UNITED STATES DEPARTMENT OF ENERGY (DOE)
Announcement of Scientific and Technical Information (STI)
(For Use By Financial Assistance Recipients and Non-M&O/M&I Contractors)

OMB CONTROL NO.
1910-1400

PART I: STI PRODUCT DESCRIPTION
(To be completed by Recipient/Contractor)

A. STI Product Identifiers

1. REPORT/PRODUCT NUMBER(s)
None

2. DOE AWARD/CONTRACT NUMBER(s)
DE-FC36-97ID13554

3. OTHER IDENTIFYING NUMBER(s)
None

B. Recipient/Contractor
Purdue University – Calumet, Dept. of Mechnaical Engineering, Hammond, IN 46321

C. STI Product Title
CFD Modeling for High Rate Pulverized Coal Injection (PCI) into the Blast Furnace

D. Author(s)
Dr. Chenn Zhou

E-mail Address(es):
gzhou@calumet.purdue.edu

E. STI Product Issue Date/Date of Publication
10 (MM) 15 (DD) 2008 (YYYY)

F. STI Product Type (*Select only one*)

☒ 1. TECHNICAL REPORT
☒ *Final* ☐ *Other (specify)*

☐ 2. CONFERENCE PAPER/PROCEEDINGS
Conference Information (title, location, dates)

☐ 3. JOURNAL ARTICLE
a. TYPE: ☐ *Announcement Citation Only*
☐ *Preprint* ☐ *Postprint*
b. JOURNAL NAME
c. VOLUME *d. ISSUE*
e. SERIAL IDENTIFIER (e.g. ISSN or CODEN)

☐ 4. OTHER, SPECIFY

G. STI Product Reporting Period
05 (MM) 10 (DD) 2005 (YYYY) Thru 10 (MM) 15 (DD) 2008 (YYYY)

H. Sponsoring DOE Program Office
Office of Industrial Technologies (OIT)(EE20)

I. Subject Categories *(list primary one first)*
32 Energy Conservation, Consumption and Utilization
Keywords: PCI, Blast Furnace, CFD

J. Description/Abstract

Pulverized coal injection (PCI) has been recognized as an effective way to decrease the coke and total energy consumption along with minimization of environmental impacts. However, increasing the amount of coal injected into the BF is currently limited by the lack of knowledge of some issues related to the process. It is therefore important to understand the complex physical and chemical phenomena in the PCI process. Due to the difficulty in measurements, computational fluid dynamics (CFD) has been identified as a useful technology to provide such knowledge. CFD simulation is powerful for providing detailed information on flow properties and performing parametric studies for process design and optimization. In this project, comprehensive 3-D CFD models have been developed to simulate the PCI process under actual furnace conditions. These models provide raceway size and flow property distributions. The results have provided guidance for optimizing the PCI process.

K. Intellectual Property/Distribution Limitations
(must select at least one; if uncertain contact your Contracting Officer (CO))

☒ 1. UNLIMITED ANNOUNCEMENT *(available to U.S. and non-U.S. public; the Government assumes no liability for disclosure of such data)*

☐ 2. COPYRIGHTED MATERIAL: *Are there any restrictions based on copyright?* ☐ *Yes* ☐ *No.*
If yes, list the restrictions as contained in your award document

☐ 3. PATENTABLE MATERIAL: THERE IS PATENTABLE MATERIAL IN THE DOCUMENT.
INENTION DISCLOSURE SUBMITTED TO DOE:
DOE Docket Number: S-
(Sections are marked as restricted distribution pursuant to 35 USC 205)

☐ 4. PROTECTED DATA: ☐ CRADA ☐ *Other, specify*
Release date (required) no more than 5 years from date listed in Part I.E. above MM DD YYYY

☐ 5. SMALL BUSINESS INNOVATION RESEARCH (SBIR) DATA
Release date (required) no more than 4 years from date listed in Part I.E. above MM DD YYYY

☐ 6. SMALL BUSINESS TECHNOLOGY TRANSFER RESEARCH (STTR) DATA
Release date (required) no more than 4 years from date listed in Part I.E. above MM DD YYYY

☐ 7. OFFICE OF NUCLEAR ENERGY APPLICED TECHNOLOGY

L. Recipient/Contract Point of Contact *Contact for additional information (contact or organization name To be included in published citations and who would Receive any external questions about the content of the STI Product or the research contained herein)*
Dr. Chenn Zhou
Name and/or Position
gzhou@calumet.purdue.edu (219)989-2665
E-mail *Phone*
Dept. of Mechanical Engineering, Purdue University - Calumet, Hammond, IN 46321

UNITED STATES DEPARTMENT OF ENERGY (DOE)
Announcement of Scientific and Technical Information (STI)
(For Use By Financial Assistance Recipients and Non-M&O/M&I Contractors)

OMB CONTROL NO.
1910-1400

PART II: STI PRODUCT MEDIA/FORMAT and LOCATION/TRANSMISSION
(To be completed by Recipient/Contractor)

A. Media/Format Information:

1. MEDIUM OF STI PRODUCT IS:
   [X] Electronic Document [ ] Computer Medium
   [ ] Audiovisual Material [ ] Paper [ ] No Full-text
2. SIZE OF STI PRODUCT 107 Pages, 3,449KB
3. SPECIFY FILE FORMAT OF ELECTRONIC DOCUMENT BEING TRANSMITTED, INDICATE:
   [ ] SGML [ ] HTML [ ] XML [X] PDF Normal
   [ ] PDF Image [ ] TIFFG4
   [ ] WP-indicate Version (*5.0 or greater)* _____
   Platform/operation system _____
   [ ] MS-indicate Version (*5.0 or greater)* _____
   Platform/operation system _____
   [ ] Postscript _____
4. IF COMPUTER MEDIUM OR AUDIOVISUAL MATERIAL:
   a. Quantity/type (*specify)* _____
   b. Machine compatibility (*specify)* _____
   c. Other information about product format a user needs to know:
   _____

B. Transmission Information:

1. STI PRODUCT IS BEING TRANSMITTED:
   [X] a. Electronically via E-Link
   b. Via mail or shipment to address indicated in award document (*Paper product, CD-ROM, diskettes, video cassettes, etc.)*
   _____
2. INFORMATION PRODUCT FILE NAME
   [X] *(of transmitted electronic format)*
   TRP9945NonPropFinalReport

PART III: STI PRODUCT REVIEW/RELEASE INFORMATION
(To be completed by DOE)

A. STI Product Reporting Requirements Review.

[ ] 1. THIS DELIVERABLE COMPLETES ALL REQUIRED DELIVERABLES FOR THIS AWARD
[ ] 2. THIS DELIVERABLE FULFILLS A TECHNICAL INFORMATION REPORTING REQUIREMENT, BUT SHOULD NOT BE DISSEMINATED BEYOND DOE.

B. Award Office Is the Source of STI Product Availability

[ ] THE STI PRODUCT IS NOT AVAILABLE IN AN ELECTRONIC MEDIUM. THE AWARDING OFFICE WILL SERVE AS THE INTERIM SOURCE OF AVAILABILITY.

C. DOE Releasing Official

[ ] 1. I VERIFY THAT ALL NECESSARY REVIEWS HAVE BEEN COMPLETED AS DESCRIBED IN DOE G 241.1-1A, PART II, SECTION 3.0 AND THAT THE STI PRODUCT SHOULD BE RELEASED IN ACCORDANCE WITH THE INTELLECTUAL PROPERTY/DISTRIBUTION LIMITATION ABOVE.

Release by (*name)* _____

Date ___ ___ _____
MM DD YYYY

E-Mail _____

Phone _____

REPORT DOCUMENTATION PAGE

Title and Subtitle:

AISI/DOE Technology Roadmap Program for the Steel Industry
TRP 9945: CFD Modeling for High Rate Pulverized Coal Injection (PCI) to Blast Furnaces

Authors:

Dr Chenn Q Zhou,
Department of Mechanical Engineering
Purdue University Calumet
Hammond, Indiana 46323, USA

Performing Organizations:

Purdue University Calumet, 2200 169th Street, Hammond, IN 46323
ArcelorMittal Steel USA R&D Center, Mittal Steel Company, East Chicago, IN 46312
ArcelorMittal-Dofasco, 1330 Burlington Street East, Hamilton, Ontario L8N 3J5
Union Gas Limited, Chatham, Ontario, Canada, N7M 5M1
US Steel Canada, Hamilton, Ontario, Canada, L8L 8K5
US Steel, Research and Technology Center, Munhall, PA, 15120

Abstract:

A blast furnace (BF) that converts iron ore into molten iron is an important component in iron-steel making and a capital and energy intensive process. Pulverized coal injection (PCI) has been recognized as an effective way to decrease the coke and total energy consumption along with minimization of environmental impacts. However, increasing the amount of coal injected into the BF is currently limited by the lack of knowledge of some issues related to the process. It is therefore important to understand the complex physical and chemical phenomena in the PCI process. Due to the difficulty in measurements, computational fluid dynamics (CFD) has been identified as a useful technology to provide such knowledge. CFD simulation is powerful for providing detailed information on flow properties and performing parametric studies for process design and optimization. In this project, comprehensive 3-D CFD models have been developed to simulate the PCI process under actual furnace conditions. These models provide raceway size and flow property distributions such as velocity, temperature, pressure, species, particle number density, reaction rates, and unburned char concentration. Validations have been made by comparing CFD results with experimental data. A number of simulations have been performed for different blast furnaces. The results have provided guidance for optimizing the PCI process.

DOCUMENT AVAILABILITY

Reports are available free via the U.S. Department of Energy (DOE) Information Bridge:

Website: http://www.osti.gov/bridge

Reports are available to DOE employees, DOE contractors, Energy Technology Data Exchange (ETDE) representatives, and Informational Nuclear Information System (INIS) representatives from the following source:

Office of Scientific and Technical Information
P.O. Box 62
Oak Ridge, TN 37831
Tel: (865) 576-8401
Fax: (865) 576-5728
E-mail: reports@osti.gov
Website: http://www.osti.gov/contract.html

Acknowledgement: "This report is based upon work supported by the U.S. Department of Energy under Cooperative Agreement No. DE-FC36-97ID13554."

Disclaimer: "Any findings, opinions, and conclusions or recommendations expressed in this report are those of the author(s) and do not necessarily reflect the views of the Department of Energy."

AISI/DOE Technology Roadmap Program

Final Report

CFD MODELING FOR HIGH RATE PULVERIZED COAL INJECTION (PCI) TO BLAST FURNACES

by

Dr. Chenn Q Zhou

October 15, 2008

Work performed under Cooperative Agreement
DE-FC36-97ID13554

Prepared for
U.S. Department of Energy

Prepared by
American Iron and Steel Institute
Technology Roadmap Program Office
Pittsburgh, PA 15220

TABLE OF CONTENTS

TABLE OF CONTENTS i
LIST OF TABLES ii
LIST OF FIGURES iii
EXECUTIVE SUMMARY vi
1 INTRODUCTION 1
1.1 Background 1
1.2 Blast Furnace and PCI Process 1
1.3 Existing CFD Models 3
1.4 Objective and Accomplishment 4
2 CFD MODELS AND METHODOLOGY 5
2.1 Multiphase Flow and Reaction Models 5
2.1.1 CFD Model for Injection System Simulations 5
2.1.2 CFD Models for Raceway Formation Simulations 7
2.1.3 CFD Model for Raceway Combustion Simulations 8
2.2 Methodology 14
3 RESULTS AND DISCUSSION 16
3.1 Validations 16
3.2 Applications of CFD Models to Actual Blast Furnaces 20
3.2.1 Investigation of Coal Devolatization in a Lance 20
3.2.2 Investigation of Raceway Formation Kinetics 31
3.2.3 Investigation of Coal and Coke Combustion inside Raceway 39
3.2.4 Investigation of Natural Gas Co-Injection 59
3.2.5 Design of PCI Conditions 77
4 CONCLUSIONS 90
5 LIST OF REFERENCES 92

LIST OF TABLES

Table 3.1 Raceway formation model validation conditions 17
Table 3.2 Coal combustion model validation conditions..... 19
Table 3.3 Coal properties 21
Table 3.4 Gas velocity, gas temperature and coal flow rate in the baseline case 21
Table 3.5 Parameters studied 21
Table 3.6 Effect of blast temperature on total coal devolatilization inside the lance 26
Table 3.7 Effect of blast temperature on coal devolatilization before raceway..... 27
Table 3.8 Effect of coal size on coal devolatilization before raceway 29
Table 3.9 Effect of coal size on total coal devolatilization inside the lance 29
Table 3.10 Effect of coal size on total coal devolatilization inside the lance..... 30
Table 3.11 Effect of coal size on coal devolatilization before exiting the tuyere..... 30
Table 3.12 Basic simulation conditions 32
Table 3.13 Parametric study conditions..... 32
Table 3.14 Basic conditions for raceway combustion simulations..... 40
Table 3.15 Coal properties for raceway combustion simulations..... 40
Table 3.16 Parametric study cases for raceway combustion 40
Table 3.17 Summary of coke and coal burnout 59
Table 3.18 Operating conditions for natural gas co-injection..... 60
Table 3.19 Coal properties for natural gas co-injection..... 60
Table 3.20 Baseline operating conditions for PCI design..... 77
Table 3.21 Parameters Studied for PCI design 78

LIST OF FIGURES

Figure 1.1 Blast furnace process 2
Figure 1.2 Schematic of combustion in the blast furnace 2
Figure 2.1 Schematic of computational domain of injection system 6
Figure 2.2 Computational domain for raceway formation simulations 8
Figure 2.3 Computational domain for raceway combustion simulations 8
Figure 2.4 Methodology for the complete simulation of PCI process 14
Figure 2.5 Illustration of the multi-step methodology 15
Figure 3.1 Experimental apparatus 16
Figure 3.2 Comparison of predicted and measured raceway shape 16
Figure 3.3 Comparison of predicted and measured raceway depth 18
Figure 3.4 Comparison of predicted and measured gas species 18
Figure 3.5 Schematic of coal combustor 19
Figure 3.6 Comparison of predicted and measured O2 and CO concentrations 20
Figure 3.7 Locations for the analysis of temperature and velocity profiles 22
Figure 3.8 Lance wall temperature profiles along its length 23
Figure 3.9 Velocity variations near the blowpipe and tuyere zones 23
Figure 3.10 Gas velocity variations near the lance outer surface 24
Figure 3.11 Lance wall temperature and gas velocity distribution around the lance 24
Figure 3.12 Gas and particle temperature inside the lance 25
Figure 3.13 Total local coal de-volatilization inside the lance 25
Figure 3.14 Effect of blast temperature on lance wall and gas temperatures along the lance 26
Figure 3.15 Effect of blast temperature on gas temperature distributions in a plane across the lance centerline 27
Figure 3.16 Effect of blast velocity on gas temperature distributions in a plane across the lance centerline 28
Figure 3.17 Effect of coal size on gas temperature distributions across the lance centerline 29
Figure 3.18 Effect of PCI rate on average temperature of the lance wall 30
Figure 3.19 Effect of PCI rate on average temperature of the carrier gas 30
Figure 3.20 Effect of coal size on gas temperature distribution in a plane across the lance centerline 31
Figure 3.21 Geometry used for raceway formation simulations 32
Figure 3.22 Coke volume fraction 33
Figure 3.23 Raceway shape defined by the initial porosity of 0.5 33
Figure 3.24 Gas vector field and stream lines near the tuyere 34
Figure 3.25 Effect of the coke bed fluidization on raceway formation 34
Figure 3.26 Two-zone distributions on raceway formation 35
Figure 3.27 Four-zone distributions on raceway formation 35
Figure 3.28 Effect of coke bed porosity distribution on raceway formation 36
Figure 3.29 Effect of coke diameter on raceway formation 36
Figure 3.30 Effect of dead-man porosity on raceway formation 37
Figure 3.31 Effect of tuyere velocity on raceway formation 38
Figure 3.32 Effect of tuyere velocity on raceway formation – top view 38
Figure 3.33 Effect of tuyere diameter and length extended over lining 39
Figure 3.34 Raceway formation 41
Figure 3.35 Gas and coal particle flow patterns 42

Figure 3.36 Temperature field and gas species profiles 43
Figure 3.37 Coal and coke flow property distributions 45
Figure 3.38 Comparison between all coke and PCI operations 47
Figure 3.39 Comparison between all coke and PCI operations: gas species and temperature distributions 49
Figure 3.40 Effect of coal type on raceway combustion 50
Figure 3.41 Effect of coal type on species concentration distributions 52
Figure 3.42 Effect of coal type on species and temperature distribution 52
Figure 3.43 Effect of PCR on combustion process 53
Figure 3.44 Effect of PCR on gas species distributions 55
Figure 3.45 Effect of PCR on species and temperature distributions 55
Figure 3.46 Effect of PCR on raceway combustion 55
Figure 3.47 Effect of oxygen enrichment on gas species distributions 57
Figure 3.48 Effect of oxygen enrichment on raceway combustion 58
Figure 3.49 Effect of oxygen enrichment on gas species and temperature distributions 58
Figure 3.50 Schematic of the injection system 61
Figure 3.51 Baseline velocity, temperature and devolatilization 62
Figure 3.52 Species concentrations of the baseline case 63
Figure 3.53 Effect of carrier air flow on the devolatization 64
Figure 3.54 Effect of natural gas flow rate on the devolatization 65
Figure 3.55 Contours of oxy-lance outer wall temperature (K) 65
Figure 3.56 Effect of oxygen lance flow rate on devolatization 66
Figure 3.57 Effect of oxygen enrichment on oxygen lance wall temperatures 66
Figure 3.58 Effect of blast air temperature on lance wall temperature 67
Figure 3.59 Data used as input to in-house code for the baseline case 68
Figure 3.60 Coke particle distribution for baseline case (volume fraction of coke) 69
Figure 3.61 Gas temperature and compositions for baseline case 70
Figure 3.62 Gas flow filed and CO distribution for baseline case 70
Figure 3.63 Effect of carrier gas flow rate on raceway combustion 71
Figure 3.64 Effect of natural gas flow rate on raceway combustion 72
Figure 3.65 Coke consumption and major species distributions 73
Figure 3.66 Effect of oxygen lance flow rate on raceway combustion 74
Figure 3.67 Effect of blast temperature on temperature distribution 74
Figure 3.68 Species concentrations and coke consumption in the raceway 75
Figure 3.69 Average gas temperature (˚C) for all cases 75
Figure 3.70 Coke consumption ratio for all cases 76
Figure 3.71 Geometry used for injection system simulation 77
Figure 3.72 Gas and solid flow characteristics in the injection system 78
Figure 3.73 Gas temperature (K) 79
Figure 3.74 Devolatilization rate (kg/s) 79
Figure 3.75 Mass fraction of CO2 79
Figure 3.76 Mass fraction of H2O 79
Figure 3.77 Effect of blast temperature on the coal temperature along the tuyere centerline 80
Figure 3.78 Effect of blast temperature on the devolatilization rate (kg/s) 80
Figure 3.79 Effect of blast temperature on the mass fraction of CO_2 80
Figure 3.80 Effect of tuyere diameter on the devolatilization rate (kg/s) 81

Figure 3.81 Effect of tuyere diameter on the mass fraction of CO_2 81
Figure 3.82 Effect of tuyere diameter on the coal temperature along the tuyere centerline 82
Figure 3.83 Effect of oxygen enrichment on the gas temperature distributions (K) 82
Figure 3.84 Effect of oxygen enrichment on the devolatilization rate (kg/s) 83
Figure 3.85 Gas temperature distribution 83
Figure 3.86 Species distribution along the tuyere central line 84
Figure 3.87 Gas temperature (K) for different blast temperature 85
Figure 3.88 Exit temperature at different blast temperature 85
Figure 3.89 Percentage of burned coal vs. blast temperature 86
Figure 3.90 Gas temperature as the effects of oxygen (K) 87
Figure 3.91 Exit temperatures at different PCI injection rate 87
Figure 3.92 Burned coal % at different PCI injection rate 88
Figure 3.93 Gas temperature vs. different tuyere diameter 88
Figure 3.94 Coal burnt ratio at different tuyere diameter 89

EXECUTIVE SUMMARY

The blast furnace that converts iron ore into molten iron is an important component in iron-steel making and a capital and energy intensive process. To maintain and improve the competitiveness of the blast furnace process, it is necessary to achieve a considerable decrease in the coke and total energy consumption for primary metal production along with minimization of environmental impacts. Injection of auxiliary fuels such as pulverized coal has continuously made a considerable contribution toward coke saving in the last two decades. Efforts have been made to increase the pulverized coal injection (PCI) rate. According to projections in the Steel Industry Technology Roadmap, the PCI rate is expected to rise from 300 to 500 lbs/NTHM (net ton of hot metal) by 2015. However, with increasing PCI rates, some coal related technical difficulties intensify. It is therefore essential to understand the complex physical and chemical phenomena in the PCI process for optimizations.

The goal of the research is to improve the competitive edge of steel mills by using advanced computational fluid dynamics (CFD) to increase yield, maximize fuel efficiency, save energy, and improve the environment. Advanced CFD modeling is a powerful tool for providing detailed information on furnace conditions and parametric effects on performance. In this project, comprehensive three-dimensional CFD models have been developed to simulate raceway formation, flow characteristics, and combustion of coke, coal and natural gas combustion behavior in the process of pulverized coal injection (PCI) into a blast furnace. A methodology has been developed to integrate these models to simulate the whole PCI process. A state-of-the-art multiphase reacting flow CFD software package has been developed. The CFD models provide detailed information of velocity, temperature, species, particle number density, reaction rate, unburned char concentration, and raceway size. Validations have been made by comparing CFD results with experimental data. The CFD models and the methodology have been applied to simulating the PCI process in various actual blast furnaces. A large number of simulations have been performed and the results have been used to help industry gain insights of the PCI process, identify the causes of problems encountered during operations, provide guidance for lance design and protection, and give directions for optimization strategies for PCI performance.

The collaborative efforts of the academic and industrial investigators/participants have made contributions not only to the PCI process, but also to the education of engineering students at Purdue University Calumet which is centrally located near the center of the United States industry. Numerous students involved in the project gained valuable research experience as well as excellent training in solving real world problems. The project has laid a solid foundation for the development of a comprehensive whole blast furnace model.

1 INTRODUCTION

1.1 Background

The blast furnace (BF) represents the predominant ironmaking process in the U.S. More than 95% hot metal produced from iron ore comes from blast furnaces. It is apparent that the lead role of blast furnaces in hot metal production will remain unchanged well into the future. A blast furnace is capital and energy intensive [1]. To maintain and improve the competitiveness of the blast furnace process, it is necessary to achieve a considerable decrease in coke and total energy consumption for primary metal production along with minimization of environmental impacts.

Pulverized coal injection (PCI), which provides auxiliary fuel for partial coke replacement, has proven both economically and environmentally favorable. It can result in substantial improvement in the furnace efficiency and thus contribute to the reductions of energy consumption and environmental emissions. In order to accelerate reducing the coke consumption, it is necessary to increase the PCI rate to overcome the productivity barrier due to the reliance of coke. According to projections in the Steel Industry Technology Roadmap, the PCI rate is expected to rise to 227 kg/NTHM (500 lbs/NTHM) by 2015, up from current levels of about 136 kg/NTHM (300 lbs/NTHM). However, with increasing PCI rates, some coal related technical difficulties intensify such as insufficient coal combustion due to extremely short residence time in the raceway. Poor coal combustion can result in many operational problems such as reduced permeability, undesirable gas and temperature distribution, and hence reduced BF productivity and stability. Therefore, to realize the high rate PCI, a better understanding of the essential behavior and the combustion process is required. Due to the difficulties in measurements, such knowledge can be most readily obtained through the development of high fidelity computational fluid dynamics (CFD) numerical simulations.

Recent rapid advancements in computer technology have made the development of high fidelity CFD simulations possible. Such simulations are a powerful tool that can provide detailed information on hydrodynamics, heat transfer, and chemical kinetics in complex flows, and can be used to conduct extensive computer experiments for parametric and optimization studies of flow systems. Specifically, the simulations can be used to (1) investigate the impact of key operation and design parameters and (2) develop strategies to maximize PCI rate with high coal to coke replacement ratio and furnace productivity. Currently, most U.S. steel producers use inadequate, simple models to compute multi-stage energy and material balances; moreover, there is no comprehensive blast furnace model that includes fluid flow and chemical kinetics. The development of advanced CFD models for blast furnaces will thus represent a significant technological leap for the U.S. steel industry.

1.2 Blast Furnace and PCI Process

The BF process is a counter current moving bed chemical reactor to reduce iron oxides to iron. As shown in

Figure 1.1, iron-bearing materials, fuel (coke), and flux (limestone and/or dolomite) are charged in alternate layers into the top of the furnace. Hot air (blast) enters into a bustle pipe that encircles the furnace and is then introduced into the furnace through tuyeres. The hot air with a

high velocity creates a void space in front of the tuyere called a raceway, which is surrounded by a bed of lose coke. Auxiliary fuels such as natural gas, pulverized coal and oxygen can also be injected through a lance inserted into the blowpipe leading up to the tuyere into a blast furnace. The injected fuels and some of the coke descending from the top of the furnace are combusted and gasified to produce heat and reducing gas for reducing the iron ores as shown in

Figure 1.2 [2] . The raw materials take 6 to 8 hours to descend to the hearth of the furnace where they become the hot metal and molten slag drained out through tap holes [3, 4].

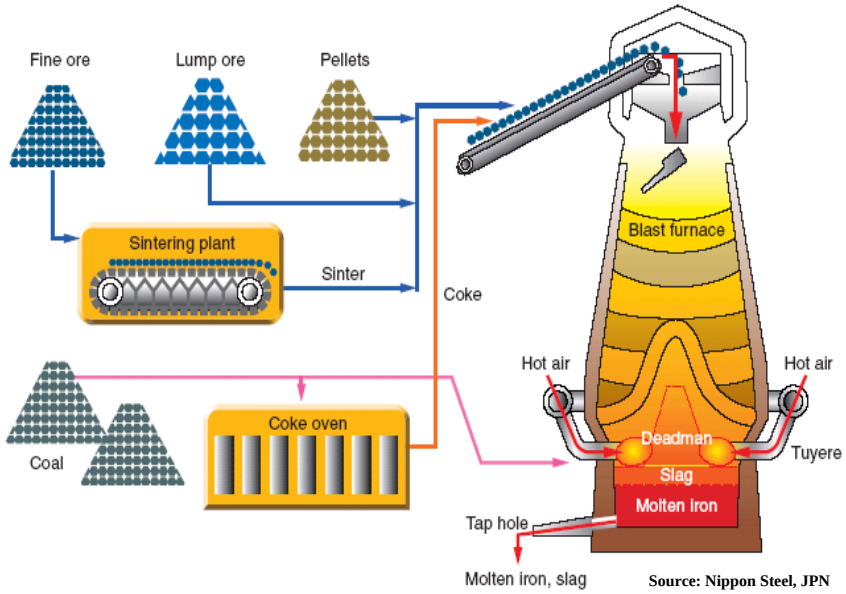

Figure 1.1 Blast furnace process

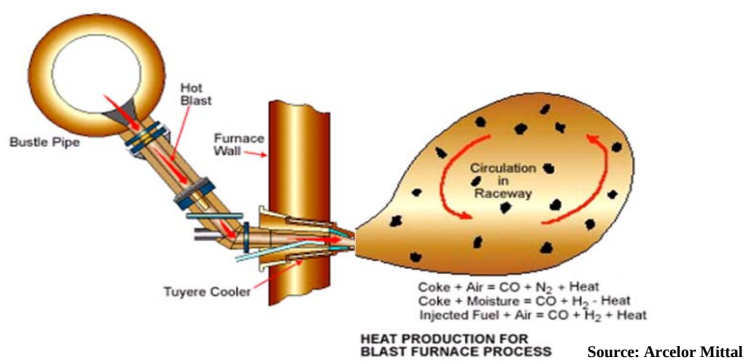

Figure 1.2 Schematic of combustion in the blast furnace

Use of auxiliary fuels can substantially decrease the hot metal production cost as well as improve the environment because the coke making process is very costly and produces harmful emissions. During the 1950s, oil was the preferred injectant, due to its low price relative to natural gas and coal. Due to the shortage and high cost of fuel oil around 1979, pulverized coal injection (PCI) potential as a coke replacement began to be realized. Experiments with PCI

showed that coal was a good replacement for oil which resulted in the rapid application of PCI in both Europe and Japan. As a result, PCI technology for blast-furnace operation has progressed rapidly during the 1980's. It is now recognized that although the capital cost associated with natural gas injection is lower than that for pulverized coal injection, PCI provides the means to ultimately achieve higher coke replacement, simply by permitting higher injection rates [5-15].

In general, the total fuel consumption of approximately 500 kg/NTHM is representative of a stable operation as current blast furnace practices suggest [16]. Although operating targets differ from steelmaker to steelmaker, the trend in PCI rates is towards a long term operating average of 200 kg/thm, representing 40% of the total fuel rate. However, at high PCI rates, insufficient combustion and gasification of pulverized coal in the raceway may result in the presence of un-burned char which flows upwards in the furnace and may block the void spaces of the burden [17]. Due to the complex phenomena involved in the blast furnace and PCI process, a better understanding of the process mechanisms and their parametric effects is essential in order to provide a guide to the setting and optimizing of furnace operating parameters for achieving high coal to coke replacement ratios. Because of the difficulties in measurements, such knowledge can be most readily obtained through the development of high fidelity computational fluid dynamics (CFD) numerical simulations.

1.3 Existing CFD Models

A CFD model based on heat, mass and momentum balance, and reaction kinetics is one of the most useful tools for designing and optimizing combustion devices. Although there are many difficulties involved in precise modeling of the raceway phenomena in the PCI process of the BF, several models have been used as guidelines to improve the PCI facilities and operation.

Earlier modeling efforts assumed one-dimensional plug flow for the tuyere and the raceway [18, 19] which ignored the mixing process between the injected coal and the blast, and thus could not predict correctly the commencement of coal de-volatilization and combustion of released volatiles. Two-dimensional models consisting of a coal combustion model in the blowpipe and a coal/coke combustion model in the raceway were later developed. Turbulent features of the gas phase in the raceway were either ignored [20] or simulated with a modified turbulence model [21]. However, two-dimensional models can only be used in simple geometry conditions. For complex geometries such as different lance arrangements used to enhance injected coal combustion in the blowpipe-tuyere-raceway system, a more practical and realistic three-dimensional model is required.

More recently, commercial software was utilized to simulate coal de-volatilization and combustion in a combustion chamber [22] and in a tuyere-raceway system with an assumed raceway shape [23]. The particle phase was treated as a dispersed phase using a Lagrangian method and a stochastic model was used to calculate particle turbulent dispersion. A pure two-fluid model for turbulent reacting flows was also recently reported [24], in which both the gas phase and the particle phase were treated as two interpenetrating continua in an Eulerian frame of reference. The model was used to simulate pulverized coal combustion in a tubular combustor

with a slanted oxygen jet. Simulation results indicated that the coal particle size had significant effects on coal de-volatilization and char combustion in an actual blowpipe of a blast furnace.

In the previous decades, tremendous work had been conducted to investigate the kinetics of raceway formation. As an example, a simplified two-dimensional physical model was built to study what factors determined the raceway size. Assuming a spherical raceway and using dimensional analysis, the experimental results were applied for the raceway radius calculation [25, 26]. Similarly, assuming the shape as a sphere [27, 28], numerical studies was conducted on the basis of mass and momentum balance to predict the raceway size. More recently, Mondal et al [29], using a two phase Eulerian-Eulerian model, investigated the impact of coke bed and wind rates on the raceway shape and size. It has been recognized for many years that other blast furnace operation factors, such as the cohesive zone, cast practice and burden distribution also play an important role in the raceway shape, size and position. However, the effect of all those practical conditions on the raceway formation has not been studied very well.

1.4 Objective and Accomplishment

In order to achieve high pulverized coal injection rates, the understanding of essential behavior and the combustion process is very critical. In the last three years, efforts have been made in this project with the following objectives:

1. To develop a comprehensive, state-of-the-art three-dimensional CFD model in order to simulate pulverized coal injection into blast furnaces.
2. To apply the CFD model for better understanding of the PCI process in real furnace conditions.
3. To provide CFD model-based strategies to optimize the PCI performance.

Highlights of some accomplishments and major activities include:

1. Developed a multiphase reacting flow model for the simulation of the injection system including blowpipe, lance, and tuyere for both PCI and natural gas co-injections.
2. Developed a multiphase flow model for the simulation of raceway formation with consideration of combustion effects
3. Developed a multiphase reacting flow model and software for the simulation of combustion of coke, coal, and natural gas inside the raceway
4. Developed a multi-step methodology for integrating all the CFD models and simulation of the entire PCI process
5. Validated CFD models using experimental data and industrial observations
6. Conducted a large number of simulations based on the needs of the industrial participants
7. Provided insights of complex phenomena in the PCI process
8. Provided guidance for the design and operation for optimization of PCI performance
9. Trained a number of students and published a number of papers [30-49].

2 CFD MODELS AND METHODOLOGY

CFD simulation has become very effective for research and development. It can also be very beneficial to the people who are involved in operating or designing a flow/reactor system. The applications are multifold. It can be used to train novice operators by providing detailed flow information. For experienced operators, it can be used to evaluate the system performance and to seek optimal operating conditions. It can be used to develop strategies to control the system automatically. Furthermore, it can be used by system designers to develop new and improved systems by conducting computational experiments of various innovative concepts.

CFD software calculates flow properties based on the fundamental conservation laws of mass, momentum and energy on a computational grid with specified boundary conditions [50]. Computed flow properties may include temperature, velocity, pressure, density, and species concentrations. Comprehensive phenomenological models may be needed to handle complicated flow processes, such as turbulent mixing, interfacial interactions, combustion kinetics, and chemical reactions.

In this project, comprehensive 3-D CFD models have been developed to simulate multiphase reacting turbulent flows in the PCI process. Both raceway and blowpipe are included. The shape and size of the raceway is calculated instead of assumed as most researchers did previously. The major processes, i.e., multiphase flow dynamics (gas, pulverized coal, and coke particles), turbulence, heat transfer, chemical reactions including coke, coal, and natural gas combustion and species transport, are considered. The CFD simulations are divided into three parts: 1) Injection system including blowpipe, lance, and tuyere, 2) raceway formation, and 3) raceway combustion. A methodology has been developed to integrate these three parts. The CFD models and the methodology are described in the following sections.

2.1 Multiphase Flow and Reaction Models

2.1.1 CFD Model for Injection System Simulations

Figure 2.1 shows a schematic of a computational domain. The injection system includes a blowpipe, a tuyere and a lance where pulverized coal is transported to the blowpipe. In some applications, natural gas co-injection may be included. A comprehensive 3-D CFD model needs to include turbulent gas flow in the blowpipe, heat transfer between the hot blast, the lance wall, and the flows inside the lance, coal particle flow carried by air inside the lance, coal devolatilization in the lance and tuyere, coal combustion in the tuyere, as well as natural gas combustion.

In this model, the gas phase flow is calculated based on the Reynolds-averaged Navier-Stokes equations. The standard k-ε turbulence model is used to describe the turbulent features of the gas phase. This model is chosen due to its excellent performance with relatively simple modeling. It is known for its robustness and economy. The k-ε model is a semi-empirical model which is based on the transport equations for the turbulence energy (k) and its dissipation rate (ε). Gas-phase continuity, momentum, species mass fraction and energy equations as well as the

equations of the turbulent kinetic energy and its dissipation rate at steady state can be written in the following generalized form:

$$div(\rho\phi u) = div(\Gamma grad\phi) + S_{\phi} + S_{\phi p} \tag{1}$$

where ϕ is the general property. When ϕ = 1, the equation represents the mass conservation equation; when ϕ = velocity, the equation represents the momentum equation; and when ϕ = specific energy, the equation represents the energy equation. Γ is the diffusivity (mass diffusion in the momentum equation, viscous term in continuity equation and heat conduction in the energy equation). S_{ϕ} and $S_{\phi P}$ are source terms of the gas phase and the source term due to the presence of coal particles, respectively.

Pulverized coal particles are treated as a discrete secondary phase. The trajectories of coal particles are calculated through the integration of the force balance equation of the particle based on the Lagrangian method with the consideration of turbulent dispersion effects.

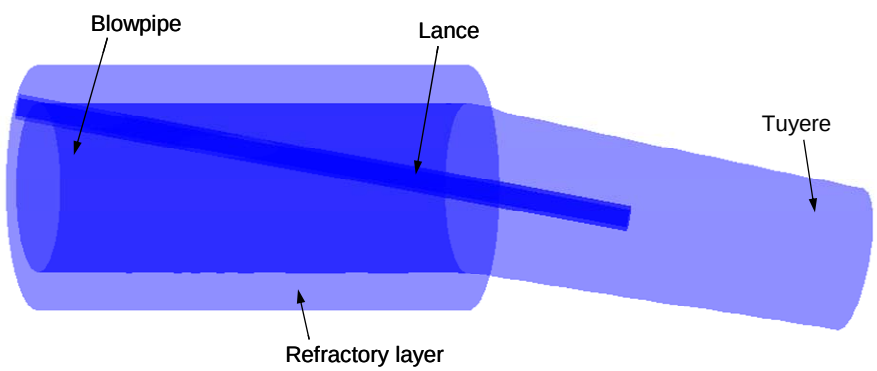

Figure 2.1 Schematic of computational domain of injection system

The commercial CFD software FLUENT© is used to solve the governing equations for the gas phase and the particle phase. The heating or cooling laws are applied when the particle temperature is less than the user defined vaporization temperature, T_{vap}, and after the volatile fraction, $f_{v,0}$, of the particle has been consumed. The heat lost or gained by the particle as it traverses each computational cell appears as a source or sink of heat in subsequent calculations of the continuous phase energy equation. During the inert heating or cooling laws, particles do not exchange mass with the continuous phase and do not participate in any chemical reaction.

The devolatilization law is applied to a combusting coal particle when the temperature of the particle reaches the vaporization temperature, T_{vap}, and remains in effect while the mass of the particle, mp, exceeds the mass of the non-volatiles in the particle. After the volatile component is completely evolved, a surface reaction begins which consumes the combustible fraction of the particle. The surface combustion law is thus active after the volatiles are evolved. When the combustible fraction has been consumed by the surface combustion law, the combusting particle may contain residual “ash” that reverts to the inert heating law. The surface

combustion law consumes the reactive content of the particle as governed by the stoichiometric requirement of the surface "burnout" reaction.

The kinetic/diffusion surface reaction rate model was chosen to model surface combustion. This model assumes that the surface reaction rate is determined either by kinetics or by a diffusion rate. The particle size is assumed to remain constant in this model while the density is allowed to decrease. The surface reaction consumes the oxidant species in the gas phase, i.e., it supplies a (negative) source term during the computation of the transport equation for this species. Similarly, the surface reaction is a source of species in the gas phase: the product of the heterogeneous surface reaction appears in the gas phase as a user-selected chemical species. The surface reaction also consumes or produces energy, in an amount determined by the heat of reaction. The gas phase reactions can be described using a species transport model with a 28-step reduced mechanism that was reported by Jazbek et. al [51].

2.1.2 CFD Models for Raceway Formation Simulations

The raceway formation has been simulated by using a most comprehensive transient 3-D Eulerian approach. The commercial CFD software FLUENT© is used to predict the shape and size of the raceway. Combustion is not included in the simulation. However, the effect of combustion on the raceway formation is considered in the methodology described later. In the Eulerian approach, the different phases are treated mathematically as interpenetrating continua. Since the volume of a phase cannot be occupied by the other phases, the concept of phasic volume fraction, α, is introduced. These volume fractions are assumed to be continuous functions of space and time and their sum is equal to one. Conservation equations for each phase are derived to obtain a set of equations, which have similar structure for all phases as shown in Equation (2).

$$\frac{\partial(\alpha_i \rho_i \phi)}{\partial t} + div(\alpha_i \rho_i \phi u) = div(\Gamma grad\,\phi) + S_\phi \qquad (2)$$

where S_ϕ stands for the mass transfer between the two phases. A multi-fluid granular flow model is used to describe the flow behavior of the fluid-solid mixture. Granular model treats the mixture to be made up of discrete solid particles which are dispersed in a fluid phase. Granular multi-fluid model consists of granular phase conservation equations and fluid phase conservation equations. The fluid-solid interaction law used is the Syamlal-O'Brian model. This model defines the fluid-solid interaction coefficient using an empirical relationship based on terminal velocity measurements in fluidized beds and settling beds. This coefficient is a function of volume fraction and Reynolds number. The solid-solid interaction is based on the assumption that there is instantaneous binary collisions between particles and that the energy dissipation is due to inelasticity of collisions.

The burden and cohesive zones are treated as porous media [52, 53]. It is modeled by the addition of a momentum source term to the standard fluid flow equations. The source term contributes to the pressure gradient in the porous cell, creating a pressure drop that is

proportional to the fluid velocity (or velocity squared) in the cell. It is composed of two parts: a viscous loss term and an inertial loss term. The computational domain is shown in Figure 2.2.

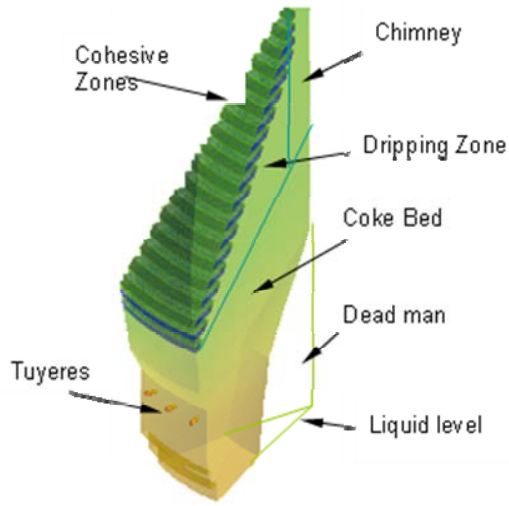

Figure 2.2 Computational domain for raceway formation simulations

2.1.3 CFD Model for Raceway Combustion Simulations

The CFD software has been developed for multiphase reacting flow simulations of raceway combustion inside a blast furnace. Eulerian approach is used to model the gas-coal particle phases. The coke bed is treated as a porous media. The computational domain includes a tuyere, a raceway and the coke bed around the raceway as shown in Figure 2.3.

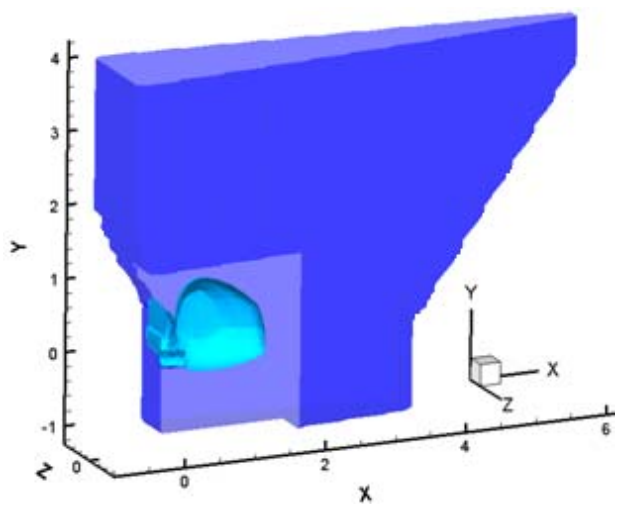

Figure 2.3 Computational domain for raceway combustion simulations

The multiphase reacting flow computer software has the following major features:

- Three-dimensional
- Steady state
- Gas-particle phases
- Turbulence
- Convective, conductive and radiative heat transfer
- Multispecies reactions
- Porous media
- Coal drying, devolatilization, combustion and gasification
- Natural gas combustion
- Coke combustion and gasification
- Easy input of kinetic data

Governing equations

Eulerian approach treats the different phases mathematically as interpenetrating continua. Mass transfer, heat transfer, and motion of gas and particle phases are described by conservation equations of mass, energy and momentum. The k- ε -k_p two-phase turbulence model is used to model the gas and particle turbulence. The radiation heat transfer is calculated by the discrete-ordinates model. The gas-particle phase continuity, momentum, species mass fraction and energy equations as well as the equations of the turbulent kinetic energy and its dissipation rate at steady state can be written in the following generalized form:

$$\frac{\partial}{\partial x}(\rho u\phi)+\frac{\partial}{\partial y}(\rho v\phi)+\frac{\partial}{\partial z}(\rho w\phi)=\frac{\partial}{\partial x}(\Gamma_{\varphi}\frac{\partial\phi}{\partial x})+\frac{\partial}{\partial y}(\Gamma_{\varphi}\frac{\partial\phi}{\partial y})+\frac{\partial}{\partial z}(\Gamma_{\varphi}\frac{\partial\phi}{\partial z})+S_{\varphi}+S_{\varphi Pg} \quad (3)$$

$$\frac{\partial}{\partial x}(\rho_P u_P\phi_P)+\frac{\partial}{\partial y}(\rho_P v_P\phi_P)+\frac{\partial}{\partial z}(\rho_P w_P\phi_P)=\frac{\partial}{\partial x}(\Gamma_{\varphi P}\frac{\partial\phi_P}{\partial x})+\frac{\partial}{\partial y}(\Gamma_{\varphi P}\frac{\partial\phi_P}{\partial y})+\frac{\partial}{\partial z}(\Gamma_{\varphi P}\frac{\partial\phi_P}{\partial z})+S_{\varphi P}+S_{\varphi Pg} \quad (4)$$

where ϕ and ϕ_P are the generalized independent variable; Γ_{ϕ} , $\Gamma_{\phi P}$ are the effective transport coefficient, S_{ϕ}, $S_{\phi P}$ and $S_{\phi Pg}$ are source terms , respectively. The detailed meanings for each equation can be found in the references [54].

Phenomenological Models

Inter-phase Momentum Transfer

The particle phase exchanges momentum with the gas phase through the drag force. When the voidage is larger than 0.8, the exchange coefficient can be expressed as:

$$\beta_{\mathrm{k}} = \frac{3}{4} C_{\mathrm{D}} \rho \frac{|\mathrm{u} - \mathrm{u}_k|(1-\varepsilon_{\mathrm{k}})^2}{d_{\mathrm{k}}} f(\varepsilon_{\mathrm{k}}) \tag{5}$$

In the above equation, $f(\varepsilon_k)$ accounts for the effect of the presence of other particles and is a correction to the Stokes law for free fall of a single particle. The following equation is used in this work.

$$f(\varepsilon_{\mathrm{k}}) = (1-\varepsilon_{\mathrm{k}})^{-3.8} \tag{6}$$

The drag coefficient is a function of the Reynolds number and can be estimated by:

$$C_D = \begin{cases} \dfrac{24}{Re_k}\left(1 + \dfrac{Re_k^{0.667}}{6}\right) & Re_k < 1000 \\ 0.44 & Re_k \geq 1000 \end{cases} \tag{7}$$

where, the Reynolds number is given by:

$$Re_{\mathrm{k}} = \frac{\rho d_k |\mathrm{u} - \mathrm{u}_k|}{\mu} \tag{8}$$

When the voidage is less than 0.8, the momentum exchange rate between gas and solid phase is calculated by the Ergun's equation:

$$S_u = (150 \frac{(1-\varepsilon_g)^2 \mu_g}{\varepsilon_g \psi_c^2 d_b^2} + 1.75 \frac{|U_g - U_b|(1-\varepsilon_g)\rho_g}{\psi_c d_b}) \times \varepsilon_g (U_g - U_b) \tag{9}$$

Inter-phase Heat Transfer

Based on the stagnant film theory, heat transfer between a single reacting particle and the gas phase can be calculated as [15]:

$$Q_{\mathrm{k}} = \pi d_{\mathrm{k}} Nu_{\mathrm{k}} \lambda_{\mathrm{s}} (T - T_{\mathrm{k}}) \frac{B_{\mathrm{k}}}{\exp(B_{\mathrm{k}}) - 1} \tag{10}$$

$$B_{\mathrm{k}} = -\frac{\dot{m}_{\mathrm{K}} C_{\mathrm{ps}}}{\pi d_{\mathrm{k}} Nu_{\mathrm{k}} \lambda_s} \tag{11}$$

$$Nu_{\mathrm{k}} = 2 + 0.5 \mathrm{Re}_{\mathrm{k}}^{0.5} \tag{12}$$

where, the so-called 1/3 Law is used to calculate the thermal conductivity λ_s and C_{ps} around the coal particles.

Moisture Evaporation Rate

The moisture evaporation rate is calculated by a diffusion model [54]. Assuming that the moisture in a coal particle diffuses to the surface of the coal particle to form a liquid film and treating this liquid film as a surface layer of a water droplet with the same diameter, the moisture evaporation rate can be calculated as:

$$\dot{m}_{wk} = \begin{cases} -\pi d_k Nu_k D_s \rho_s \ln\left(1 + \dfrac{Y_{H_2O,s} - Y_{H_2Og}}{1 - Y_{H_2O,s}}\right) & T_k < T_b \\ -\pi d_k Nu_k \dfrac{\lambda_s}{C_{ps}} \ln\left(1 + \dfrac{C_{ps}(T - T_k)}{1 - L_w}\right) & T_k \geq T_b \end{cases} \tag{13}$$

$$Y_{H_2O,s} = B_w \exp(-E_w / RT_k) \tag{14}$$

where Y_{H2Os} is the mass fraction of vapor at the surface of the coal particles. The Nusselt number, Nu_k, of heat convection is calculated as:

$$Nu_k = 2 + 0.5\,\mathrm{Re}_k^{0.5} \tag{15}$$

Coal Devolatilization Rate

When the coal particles are heated to a certain temperature, thermal decomposition of the carbon network occurs and the process releases volatile matters into the gas phase. The gaseous product contains hydrocarbons of low molecular weight, such as methane, carbon monoxide and hydrogen. The coal de-volatilization rate is proportional to the mass of the dry and ash free (daf) coal. The coal de-volatilization is modeled by two simultaneous, competing, first-order, irreversible reactions [18]:

$$\text{Raw Coal} \xrightarrow{k_{v1}} \alpha_1(\text{Volatiles})_1 + (1-\alpha_1)(\text{Char})_1$$

$$\text{Raw Coal} \xrightarrow{k_{v2}} \alpha_2(\text{Volatiles})_2 + (1-\alpha_2)(\text{Char})_2$$

where the α_1 is obtained from the volatile matter percentage in proximate analysis of coal and α_2 is equal to 2.

The volatile release rate can be calculated by:

$$\dot{m}_{vk} = -\alpha_1 m_{dk} B_{v1} \exp\left(-\frac{E_{v1}}{RT_k}\right) - \alpha_2 m_{dk} B_{v2} \exp\left(-\frac{E_{v2}}{RT_k}\right) \tag{16}$$

The daf coal mass reduction rate can be obtained by:

$$\dot{m}_{dk} = -m_{dk} B_{v1} \exp(-\frac{E_{v1}}{R T_k}) - m_{dk} B_{v2} \exp(-\frac{E_{v2}}{R T_k}) \tag{17}$$

Coal is assumed to decompose to form char and volatiles which consist of hydrocarbon C_dH_b and CO.

$$\text{Coal} = [\text{ Volatiles }] + \text{Char} \tag{18}$$

$$C_aH_bO_c = [\ C_dH_b + cCO\ ] + eC \quad (\text{ Volatiles} = C_dH_b + cCO\ ) \tag{19}$$

where, constants a to e can be determined from the coal ultimate analysis.

Char Combustion Rate

The heterogeneous char reaction rate is assumed to be of first-order with respect to oxygen, carbon dioxide and water vapor concentrations [22].

$$C + O_2 \rightarrow CO_2 \tag{20}$$

$$2C + O_2 \rightarrow 2CO \tag{21}$$

$$C + CO_2 \rightarrow 2CO \tag{22}$$

$$C + H_2O \rightarrow CO + H_2 \tag{23}$$

The char reaction rates for the surface reactions (20) to (23) given in terms of the gas consumption rates can be written as:

$$\dot{m}_{ck,A} = -\pi d_k^2 \rho_s Y_{O_2,s} B_A \exp(-\frac{E_A}{R T_k}) \tag{24}$$

$$\dot{m}_{ck,B} = -\pi d_k^2 \rho_s Y_{O_2,s} B_B \exp(-\frac{E_B}{R T_k}) \tag{25}$$

$$\dot{m}_{ck,C} = -\pi d_k^2 \rho_s Y_{CO_2,s} B_C \exp(-\frac{E_C}{R T_k}) \tag{26}$$

$$\dot{m}_{ck,D} = -\pi d_k^2 \rho_s Y_{H_2O,s} B_D \exp(-\frac{E_D}{R T_k}) \tag{27}$$

Volatiles Combustion

Once the volatile matters are released in the gas phase, they undergo homogeneous combustion. In this work, it is assumed that the volatile consists of hydrocarbons and carbon monoxide only. The following gaseous reactions are considered:

$$C_dH_b + \frac{d}{2}O_2 = d\,CO + \frac{b}{2}H_2 \tag{28}$$

$$2CO + O_2 \rightarrow 2CO_2 \tag{29}$$

$$2H_2 + O_2 \rightarrow 2H_2O \tag{30}$$

The eddy breakup (EBU) turbulent combustion model is used to quantify the effect of turbulence on the combustion rates of volatiles, carbon monoxide and hydrogen. The reaction rate is determined as: $W_s = min\ (W_{s,EBU},\ W_{s,Arr})$, in which:

$$W_{s,\mathrm{Arr}} = B_s \rho^2 Y_F Y_{ox} \exp(-\frac{E_s}{RT}) \tag{31}$$

$$W_{s,\mathrm{EBU}} = C_R \rho \frac{k}{\varepsilon} \min(Y_F, \frac{Y_{ox}}{\beta}) \tag{32}$$

Coke Combustion Model

Coke combustion inside raceway and coke bed is considered. The following heterogeneous reactions are taken into account for the coke combustion [55]:

$$C + O_2 \rightarrow CO_2 \tag{33}$$

$$C + CO_2 \rightarrow 2CO \tag{34}$$

$$C + H_2O \rightarrow CO + H_2 \tag{35}$$

$$\dot{m}_{\mathrm{ck,D}} = -\pi d_k^2 \rho_s Y_{H_2O,s} B_D \exp(-\frac{E_D}{R T_k}) \tag{36}$$

The rate of above reactions can be expressed as:

$$R_i = k_i\, C_i \tag{37}$$

$$k_i = \frac{1}{\frac{1}{k_{fi} a} + \frac{1}{\eta_i k_{mi} \rho_{bc}}} \tag{38}$$

where the k_{fi} is the mass transfer coefficient, a is specific surface area, η_i is the effectiveness factor of catalytic reaction, k_{mi} is the chemical rate constant, and ρ_{bc} is the bulk density. The mass transfer coefficient can be expressed as:

$$k_{fi} = \frac{D_i}{\phi d_p} Sh \tag{39}$$

The Sh is the Sherwood number, it can be calculated by:

$$Sh = 1.5 \mathrm{Re}_p^{0.55} \tag{40}$$

2.2 Methodology

The CFD models described above can be used to simulate each individual part to obtain useful information on the flow characteristics and parametric effects. In order to simulate the complete PCI process, a multi-step methodology was developed to integrate CFD models described above as shown in Figure 2.4.

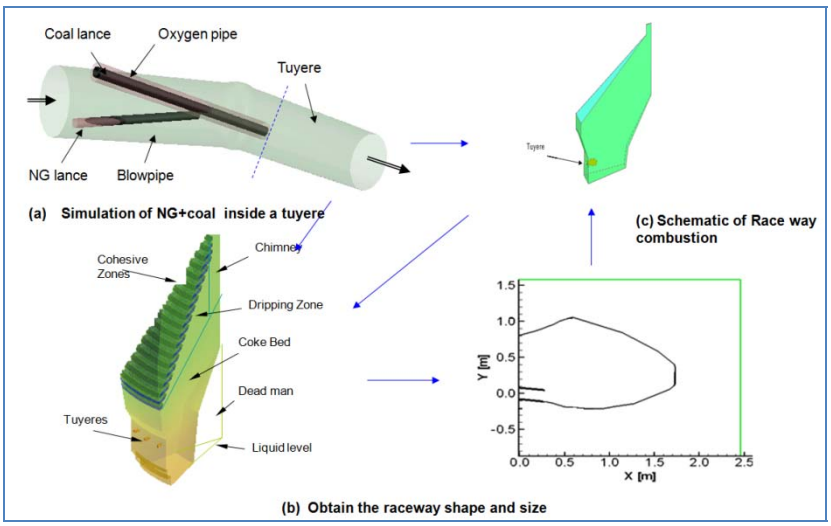

Figure 2.4 Methodology for the complete simulation of the PCI process

In this multi-methodology, computations are performed based on the following steps:

Step 1: Simulate flows in the injection system including blowpipe, lance and tuyere; and record detailed distributions of flow properties at the exit cross section

Step 2: Use the flow properties at the exit in Step 1 as input conditions to simulate raceway formation

Step 3: Use the flow properties at the exit in Step 1 and the raceway shape and size in Step 2 as input conditions to simulate raceway combustion inside a blast furnace.

Step 4: Consider the effects of combustion on raceway shape and size by adding the additional gases and volume expansion from raceway combustion simulation in Step 3 in each computational cells affected

Step 5: Use information from Step 1 and Step 4 to simulate raceway formation.

Step 6: Repeat Step 3, 4, and 5 until there is little change of raceway shape and the size between steps.

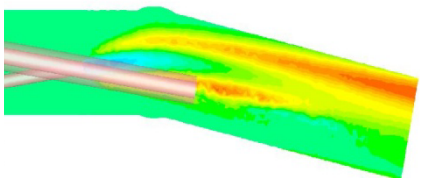

(a) Temperature distribution in a side view in blowpipe and tuyere

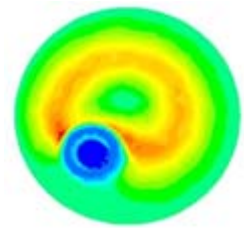

(b) Temperature distribution in a cross section at the exit of the tuyere

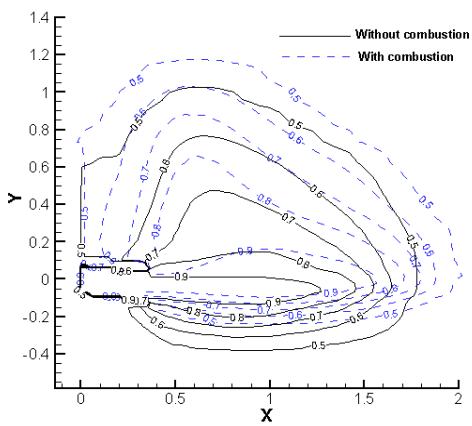

(c) Raceway with and without combustion effects

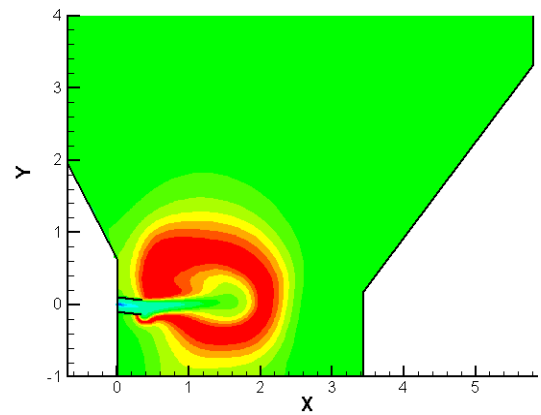

(d) Temperature distribution and coke bed

Figure 2.5 Illustration of the multi-step methodology

This methodology can be illustrated by temperature distributions in Figures 2.5 (a) to (c). In these figures, the red color indicates the highest temperature and the blue color indicates the lowest temperature. Figures 2.5(a) and 2.5(b) is the temperature distributions in a blowpipe and tuyere in a side view and the exit cross section respectively calculated in Step 1. The detailed temperature along with other flow property distributions is used for the simulations of raceway formation and combustion. Figure 2.5 (c) indicates the raceway before and after consider the effect of combustion. Figure 2.5(d) shows the temperature distributions inside the blast furnace. This methodology appears very effective.

3 RESULTS AND DISCUSSION

3.1 Validations

Because of the complexity of a multi-phase reacting flow system, a CFD code often needs to include new sub models specifically developed for the flow system as described above. Validation of these sub models is essential for CFD applications. Figure 3.1 shows a typical validation process for the development of CFD sub models. In the PCI process, the measurement in the BF is extremely difficult. The validation of the developed CFD models have been based on published data in the literature as well as observations by industrial collaborators.

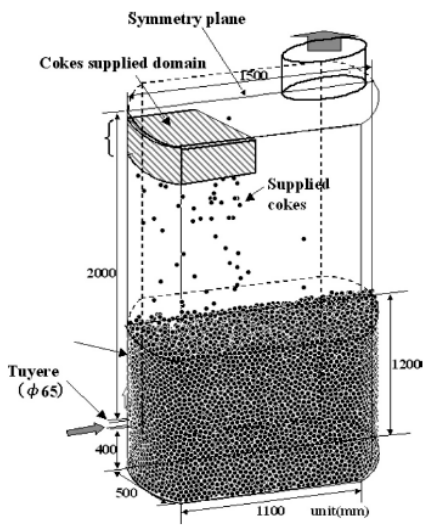

Figure 3.1 Experimental apparatus

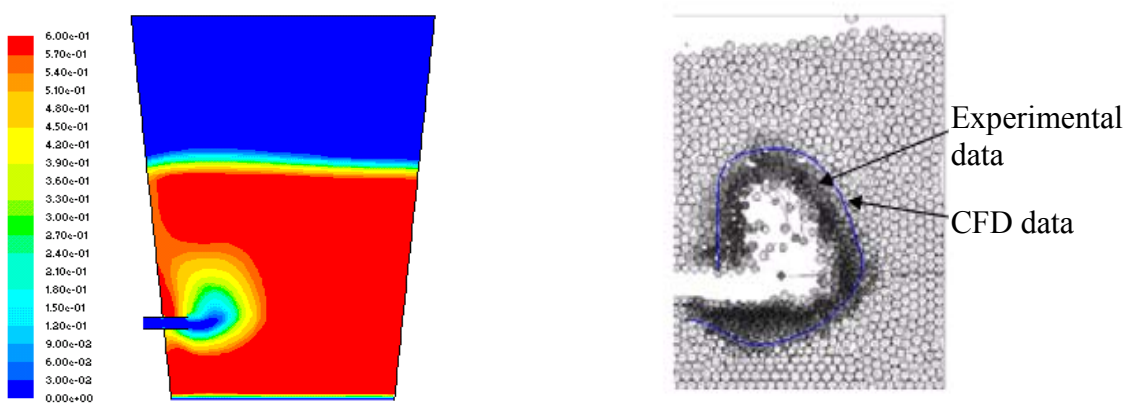

(a) Coke volume fraction from CFD model (b) Experimental vs. predicted

Figure 3.2 Comparison of Predicted and Measured Raceway Shape

Figures 3.1 and 3.2 show the validation of a raceway formation model. The experimental data are obtained from a reference by Nogami et al [56]. The experiment facility is shown in Figure 3.1. The parameters used in the validation case are listed in Table 3.1. Figure 3.2(a) shows the coke volume fraction computed from the CFD model. Figure 3.2(b) shows the raceway shapes from experiments and CFD simulations. It is clear that the CFD prediction is in agreement with the measured result.

Table 3.1 Raceway formation model validation conditions

Coke bed Porosity	0.4
Coke Diameter	0.03m
Bed Height	1.2m
Tuyere exit diameter	0.065 m
Total model height	2m
Bed Width	0.5m

Another validation of a raceway formation model is performed using the work by Rajneesh et al [57]. This work uses 2D experimental work to measure the effect of various parameters and a dimensional analysis is carried out using π-theorem to obtain a correlation for the raceway depth. The correlation thus obtained is listed below.

$$D_r = 164\left(\frac{\rho_g v_b^{\,2} D_T^2}{\rho_{eff}\, g d_p H W}\right)^{0.8} \mu_w^{-0.25} D_T \tag{41}$$

where D_r is the raceway depth, D_T is the tuyere diameter, ρ_{eff} is the effective density, H is the bed height, W is bed width, d_p is the particle diameter, g is acceleration due to gravity, v_b is the tuyere velocity, ρ_g is the gas density and μ_w is the wall friction coefficient. The results obtained from CFD and the raceway depth obtained from the equation (41) is compared in Figure 3.3. Effects of initial porosity, blast velocity and coke particles were investigated. The agreement between CFD predictions and experimental correlations is well within the acceptable range in terms of both magnitude and the trends.

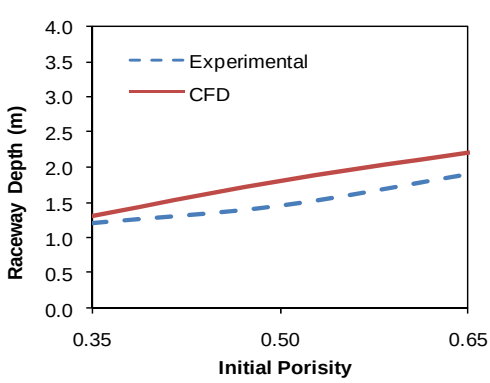

(a) Effect of initial porosity

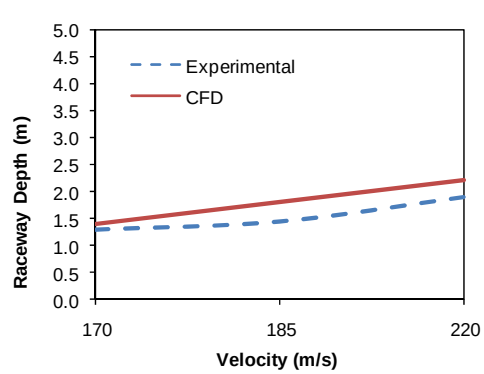

(b) Effect of blast velocity

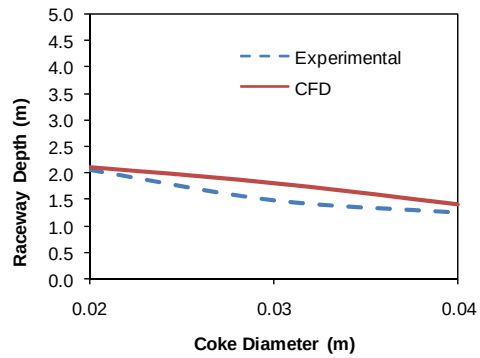

(c) Effect of coke diameter

Figure 3.3 Comparison of predicted and measured raceway depth

The measured data from the same experimental apparatus in Figure 3.1 is used to validate the coke combustion model [56]. Figure 3.4 shows the mass fractions of O_2, N_2, CO, and CO_2 along the distance from tuyere nose. The measured data indicated by individual points agrees well with the CFD data indicated by lines in terms of both magnitude and the trends.

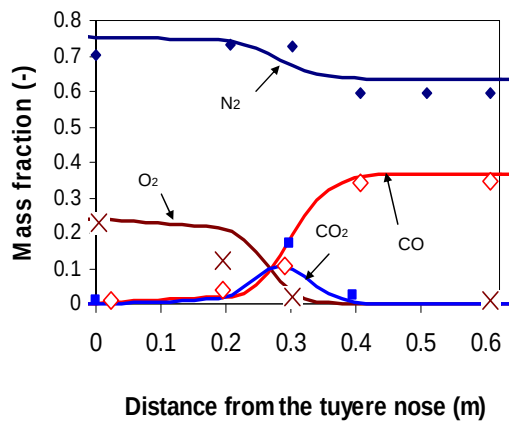

Figure 3.4 Comparison of predicted and measured gas species

The experimental data from Zhang et al [58] is used to validate the coal combustion model. Figure 3.5 illustrates the schematic of the coal combustor. It is an electrical heated reactor having five regulated heating zones; the reactor is 2.5m long and has a diameter of 0.2m. The carrying air with pulverized coal enters the burner center. The combustion air can be heated up to 673K, a gravimetric screw conveyor ensures a constant coal feeding rate. The simulation parameters are shown in Table 3.2. Figure 3.6 shows the comparison results. The agreement between the predicted and measured CO_2 and O_2 concentrations are acceptable.

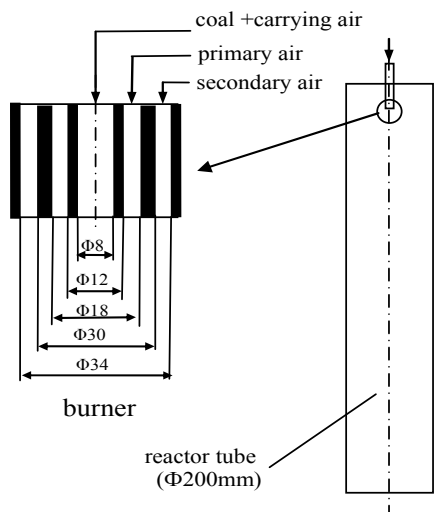

Figure 3.5 Schematic of coal combustor [58]

Table 3.2 Coal combustion model validation conditions

Coal flow rate (kg/h)	1.0
Wall temperature (K)	1523
Coal carrying air (Nm^3/h)	1.5
Temperature of carrying air (K)	473
Primary and second air flow rate(Nm^3/h)	8.0
Primary air : second air	1 : 2
Temperature of primary air (K)	523
Temperature of second air (K)	623
Coal size distribution (μm) (%)	16(30%), 52(35%), 160(25%), 350(10%)

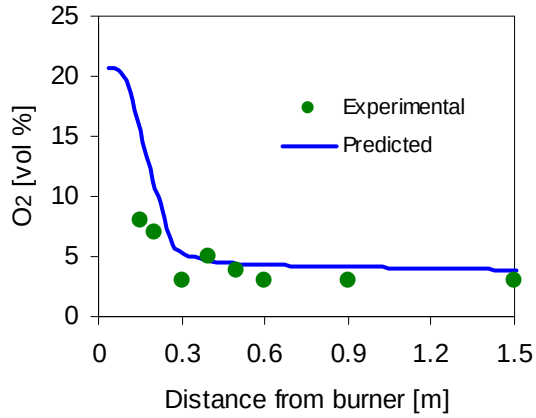

(a) Oxygen Concentration

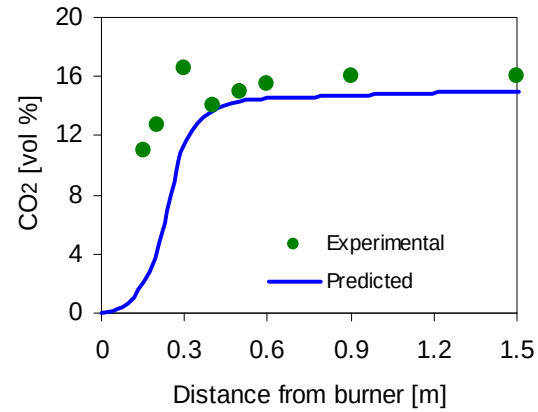

(b) Carbon dioxide Concentration

Figure 3.6 Comparison of predicted and measured O_2 and CO Concentrations

3.2 Applications of CFD Models to Actual Blast Furnaces

A large number of simulations have been performed for various blast furnaces based on requests from the industrial participants. The results and discussions of these applications are presented in the following sections.

3.2.1 Investigation of Coal Devolatization in a Lance

During the operation of a blast furnace at the site of one of industrial participants, it was found that there was a layer of black material formed on the inner surface of the lance after a period of time. This may be caused by the coal devolatilization inside a lance. Therefore, the objective of this application is to investigate the cause of the deposit by analyzing the coal devolatization as well as to conduct parametric studies to reduce or eliminate the deposit.

The computational domain includes a blowpipe, a tuyere and a lance where pulverized coal is transported to the blowpipe. The geometry is based on actual blast furnace conditions as shown in Figure 2.1. The centerline of the blowpipe is perpendicular to the centerline of the blast furnace. The tuyere exit is tilted downward with an angle of 6° between the centerlines of the blowpipe and the tuyere. The inner diameter of the tuyere exit is 0.15 m and the tuyere length is 0.437 m. The lance inlet is inclined 10° upward and then to the right of the blowpipe inlet with an angle of 10.8°. The lance has an inner diameter of 0.019 m and an outer diameter of 0.027 m. The lance exit is located at the centerline of the tuyere. The inner diameter of the blowpipe is 0.178 m and its length is 0.463 m; the blowpipe has an refractory layer with a thickness of 0.044 m and a thermal conductivity of 1.51 W/(m·K). On the outer surface of the insulation, there is a thin layer (12.7 mm) of insulation fiber with a thermal conductivity of 0.15 W/(m·K).

Coal proximate and ultimate analyses are given in Table 3.3. An average particle size of 60 μm is used in the simulations. Nitrogen is the carrier gas for the coal injection. The blast is

oxygen-enriched with 8 m^3 oxygen/100 m^3 air and containing 1% moisture. Operating conditions are summarized in Tables 3.4 and 3.5.

Table 3.3 Coal properties

(a) Proximate analysis (wt. %)

Fixed carbon	Volatile matter	Ash
58.6	35.6	5.8

(b) Ultimate analysis (wt. %)

C	H	O	N	S	Ash
81.7	5.0	4.9	1.5	0.87	5.8

Table 3.4 Gas velocity, gas temperature and coal flow rate in the baseline case

	Parameter	Value
Lance	Inlet nitrogen velocity (m/s)	9.0
	Inlet nitrogen temperature (K)	300
	PCI rate (kg/s)	0.50
Blowpipe	Inlet air velocity (m/s)	107.5
	Inlet air temperature (K)	1493
	Operating pressure (kPa)	461.3

Table 3.5 Parameters studied

Parameter	Ranges for different cases
Blast temperature (K)	1493 -1543
PCI flow rate (kg/s)	0.375 – 0.620.5
N_2 velocity (m/s)	6.8 – 11.3
Blast velocity (m/s)	100 - 115
Coke Particle size (μm)	30 - 90

Baseline Case

In the simulations, a baseline case is established and then parametric effects are studied. Detailed analyses of flow pattern, heat transfer, coal devolatization and combustion are conducted. Figure 3.7 shows the locations where temperature and gas flow field are analyzed.

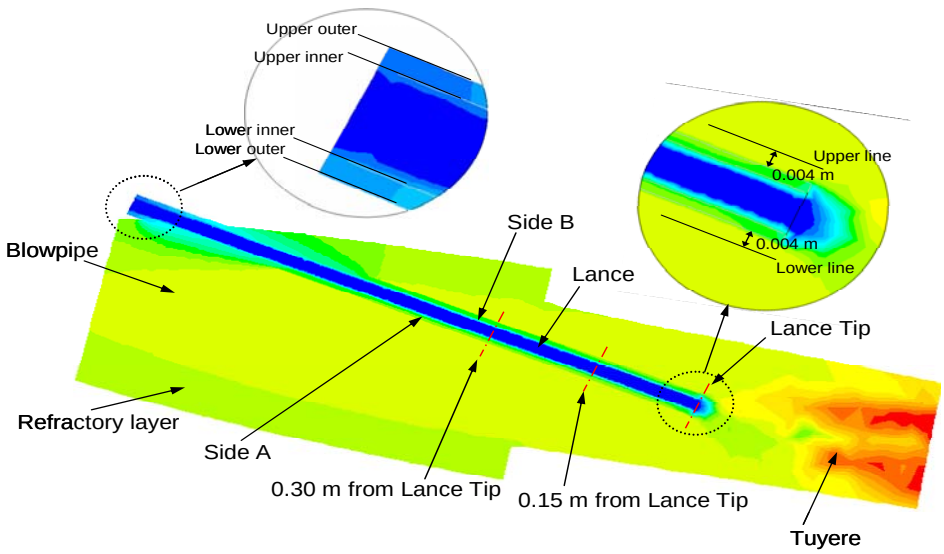

Figure 3.7 Locations for the analysis of temperature and velocity profiles

Variations of the average lance wall temperature and local lance wall temperature along the lance length are shown in Figure 3.8. Lance wall temperature increases rapidly in the section in contact with the refractory layer, and then increases slightly in the section immersing in the hot blast. The former is due to a greater temperature difference between the lance wall and the blowpipe refractory. For the lance section in direct contact with the blast, heat transfer between the lance and the blast is mainly through convection. A slow increase in the lance wall temperature is attributed to a smaller temperature difference between the lance wall and the blast.

Scrutiny of the lance wall temperature profile indicates that the lance temperature increases slightly faster near the exit of the lance. This is because the blast velocity increases somewhat at these locations since the diameter of the tuyere exit is smaller than that of the blowpipe. At the exit of the lance, a local low gas temperature is evident since the carrier gas with a low temperature mixes with the hot blast, lowering the blast temperature. At this point, the injected coal particles are in direct contact with the hot blast, causing the particle temperature increase rapidly. Thus, coal devolatilization commences followed by combustion of the evolved volatiles, resulting in a higher gas temperature near the exit of the tuyere.

Figure 3.9 shows a plan view of the gas flow field. Clearly, the gas velocity around the lance increases once the flow enters the tuyere zone; this can be seen more evidently in Figure 3.10. In this figure, the local gas velocity along an upper line and a lower line near the outer surface of the lance as shown in Figure 3.7 is illustrated. It can be seen that for both lines the

local velocity is nearly constant in the blowpipe section with a constant diameter. The gas velocity starts to increase steadily once the blast leaves the constant-diameter blowpipe section, leading to a marginally higher increase in the heat transfer to the lance.

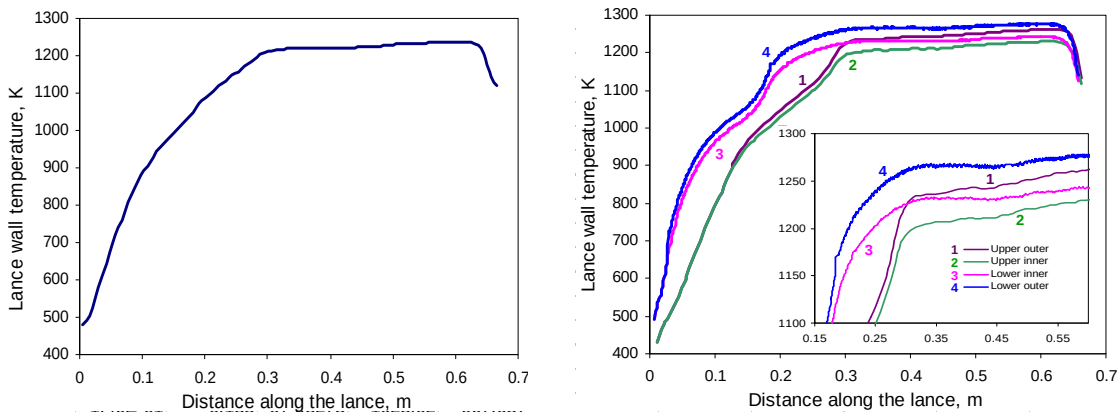

(a) Average lance wall temperature (b) Local lance wall temperature

Figure 3.8 Lance wall temperature profiles along its length

Figure 3.11(a) represents the temperature profile of the lance wall at a location of 0.15 m from the lance tip as given in Figure 3.7. In Figure 3.11, the lance wall temperature is higher near the top than that near the bottom of the figure. The top of Figure 3.11 corresponds to Side A as shown in Figure 3.7, where the blast velocity is slightly higher than that near Side B in which the effect of the blowpipe walls leads to a lower blast velocity; the corresponding gas flow distribution is also presented in the figure. A higher gas velocity near Side A results in a higher convective heat transfer between the blast and the lance wall, and hence higher lance wall temperatures.

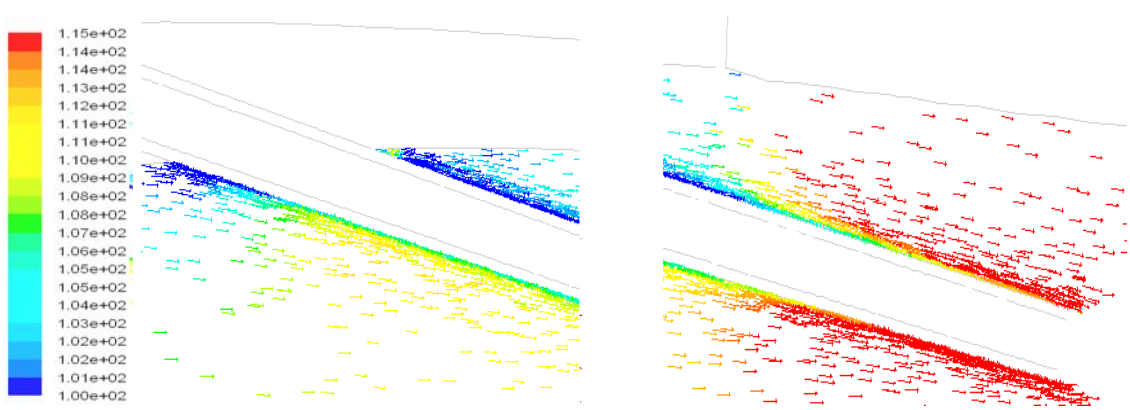

(a) Blowpipe zone (b) Tuyere zone

Figure 3.9 Velocity variations near the blowpipe and tuyere zones

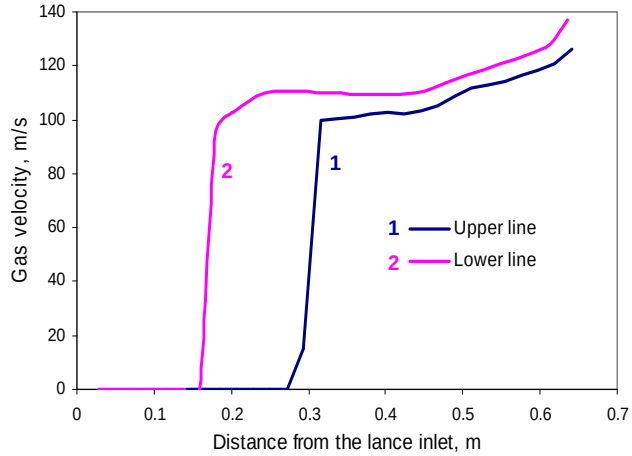

Figure 3.10 Gas velocity variations near the lance outer surface

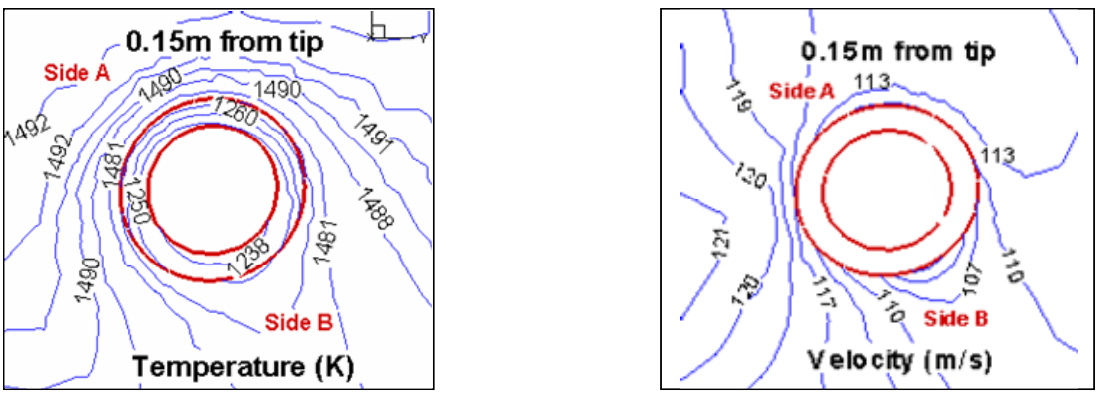

(a) Temperature field (b) Contour of gas velocity

Figure 3.11 Lance wall temperature and gas velocity distribution around the lance

The average and maximum gas temperatures inside the lance as functions of the distance from the lance inlet are elucidated in Figure 3.12. It indicates that both the average and maximum gas temperatures increase gradually inside the lance. At the lance exit, the average gas temperature is about 335 K. Also shown in the figure is the variation of the coal particle temperature. The average particle temperature is somewhat lower than the average gas temperature.

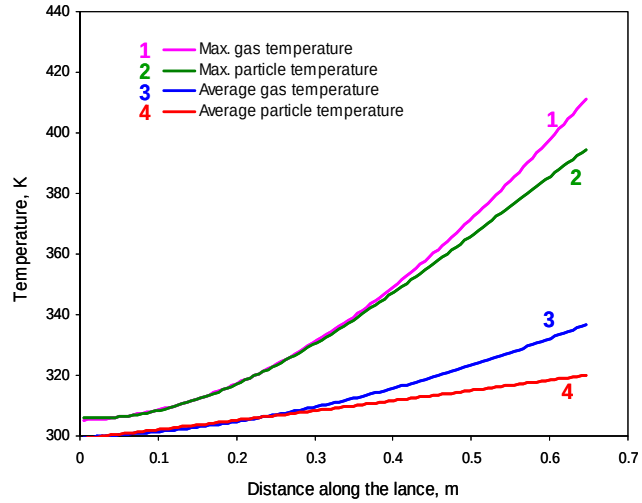

Figure 3.12 Gas and particle temperature inside the lance

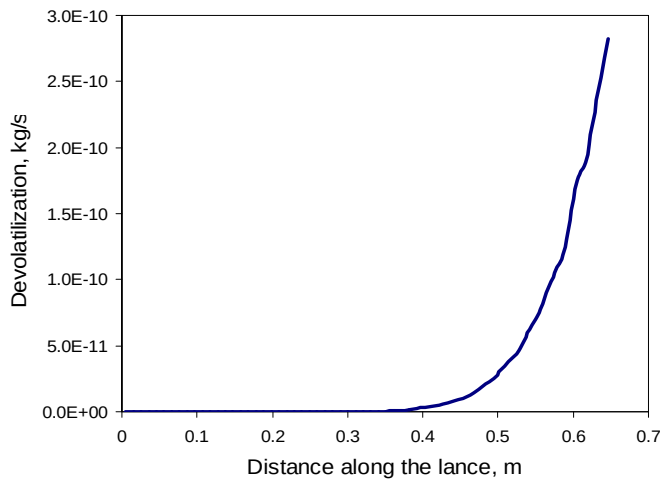

Figure 3.13 Total local coal de-volatilization inside the lance

Figure 3.13 shows total local devolatilization rate of coal particles along the lance. The coal devolatilization takes place inside the lance, because local higher temperatures obtain near the lance wall. It can be seen that the devolatilization rate increases as the particles move to the exit of the lance due to an increase in the particle temperature. For the baseline case, the total devolatilization rate inside the lance is predicted to 2.5×10^{-8} kg/s. Assume that 30% of the released volatiles form soot and deposit on the inner surface of the lance, it can be estimated that, for a lance in operation for a period of 3 months, the thickness of coal black is about 2.5 mm. However, the thickness of the deposit layer may not grow continuously because of the "washing" effect of the coal-nitrogen flow. In above calculation, it is assumed that the coal black has a density of 1000 kg/m^3 and all the soot formed deposits on the inner wall of the lance section immersing in the blast, in which coal devolatilization occurs.

Effect of Blast Temperature

Simulations using different blast temperatures are also performed to investigate the effect of blast temperature on the lance wall temperature and gas temperature inside the lance. In the simulations, the blast velocity is adjusted such that the blast mass flow rate remained the same for all the cases. The results are presented in Figure 3.14. As expected, as the blast temperature increases, both the lance wall temperature and the gas temperature inside the lance increase; thus, particle temperature also increases. For a blast temperature of 1543 K, the gas temperature at the lance exit is 338 K. Inside the lance, total coal devolatilization increases as a result of an increase in the blast temperature, as presented in Table 3.6.

The extent of coal devolatilization at the tuyere exit for blast temperatures of 1443, 1493 and 1543 K is summarized in Table 3.7, for different cases. It is clear that as the blast temperature increases the extent of coal devolatilization also increases. Due to the close proximity of the lance exit and the tuyere outlet, for all the three cases under consideration, coal devolatilization is not complete and char combustion does not start before exiting the tuyere. Gas temperature distribution in a plane across the lance centerline for the three cases is shown in Figure 3.15. It is evident that for a higher blast temperature, the size of the flame is somewhat larger with a slightly higher gas temperature and the flame is more attached.

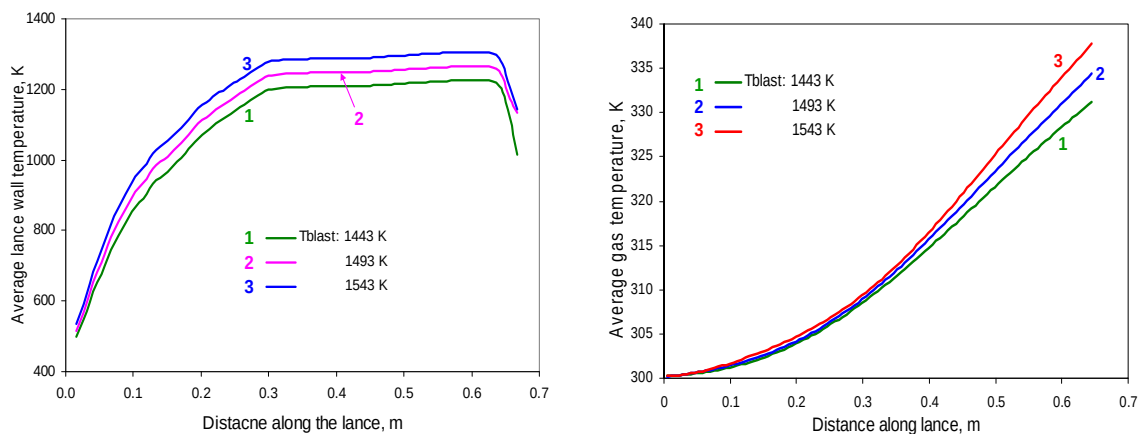

(a) Average temperature of lance wall (b) Average temperature of carrier gas

Figure 3.14 Effect of blast temperature on lance wall and gas temperatures along the lance

Table 3.6 Effect of blast temperature on total coal devolatilization inside the lance

Parameter/Case	1493K	1543K	1443K
Total devolatilization (×10-9 kg/s)	24.8	58.8	22.9

Table 3.7 Effect of blast temperature on coal devolatilization before raceway

Parameter/Case	1493K	1543K	1443K
Volatiles released (%)	57	67	48

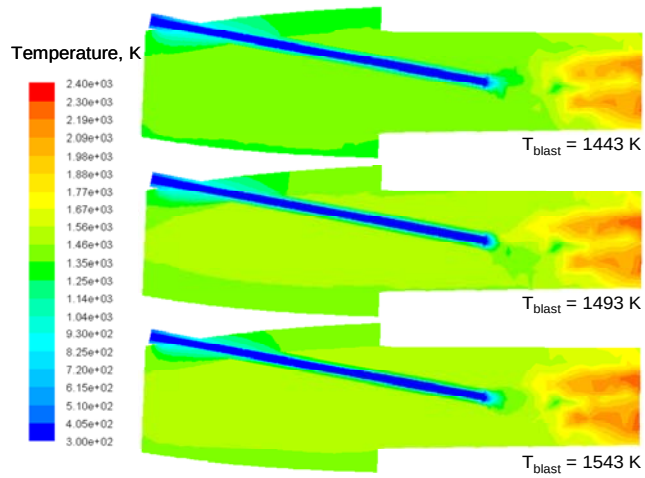

Figure 3.15 Effect of blast temperature on gas temperature distributions in a plane across the lance centerline

Effect of Blast Velocity

Simulations are performed to investigate the effect of blast velocity on the lance wall temperature, devolatilization and gas temperature inside the lance. The blast velocity selected is based on the values obtained from the above study of the effect of blast temperature. The results are presented in Figure 3.16. It is seen that as the blast velocity increases, the temperature profile remains almost the same. Same results are obtained for the coal devolatilization and the burn out rate. Thus it can be inferred that the blast temperature is the main factor that affects the devolatilization inside the lance.

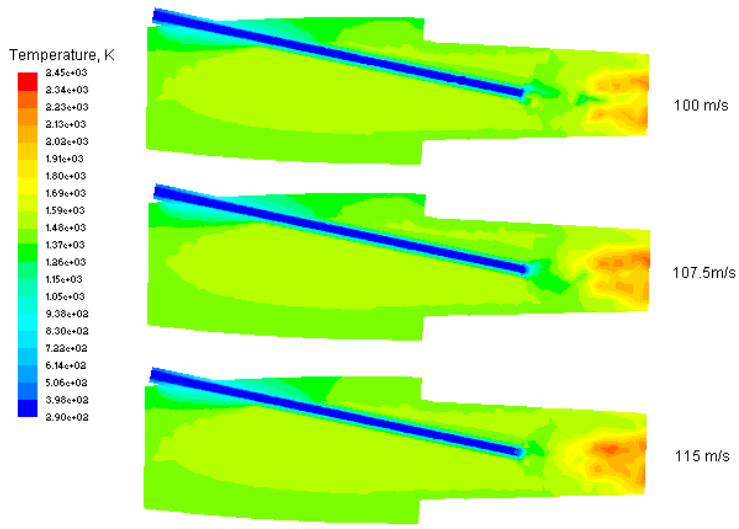

Figure 3.16 Effect of blast velocity on gas temperature distributions in a plane across the lance centerline

Effect of Coal Particle Size

Simulations were also performed to investigate the effect of coal particle diameter on the lance wall temperature and gas temperature inside the lance. In the simulations, the coal particle diameter was varied from 30 microns to 60 microns and 90 microns. The results are presented in Figure 3.17. As the particle diameter increases the specific surface area increases. Therefore, particle temperature also increases, increasing the coal devolatilization rate and the coal burnout rate.

The extent of coal devolatilization at the tuyere exit and in the lance for coal diameters of 30µm, 60µm, 90µm is summarized in Tables 3.8 and 3.9. It is clear that as the coal particle diameter decreases the extent of coal devolatilization also increases. For all three cases, the coal devolatilization is not complete and the char combustion does not start before exiting the tuyere, because of the close proximity of the lance exit and the tuyere outlet. Gas temperature distribution in a plane across the lance centerline for the three cases is shown in Figure 3.17. It is evident that for a higher coal diameter, the flame is more attached to the lance because coal particle's momentum is less for the larger size particle.

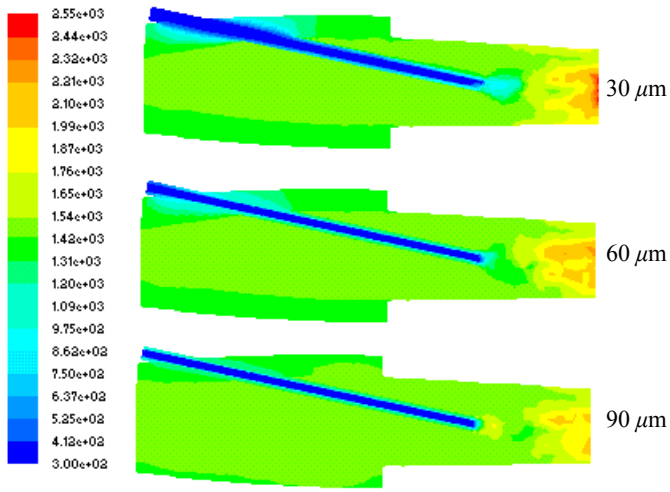

Figure 3.17 Effect of coal size on gas temperature distributions across the lance centerline

Table 3.8 Effect of coal size on coal devolatilization before raceway

Parameter/Case	30 μm case	60 μm case	90 μm case
Volatiles released (%)	59	57	53

Table 3.9 Effect of coal size on total coal devolatilization inside the lance

Parameter/Case	30 μm case	60 μm case	90 μm case
Total devolatilization (×10-9 kg/s)	26.1	24.8	23.7

Effect of PCI Rate

Parametric studies are also conducted for different pulverized coal injection rates. The carrier nitrogen flow rate is varied such that the ratio of the coal to nitrogen mass flow rates was constant, like as the concentration of coal-nitrogen flow is fixed while the PCI rate changed. The lance wall temperature and gas average temperature along the lance are shown in Figure 3.18 and 3.19. Since more energy is required to heat up the particles, as the coal injection rate increases, both the lance wall temperature and the gas average temperature decrease. The coal devolatilization decreases as the injection rate increases due to a decrease in the temperature of coal particles, as shown in Table 3.10. The extent of coal devolatilization before exiting the tuyere for coal injection rates of 0.375 kg/s and 0.625 kg/s is given in Table 3.11, in comparison with the baseline case. Clearly, as the coal injection rate increases, the extent of coal devolatilization decreases since particle temperature inside the lance decreases. For a coal injection rate of 0.375 kg/s, char combustion takes place and char burnout is about 1.7% in the tuyere. The PCI rate also has a considerable effect on the gas temperature profile as shown in Figure 3.20. For a lower injection rate, the flame temperature is substantially higher.

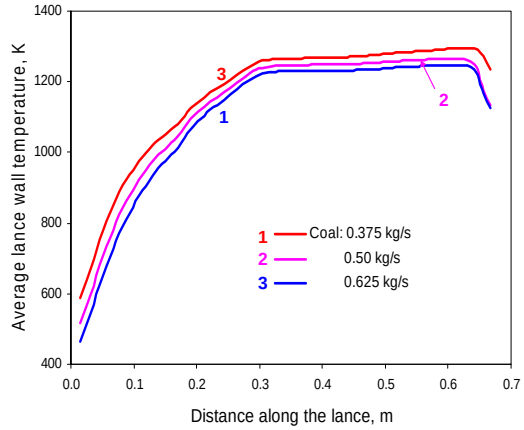

Figure 3.18 Effect of PCI rate on average temperature of the lance wall

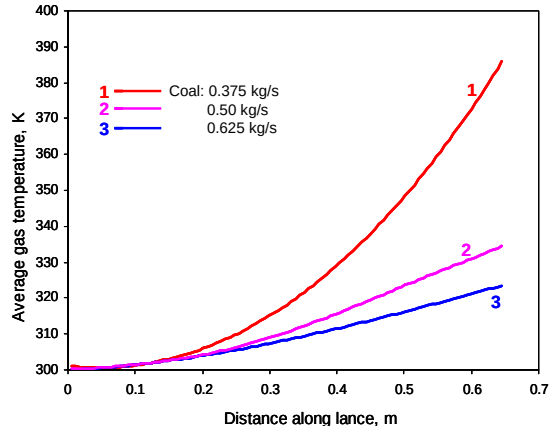

Figure 3.19 Effect of PCI rate on average temperature of the carrier gas

Table 3.10 Effect of coal size on total coal devolatilization inside the lance

	0.375 kg/s case	0.5 kg/s case	0.62 kg/s case
Total devolatilization (×10-9 kg/s)	4421.3	24.8	6.6

Table 3.11 Effect of coal size on coal devolatilization before exiting the tuyere

	0.375 kg/s case	0.5 kg/s case	0.62 kg/s case
Volatiles released (%)	88	57	45

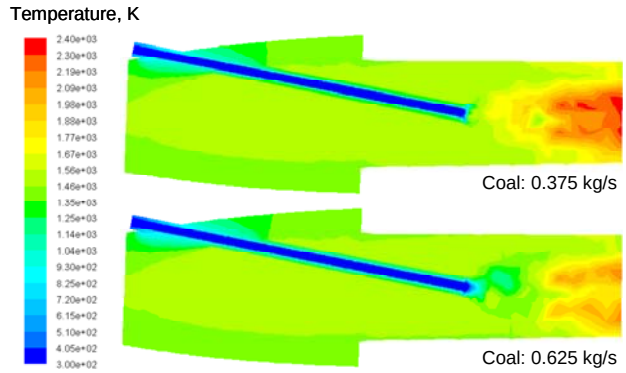

Figure 3.20 Effect of coal size on gas temperature distribution in a plane across the lance centerline

Summary

Based on the simulation results, it has been concluded that coal devolatilization inside the lance is the cause of the layer of black material formed on the inner surface. For an operation period of three months, it has been predicted that the thickness of the deposit layer on the inner surface of the lance will be a few millimeters. The effects of operating conditions on the heat transfer and coal devolatilization have indicated that both the pulverized coal injection rate and the blast temperature have a significant effect on the heat transfer and coal devolatilization. To increase the blast temperature or decrease the coal injection rate will raise the lance wall temperature and the gas temperature inside the lance, hence an increase in coal devolatilization inside the lance and in the tuyere. The simulations have provided useful results to the industrial participants.

3.2.2 Investigation of Raceway Formation Kinetics

The blast furnace raceway shape, size and position are important factors affecting gas distribution inside the furnace, consequently, affecting the operation stability and efficiency [59,60]. The blast furnace raceway shape, size and position are determined by the kinetic force of the blast from tuyeres, as well as the combustion process inside the raceway. In order to have a better understanding of the raceway formation, a number of simulations have been made to investigate the raceway formation kinetics and its parametric effects. The parameters investigated include coke bed porosity, coke particle size, deadman permeability, tuyere velocity, and tuyere geometry on the raceway formation. The simulation conditions are provided by industrial partners.

The computational domain consists of three tuyeres located 9° apart, with an inlet tuyere diameter of 0.15m. The tuyere length is 0.437m and is at an angle of 6 degrees downward. The coke bed in the hearth at the tuyere level is assumed basically as cone shape with a dead-man at its center. The detailed size, diameter and height of coke cone are dependent on the furnace inner profile and the cohesive zone shape and location. The coke bed is divided into two zones; a

denser zone 1m below the tuyere level, and a zone above the tuyere zone, which is not so dense. Figure 3.21 shows the geometry used for the simulation. The tuyere velocity for the baseline case is 184 m/s. The parameters for the baseline case are given in Table 3.12. These parameters are collected from an actual operation conditions.

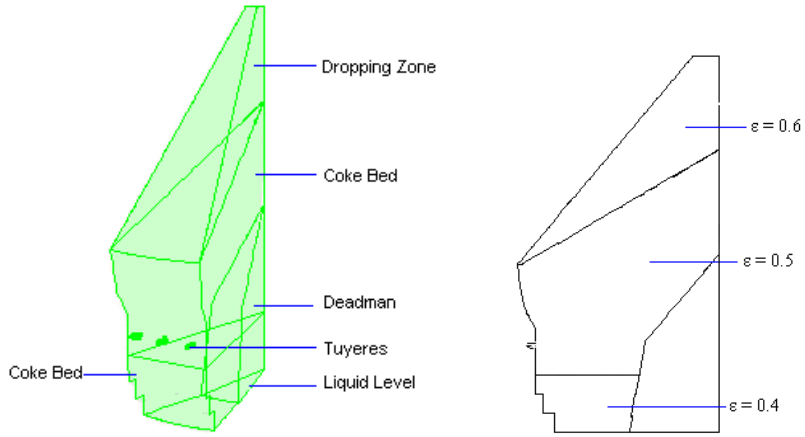

(a) Geometry (b) Porosity

Figure 3.21 Geometry used for raceway formation simulations

Table 3.12 Basic simulation conditions

Porosity	0.5/0.6/0.4
Coke Diameter	0.03m
Tuyere Velocity And Pressure	184m/s, 5 atm
Tuyere Diameter At Tuyere Exit	0.15m
Tuyere Diameter At Tuyere Inlet	0.1778m
Tuyere Length Inside Furnace	89 mm
Dead-Man Porosity	0.0
Coke Bed	Treated as Fluidized Bed

Table 3.13 Parametric study conditions

Tuyere Velocity	239 m/s, 129 m/s
Tuyere Diameter	+1”, -1”
Tuyere Length Inside Furnace	1.5”, 9.5”
Dead-Man Porosity	20%

Baseline Case

The boundary of the raceway that separates from the coke bed is defined as the iso-line of constant initial coke volume fraction. The term of porosity, ε, is defined as the volume fraction of the gas phase with respect to the total volume of gas and solid phases, αp, i.e. $\varepsilon = 1 - \alpha_p$. Figure 3.22 shows the porosity distributions of the side and top views. The raceway dimensions for the baseline case are listed in Figure 3.23. The velocity distribution inside the raceway is an important factor that decides the combustion behavior of the coke and other replacement fuels like pulverized coal or natural gas. It is observed as in Figure 3.24(a) that the flow is predominantly moving upward as expected. Also observed are stagnation zones at the top and bottom of the raceway near the wall of the furnace. The streamlines of flow are shown in Figure 3.24(b).

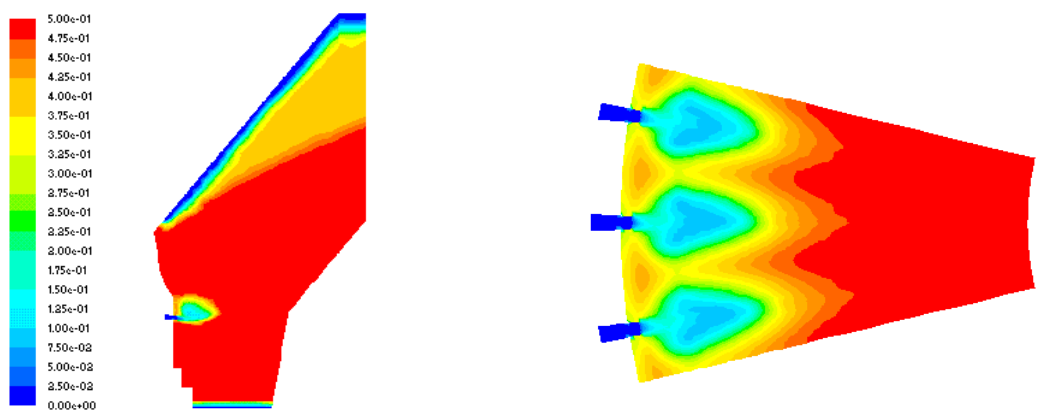

(a) Side view (b) Top view

Figure 3.22 Coke volume fraction

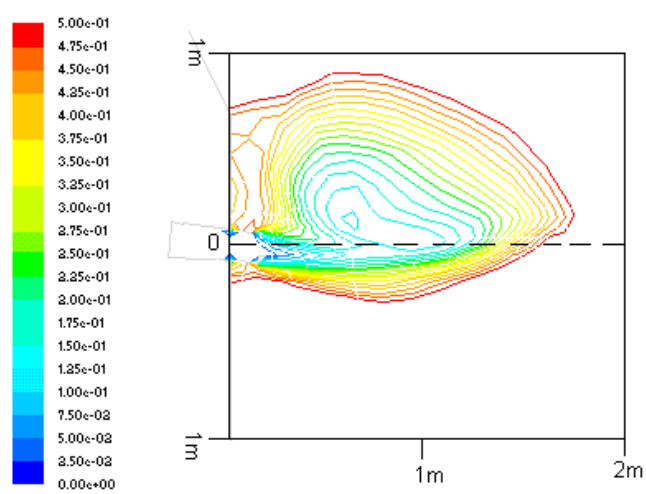

Figure 3.23 Raceway shape defined by the initial porosity of 0.5

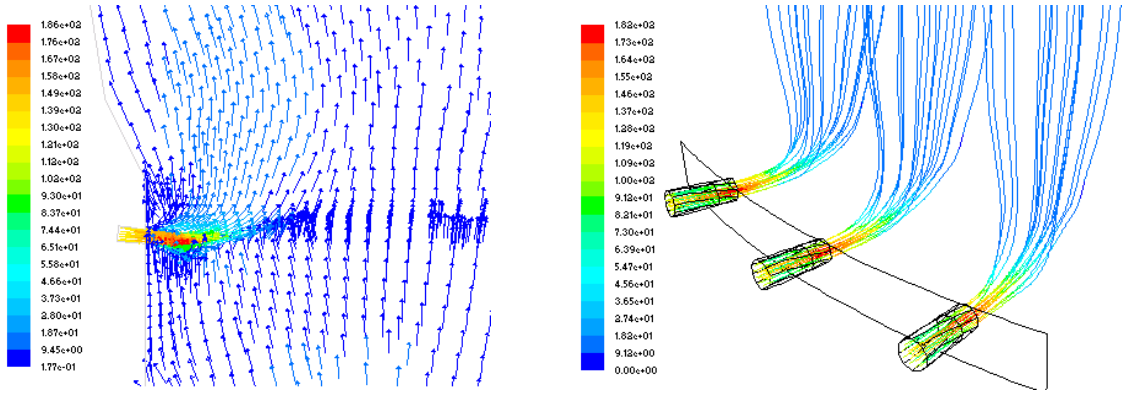

(a) Velocity vectors (b) Streamlines of the gas phase

Figure 3.24 Gas vector field and stream lines near the tuyere

Effect of Coke Bed Porosity Distributions

The coke bed porosity distribution may be affected by burden distributions and other operating conditions. This in return will affect the raceway formation as well as combustion. Studies have been made to investigate the effect of the coke bed porosity distribution. Different coke bed porosity distributions have been considered. These include uniform distribution (Figure 3.25), two-zone distribution as the base case (Figure 3.26), and four-zone distribution (Figure 3.27)

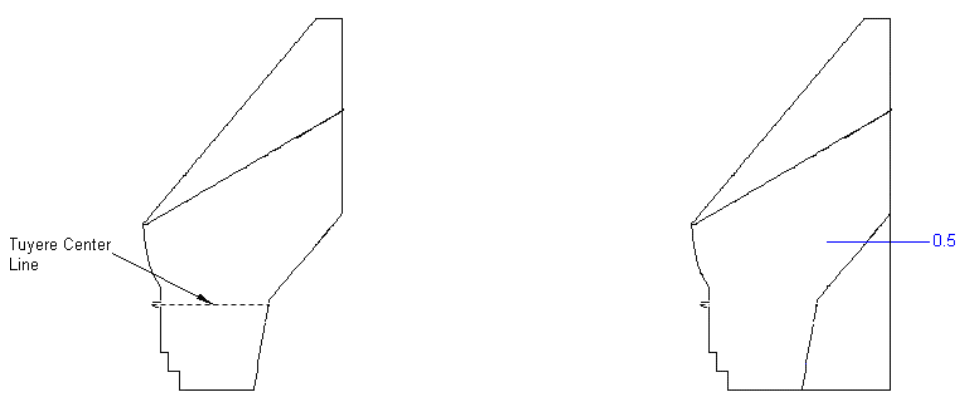

(a) Sub-zones (b) Porosity distribution

Figure 3.25 Uniform coke bed distributions on raceway formation

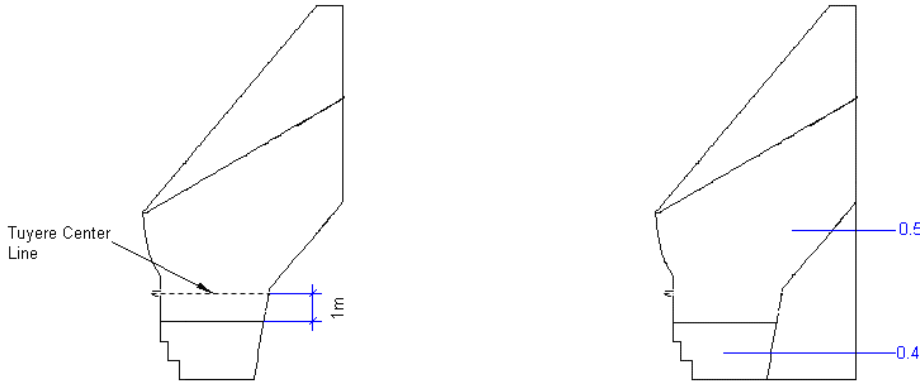

(a) Sub-zones (b) Porosity distribution

Figure 3.26 Two-zone distributions on raceway formation

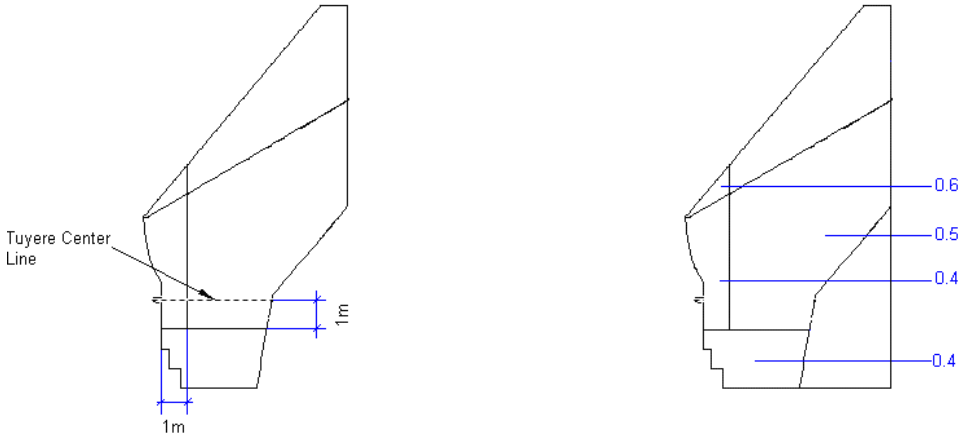

(a) Sub-zones (b) Porosity distribution

Figure 3.27 Four-zone distributions on raceway formation

As shown in Figure 3.28, when the coke bed porosity is uniform, the raceway shape tends to be predominantly downward. The raceway moves up when the coke bed porosity is denser at lower coke bed zone. In the four-zone case, it can be seen that the height of the raceway is decreased. This is because the coke bed near the tuyere zone is denser due to the effects of the weight of the descending burden particles.

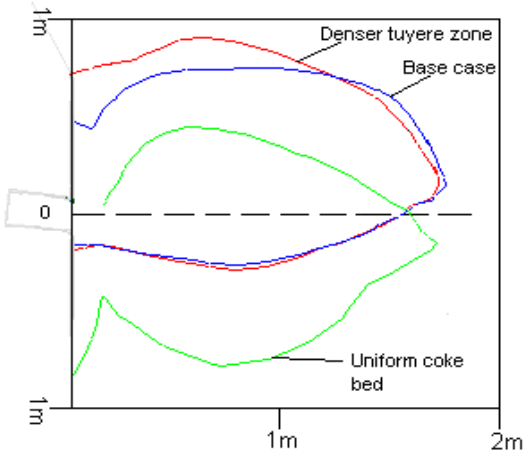

Figure 3.28 Effect of coke bed porosity distribution on raceway formation

Effect of Coke Particle Diameter

The effect of coke particle size is shown in Figure 3.29. The coke particle size is changed from 0.03m for the baseline case to 0.02m and 0.04m. The results in Figure 3.29 shows that the raceway size increases as the coke size decreases, because smaller particles have larger specific surface area and gains stronger drag force from the gas flow with respect to their mass/weight. This is in agreement with various experimental observations and correlations obtained using dimensional analysis by Rajneesh et al [25], where it is observed that the raceway shape is inversely proportional to the coke particle diameter.

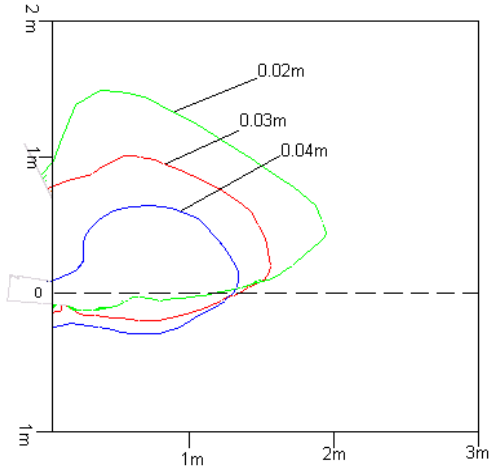

Figure 3.29 Effect of coke diameter on raceway formation

Effect of Deadman Permeability

The effect of the deadman porosity is shown in Figure 3.30. As the deadman porosity is increased to 20%, the raceway size increases due to less difficulty for particle to move. The deadman with increased porosity also offers less resistance for the gases, making the raceway deeper.

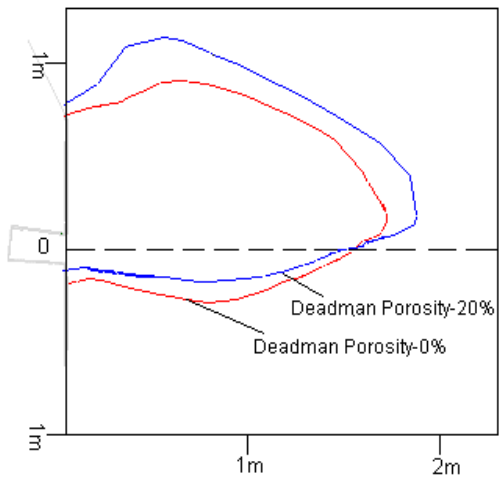

Figure 3.30 Effect of dead-man porosity on raceway formation

Effect of Tuyere Velocity

The effect of the tuyere velocity is shown in Figures 3.31-3.32. The raceway size increases as the tuyere velocity rises. An increase in the tuyere velocity increases the momentum of the gas phase, which in turn causes a larger momentum exchange with the solid particles, moving them further away from the tuyere towards the center of the furnace. The same effect is seen in Figure 3.32, in the top view comparison between the different velocities at the center of the tuyere for different velocities. The raceway is larger for a higher tuyere velocity. It is also observed that the interaction between the different raceways increases with the increase of the tuyere velocity. These results agree with the observation of the blast furnace operators.

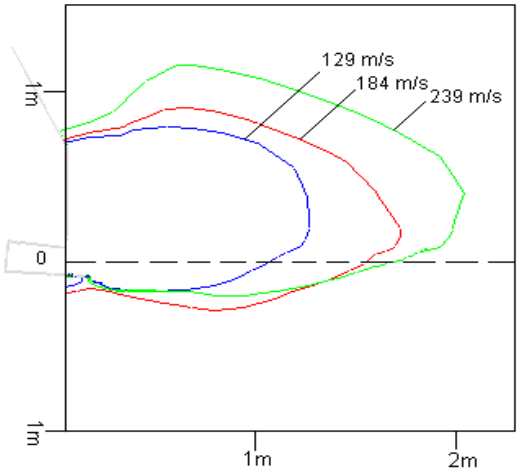

Figure 3.31 Effect of tuyere velocity on raceway formation

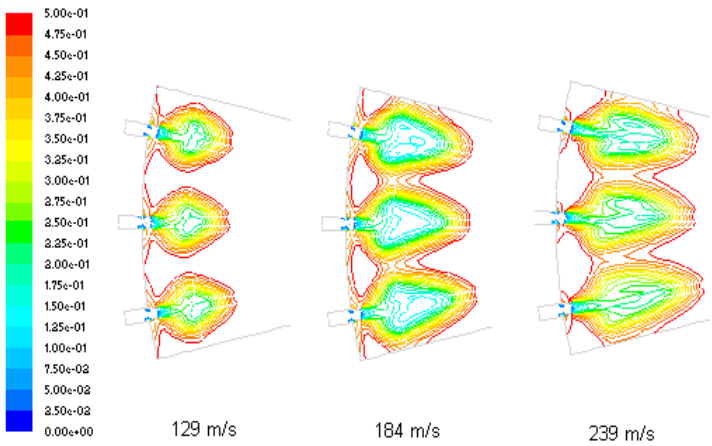

Figure 3.32 Effect of tuyere velocity on raceway formation – top view

Effect of Tuyere Diameter and Length

The effect of the tuyere diameter and the length extended over the lining are studied. The tuyere diameter is increased and decreased by 25.4 mm (1”) for a fixed wind rate. At a fixed tuyere velocity, the raceway size increases with the increase in tuyere diameter due to additional momentum of the gas phase, as additional mass is added to the system. This is seen in Figure 3.33(a). The tuyere length inside the furnace is increased by 6” and decreased by 2”. When the tuyere penetration length is increased, the raceway is moved closer to the center of the furnace and away from the wall as one might expect. This is seen in Figure 3.33(b). The position of the raceway affects the design of the bosh cooling system. Thus, if the raceway is positioned deeper, the load on the bosh cooling system reduces.

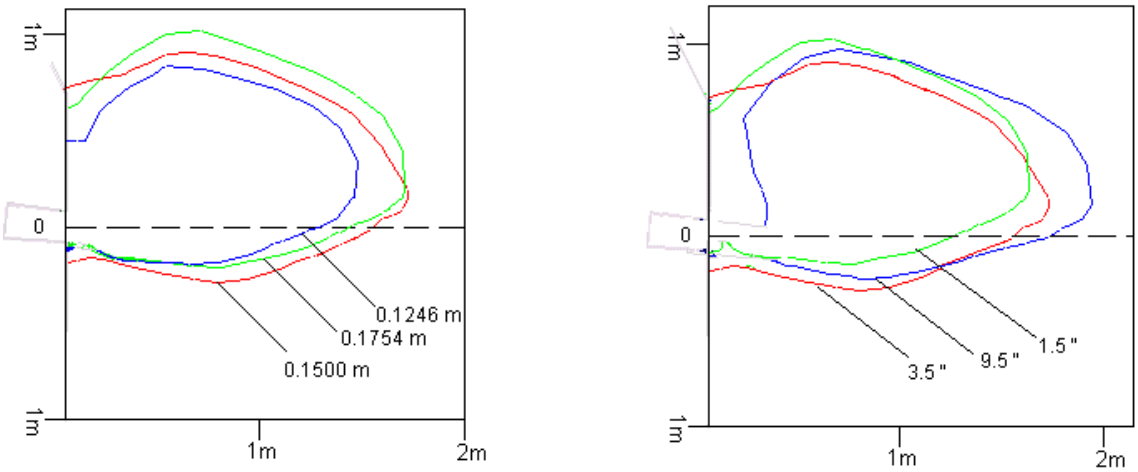

(a) Tuyere Diameter (b) Tuyere Length inside the furnace

Figure 3.33 Effect of tuyere diameter and length extended over lining

Summary

The simulations have provided detailed raceway formation kinetics and parametric effects. The raceway location, shape and size are affected by coke bed porosity distributions, coke particle diameter, deadman permeability, tuyere velocity, and tuyere diameter and length. A large raceway size will provide more residence time for coal combustion. This may be achieved by decreasing the coke particle diameter and increasing the deadman porosity as well as the tuyere momentum.

3.2.3 Investigation of Coal and Coke Combustion inside Raceway

Investigations of coal and coke combustion inside the raceway have been made based on an actual blast furnace from one of the industrial participants. The computational domain includes a tuyere, a raceway and the coke bed around the raceway as shown in Figure 3.34(a). The tuyere exit is titled downward with an angle of 7°, and its inner diameter is 0.165 m. The length inside the raceway is 0.35m. During the simulation, a slice of 10.58°of the lower part of the blast furnace is considered, since there are totally 34 tuyeres for the practical project, with the radius being 6.5m. The deadman structure is also taken into account. The pulverized coal is injected into the tuyere through a lance with an angle of 24° upward and then to the right of the tuyere with an angle of 30°. The lance has an inner diameter of 0.0254 m. The computation domain starts from the tip of lance, the carrier gas (N_2) mass flow rate and the coal particle velocity at the exit of lance is as they are in the real injection conditions. Major operating parameters can be found in Table 3.14.

The objectives of this study are to understand the coal and coke combustion behavior as well as parametric effects. The parameters investigated include coal type, PCI rate (PCR) and oxygen enrichment. As shown in Table 3.15 and 3.16, simulations have been conducted for five cases.

Table 3.14 Basic conditions for raceway combustion simulations

Lance diameter, m	0.0254
Tuyere diameter, m	0.1650
Tuyere length inside the coke bed, m	0.3500
Blast temperature, K	1414.0
Blast pressure , Pa	447451
Wind rate, kg/s	4.3500
Mass fraction of O_2	0.3039
Mass fraction of Moisture	0.0245
Mass fraction of N_2	0.6716

Table 3.15 Coal properties for raceway combustion simulations

Coal Type	Coal_A	Coal_B
Proximate Analysis (wt. %)		
Fixed Carbon	56.9	75.1
Ash	6.5	6.7
Volatile Matter	36.6	18.2
Ultimate Analysis (wt. %)		
C	79.8	84.7
H	5.3	3.9
N	1.5	1.0
O	6.1	2.9
S	0.9	0.8
Ash	6.4	6.7

Table 3.16 Parametric study cases for raceway combustion

Case Number	Coal Type	PCR (lb/tHM)	O_2 (v %)	Note
1	A	250	27.26	Baseline
2	-	0	27.26	All Coke
3	B	250	27.26	Coal Type
4	A	450	27.26	PCR
5	A	250	23.55	O_2 Enrichment

Baseline Case

In order to fully understand the combustion mechanism, a baseline case was established based on a typical industrial operating condition (Case 1). Detailed information concerning the

multiphase flow characteristics and chemical kinetics were analyzed. Figure 3.34 shown the raceway predicted using the CFD model and the methodology discussed in Section 2.

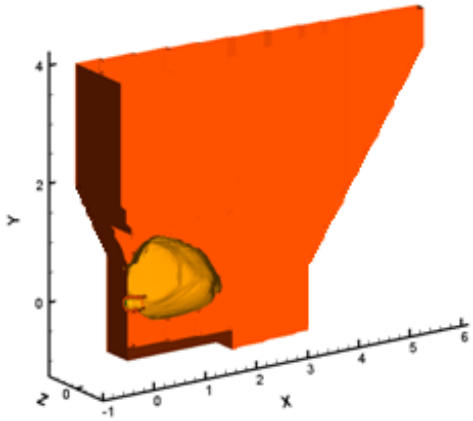

(a) 3D scheme

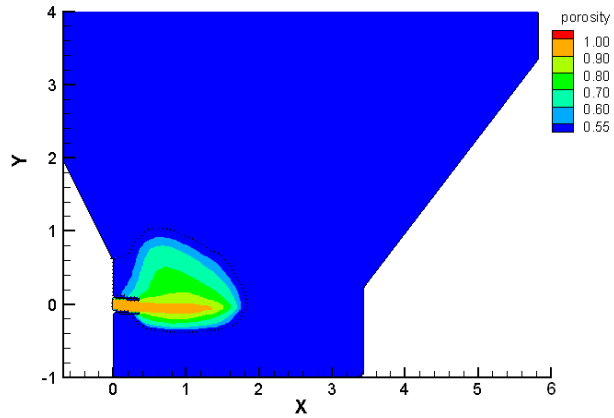

(b) Side view of porosity distribution

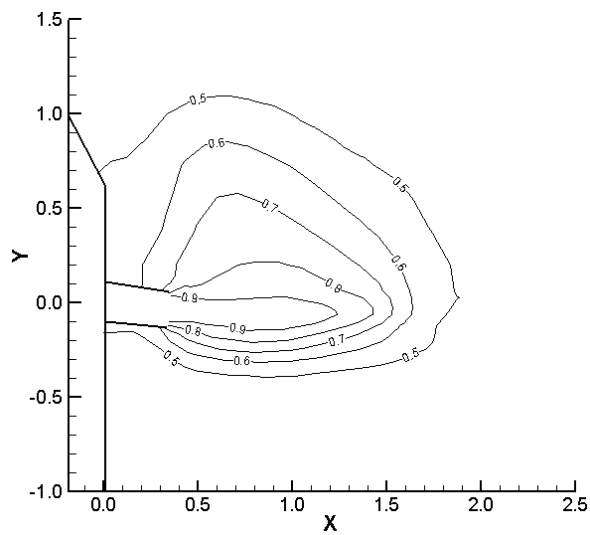

(c) Porosity iso-line

Figure 3.34 Raceway formation

Gas and coal particle flow patterns play important roles for coal and coke combustion inside a raceway. Figure 3.35 display the vector field and streamlines of both gas and coal particle flows. As shown in Figures 3.35(a) and (b), the gas proceeds horizontally as a jet on the tuyere axis owing to the jet inertia. An upward component then appears along the raceway boundary because of the increased flow resistance at the point where the gas impinges on the boundary. After passing through the raceway boundary, the gas flow tends to return to that in the packed column. Meanwhile, there is an obvious recirculation flow of the gas phase in the

corner underneath the tuyere. Figures 3.35(c) and (d) indicate that the motion of the pulverized coal particles have very similar flow patterns as the gas phase.

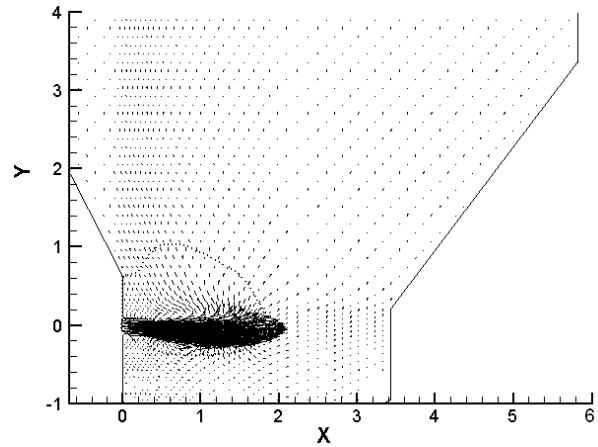

(a) Gas velocity vector field

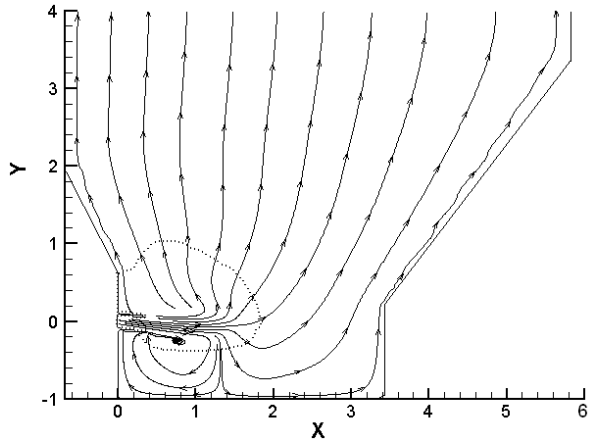

(b) Gas streamline profile

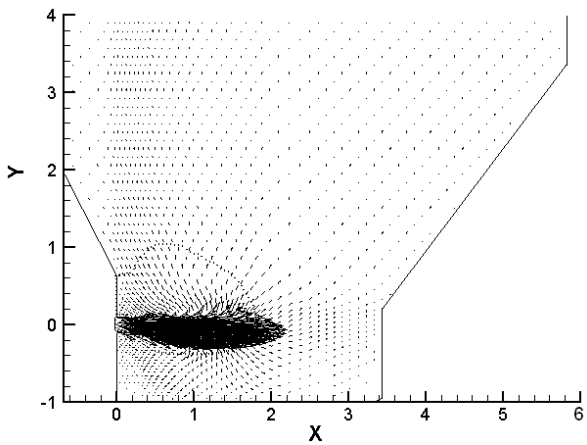

(c) Coal particle velocity vector field

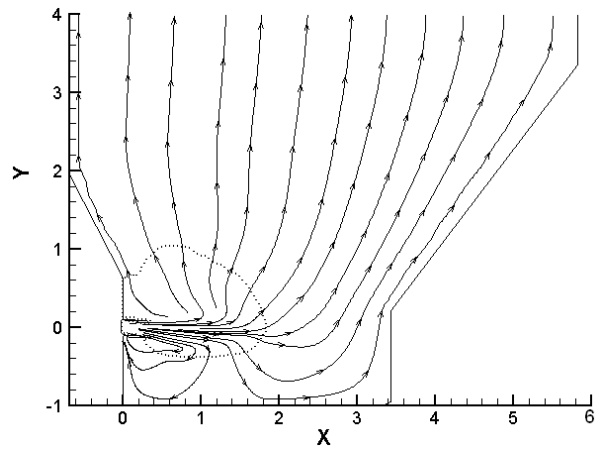

(d) Coal particle streamline

Figure 3.35 Gas and coal particle flow patterns

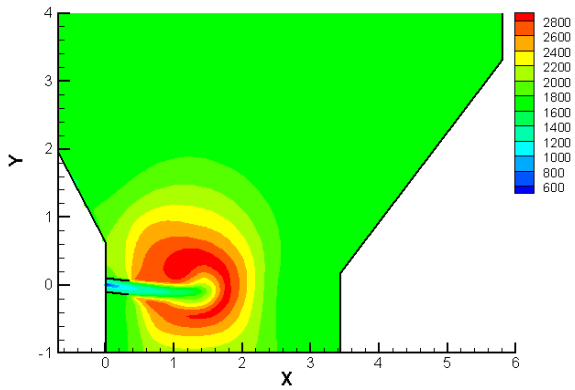

(a) Gas temperature (K)

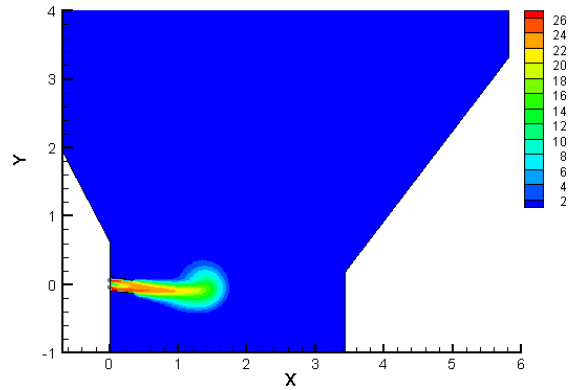

(b) O_2 concentration (v %)

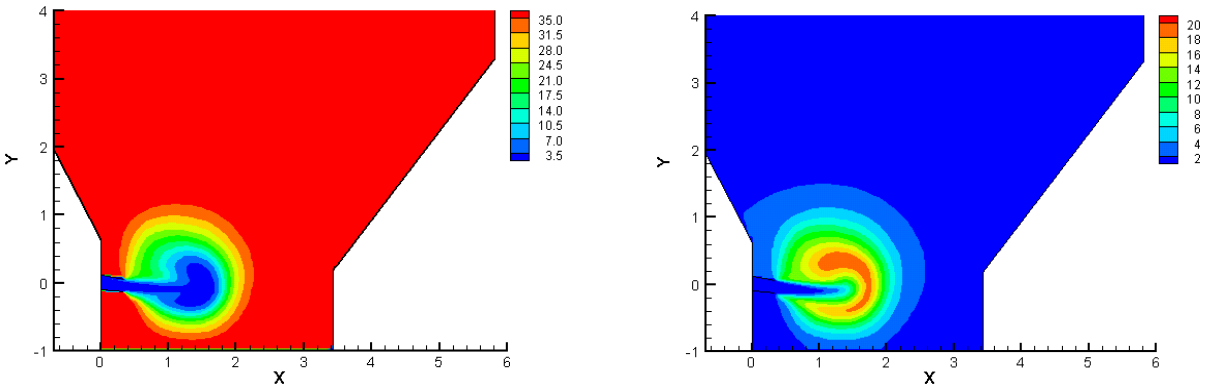

(c) CO concentration (v %) (d) CO_2 concentration (v %)

Figure 3.36 Temperature and gas species distributions

Figure 3.36(a) demonstrates the temperature distributions at a 2-D view through the center of a tuyere. When pulverized coal is injected into a lance, its temperature is low. The coal particle temperature increases rapidly due to the heat transferred from the hot blast [61,62]. The coal particles devolatilize rapidly when they move toward the exit of tuyere. The released volatile matter combusts when the volatile matter mixes well with the oxygen around the coal injected plume surface. The temperature is higher in correspondence to the combustion zone. It is also observed that the combustion process happens at the lower end of the raceway, where the oxygen from the blast air comes in contact with the coke bed. The maximum temperature is established in this space owing to successive exothermic and endothermic reactions. This vital space is known as the 'combustion focus'. The Figure 3.36(b) illustrates that oxygen concentration is relatively lean in the coal plume region. As the combustion goes on, oxygen is consumed rapidly. Additionally, the N_2 and the released volatile matter will dilute the oxygen concentration.

The carbon monoxide distribution behavior is given Figure 3.36(c). Beginning around the edge of the O_2 field, the carbon monoxide concentration is low in the high temperature zone (where combustion is predominant), and increases notably outward. Farther from the raceway, a higher concentration of carbon monoxide can be found. The outer space from the raceway is oxygen free, because of the combustion. Such reduction in the atmosphere facilitates the gasification of the coke media, i.e., the reaction of the carbon dioxide with the coke, resulting in an increasing CO fraction. Such a reaction is endothermic, which is the reason why there is a peak temperature zone in Figure 3.36 (a). The carbon dioxide distribution is shown in Figure 3.36(d). The maximum carbon dioxide concentration corresponds to the zone of maximum reaction and maximum temperature, showing that the maximum temperature corresponds to carbon dioxide production.

Many efforts have been exerted to investigate the PCI combustion. However, most of them focused on the tuyere part and few discussions provided detailed information about the pulverized coal after it has been injected into coke bed. Figure 3.37 exhibits coal and coke flow

property distributions. Figures 3.37(a) and (b) indicate the pulverized coal concentration in terms of number density and bulk density, respectively. The number density refers to the amount of the pulverized particle in unit volumetric coke bed, n/m^3; bulk density, the mass weight of the pulverized particle in unit volumetric coke bed, kg/m^3. After the pulverized coal is injected into the furnace, it penetrates through the raceway zone, under the effect of inertia momentum. It also diffuses in a vertical direction, appearing to be a torch. It appears that because of the appreciable flow resistance most of pulverized coal is trapped inside the raceway, which is favored for complete coal combustion [63].

Figures 3.37(c) to (e) demonstrate chemical kinetics characteristics of the injected coal particles. Obviously, when the particles move toward the exit of tuyere, rapid coal devolatilization occurs [18]. The released volatile matter combustion appears when the volatile matter mixes well with the oxygen around the coal injected plume surface. It is also observed that the coke combustion process happens at the lower end of the raceway, where the oxygen from the blast air comes in contact with the coke bed, see Figure 3.37(f).

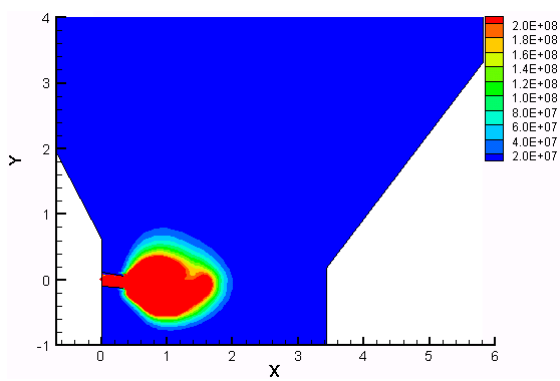

(a) Coal particle number density (n/m^3)

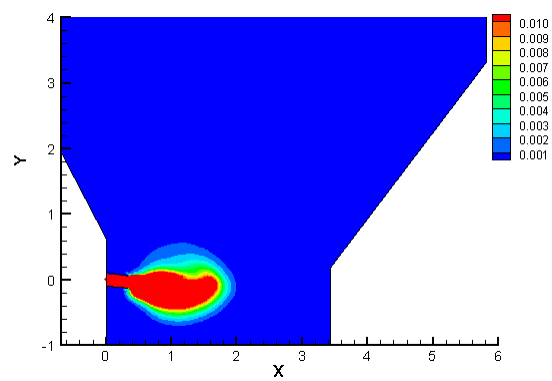

(b) Coal bulk density (kg/m^3)

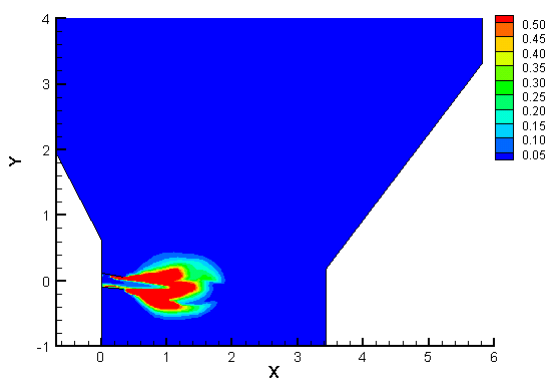

(c) Coal mass loss rate (kg/s)

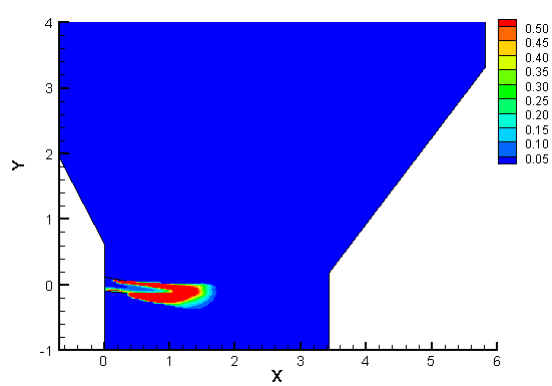

(d) Volatile release rate (kg/s)

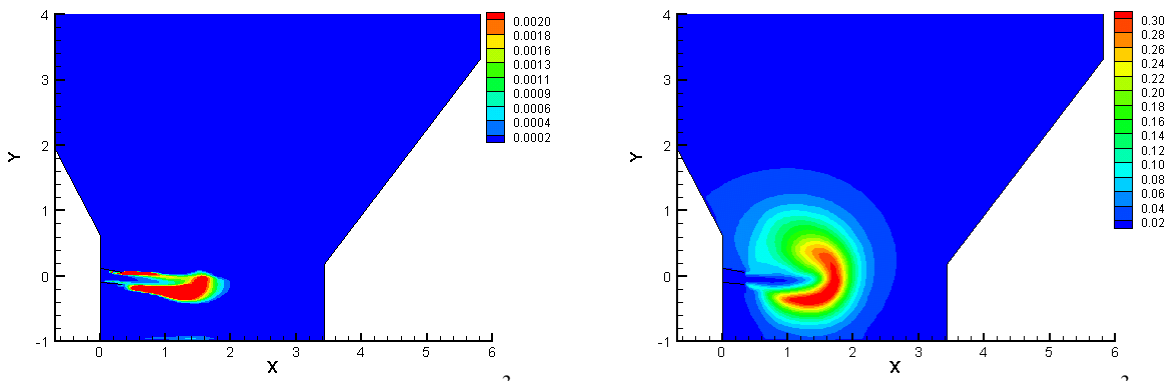

(e) Unburned char bulk density (kg/m^3) (f) Coke consumption rate (kg/m^{3}s)

Figure 3.37 Coal and coke flow property distributions

Comparisons of All-Coke Case and PCI Case

Coke plays a vital role as a heat supply and reductant source. Moreover, being the only material which does not undergo phase transformation in the blast furnace, coke helps to keep the layer structure of the burden distribution. In the early stages, coke was the only fuel feed into the blast furnace. PCI was introduced only in recent years. In order to provide better understandings, comparisons have made between two cases with and without PCI as shown in Figure 3.38.

Temperature and O_2 concentration distributions are displayed in Figures 3.38 (a), (b), (c) and (d) for cases without and with PCI respectively. These figures demonstrate that when pulverized coal is injected into the raceway, more oxygen is consumed and a higher temperature rise appears at the region closest to tuyere tip in the raceway and a lower temperature is represented in the coke bed than those of all coke operation. The residence time of PC particles in the blowpipe is quite short, so the burn-off in the blowpipe is very low and the PC particles mainly burn in the raceway cavity. Clearly, there is a remarkable change in the oxygen distribution between these two cases. In the case of all coke operation, oxygen fills most of the nose of the raceway area, indicating that O_2 is gradually consumed by the coke. While in the case of PCI operation, oxygen from the tuyere is rapidly consumed, appearing to be much narrower than that in the case of all coke operation. Due to the pulverized coal injection along with hot blast into the blast furnace, combustion occurs much earlier inside the raceway, resulting in rapid consumption of O_2. The different distribution is also caused by different reaction mechanisms of the coke and the pulverized coal. For the pulverized coal, the diameter is at the micron level, or 10^{-6} m. The size of the granular coke, being porous material - 10^{-2} m, is thousands of times larger than the pulverized coal. This indicates that granular coke has a much smaller specific area than that of coal, or much less chemical contact interface with the gas phase. In addition, due to the much larger size, the gas diffusion through the porous coke also reduces the oxygen consumption rate.

Consequently, as shown in Figures 3.38 (e) and (f), because of the lower reaction rate, residence time of oxygen is prolonged, and the coke combustion happens in a wider zone. In the case of all coke operation, this results in a larger "combustion focus", or a larger CO_2-

concentrated flame. Furthermore, the shape of the CO_2 distribution is more regular than seen with the PCI case. It is considered that, since the gas diffusion process is somewhat a controlling factor, gas-coke reaction takes place evenly as the gas phase penetrates through the coke bed. Therefore, the species distributions are quite regular. As for the PCI case, it is clear that the combustion occurs much earlier than it does with the all coke case. Correspondingly, due to the delay of the coke combustion, the carbon oxide formation takes place in a farther zone in the all coke case (Figure 3.38(g).) than in the PCI case (Figure 3.38(h)). Figures 3.38 (i) and (j) demonstrate that for the PCI case, some part of the coke has been replaced by the injected pulverized coal.

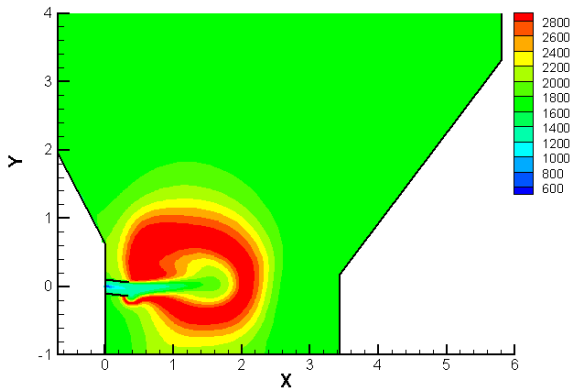

(a) Gas temperature in all coke (K)

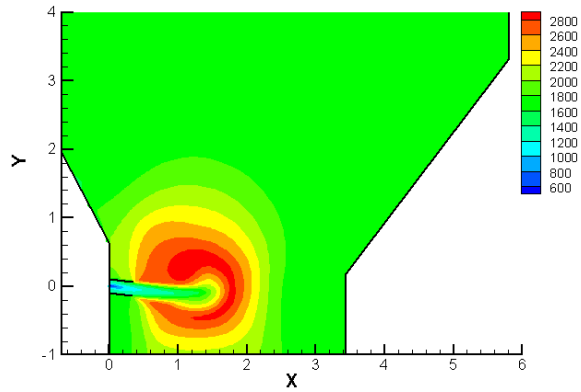

(b) Gas temperature in PCI (K)

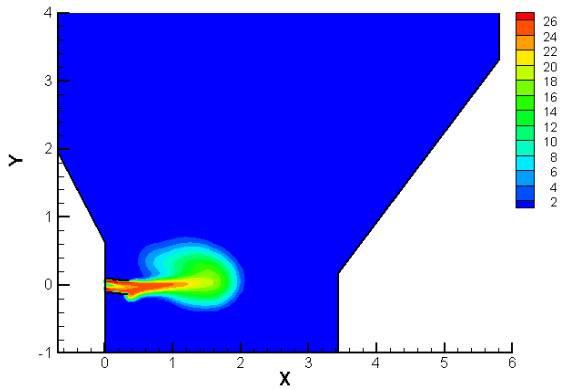

(c) O_2 concentration in all coke

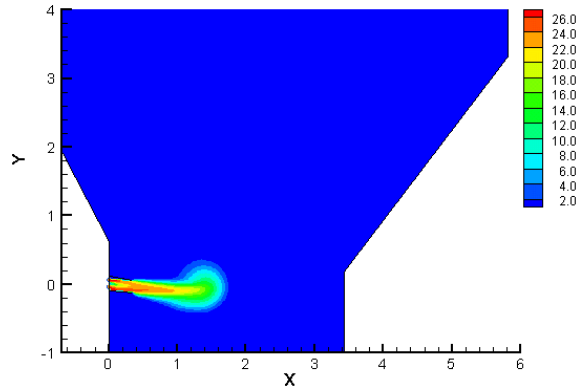

(d) O_2 concentration in PCI

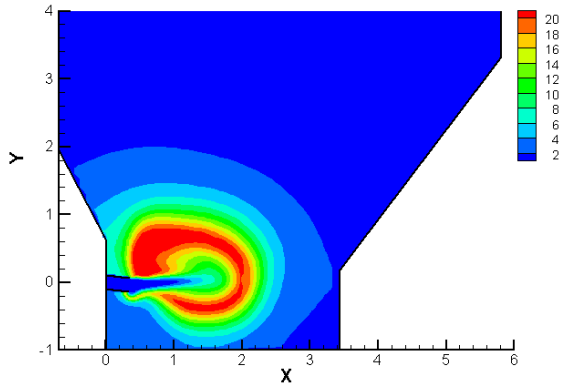

(e) CO_2 concentration in all coke

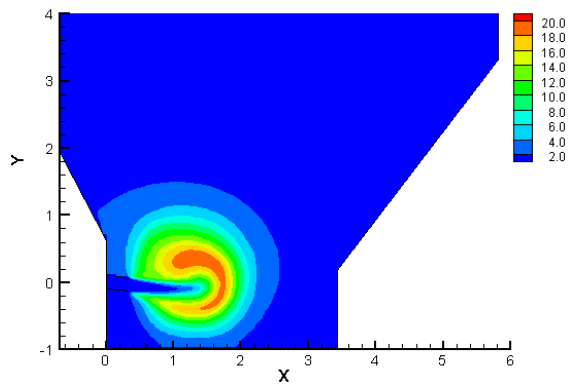

(f) CO_2 concentration in PCI

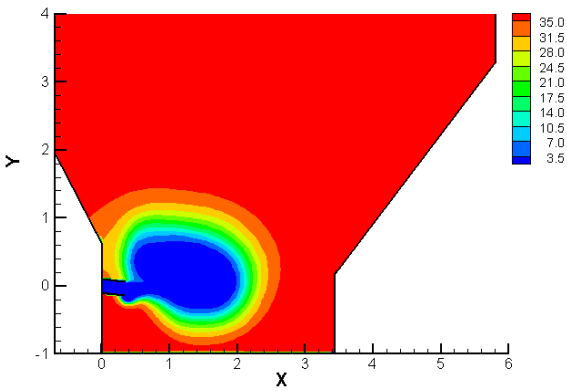

(g) CO concentration in all coke

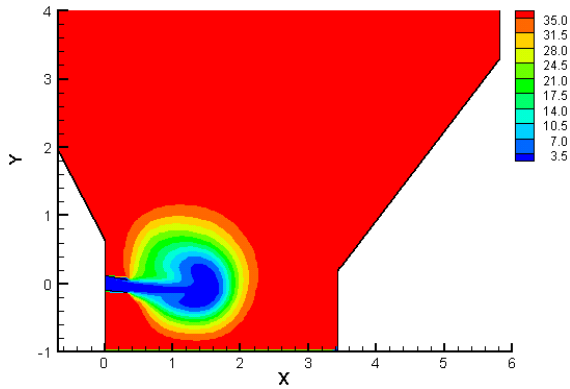

(h) CO concentration in PCI

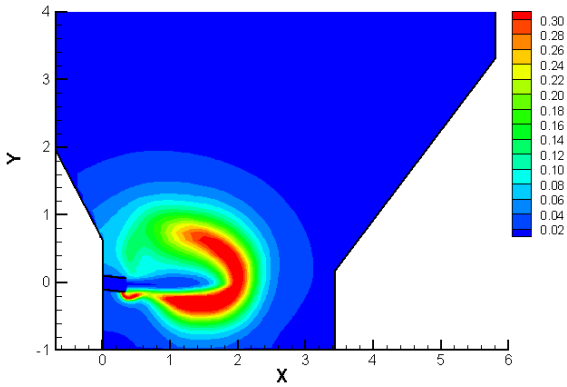

(i) Coke reaction rate in all coke (kg/ m^3s)

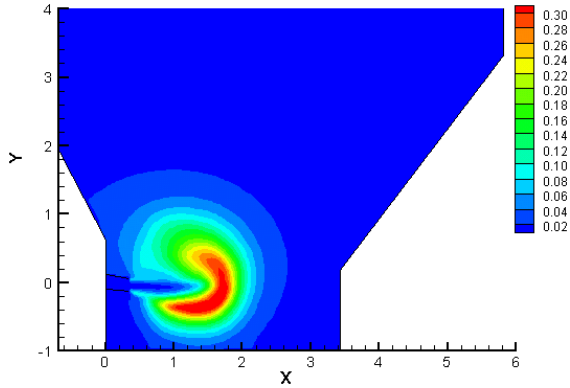

(j) Coke reaction rate in PCI (kg/ m^3s)

Figure 3.38 Comparisons between all coke and PCI operations

Gas species content along the tuyere centerline is widely used to evaluate the combustion status in the blast furnace, with the position being the dash-dotted line in Figure 3.39(a). Figure 3.39(b) demonstrates a more quantitative concept for the species distribution within the blast furnace. In terms of the O_2, its concentration increases from zero. This is because that carrier gas (pure N_2) inlet occupies the tuyere central zone. Afterward, combustion occurs and the carbon dioxide and carbon monoxide concentration increase as they move farther from the inlet accompanied with the decrease in the oxygen concentrations. The carbon dioxide concentration decreases after a peak, mainly due to the solution reaction of the coke bed, i.e., the coke gasification. It can be seen that the carbon monoxide peak corresponds to the start of the decline of the carbon dioxide concentrations. It should also be noted that the reaction rate inside the raceway is dependent on the oxygen content in the hot blast air.

As it is analyzed earlier, under the condition of pulverized coal injection operation, oxygen concentration decreases more rapidly, combustion focus comes closer to the tuyere or the wall, and CO fraction in the gaseous mixture is higher than that of all coke operation. Analysis demonstrates the combustion performance both of all coke and PCI operations. It can be found that nearly 85% of pulverized coal combusts inside the raceway zone, and the replacement ratio is nearly 98%. Rapid and efficient combustion of injected coal after the pulverized coal leaves the tuyere is critical for the energy performance and the penetrability of the burden.

In fact, the greater reactivity of the unburned coal will assure its consumption by CO_2 preferentially to the coke. So, the coke residence time in this region will increase, resulting in more pronounced degradation and generation of fines, because the mechanical collision increases among the particles.

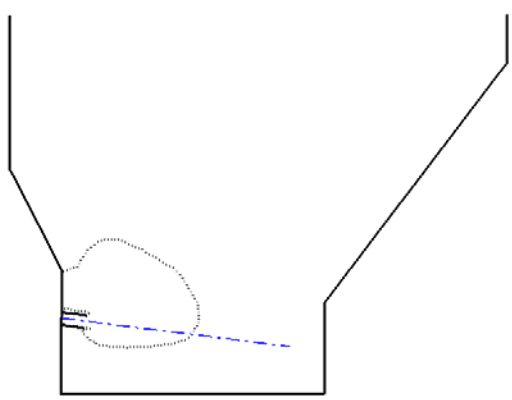

(a) Scheme of the tuyere centerline

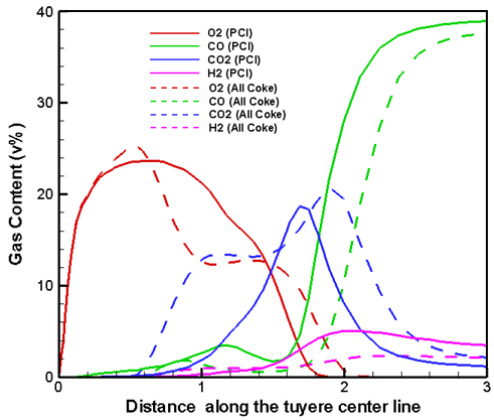

(b) Gas species

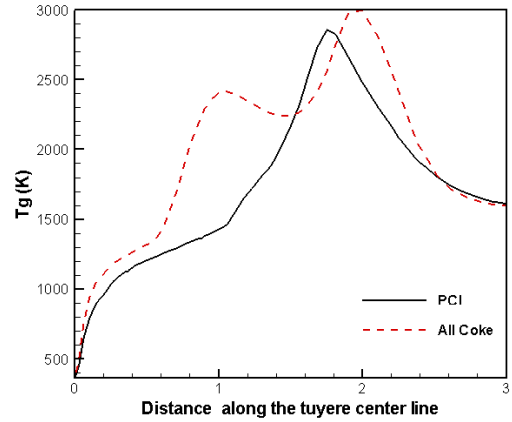

(c) Temperature

Figure 3.39 Comparisons between all coke and PCI operation: gas species and temperature distributions

Effect of Coal Type

Among the various factors that define the success of this technology, the appropriate choice of the coal to be injected plays an important role [64-66]. The effects of coal type are shown in Figures 3.40 to 3.42. Figure 3.40 provides the solid reaction information of different types of pulverized coal. Based on the burning mechanism and considering the extremely short residence time of the coal in the raceway, on the order of 20 ms, the influence of the volatile matter on the combustion efficiency becomes obvious; see Figure 3.40 (a), (b). Subsequently, more unburned coal is found with the lower volatile coal (volatile matter, VM: 18.2 v %), as indicated in Figure 3.40(c). Correspondingly, Figures 3.40 (e) and (f) more quantitatively display the coal combustion behavior along the tuyere centerline. Obviously, coal rank has notable effect on the combustion pattern inside the raceway. High volatile content helps to enhance the particle reactivity.

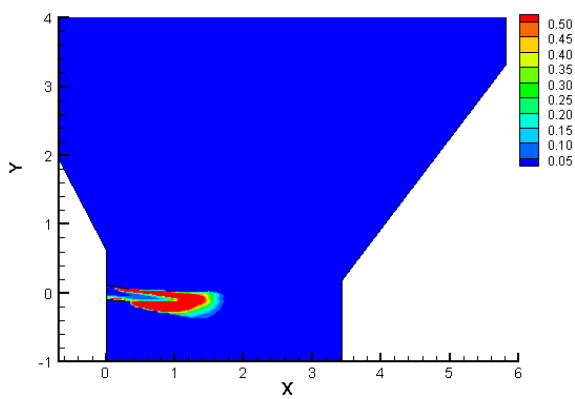

(a) Volatile Release Rate (kg/s), VM: 36.6%

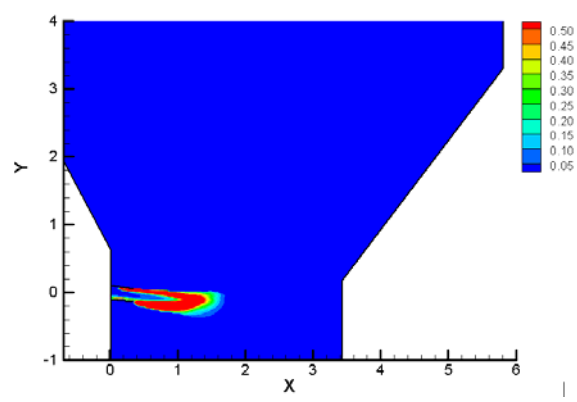

(b) Volatile Release Rate (kg/s), VM: 18.2%

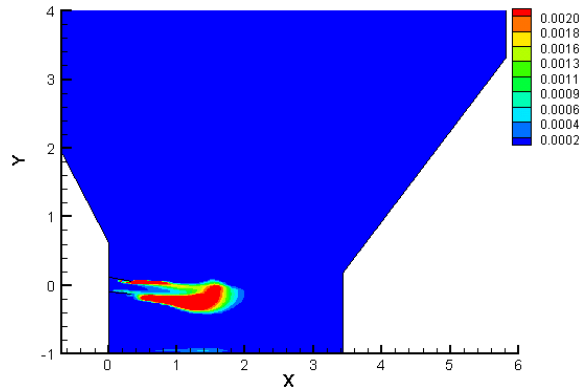

(c) Unburned char bulk density (kg/m^3)
VM: 36. %

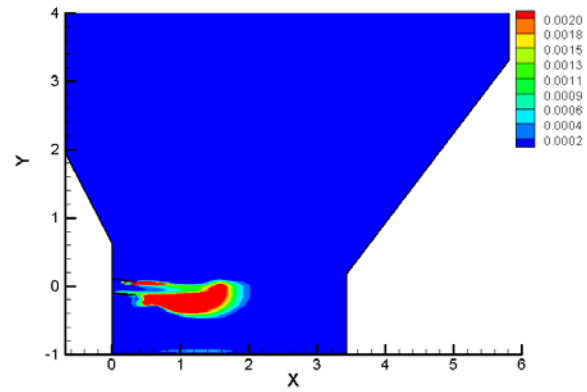

(d) Unburned char bulk density (kg/m^3),
VM: 18.2%

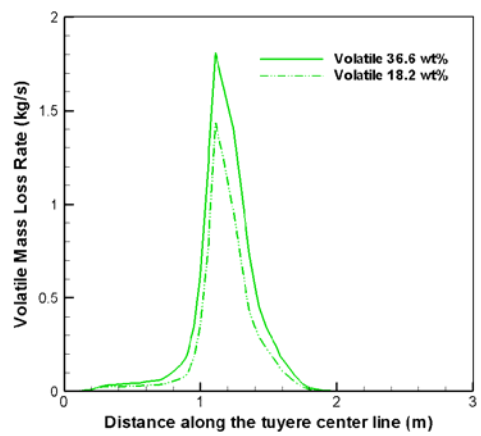

(e) Volatile Releasing Rate (kg/s)

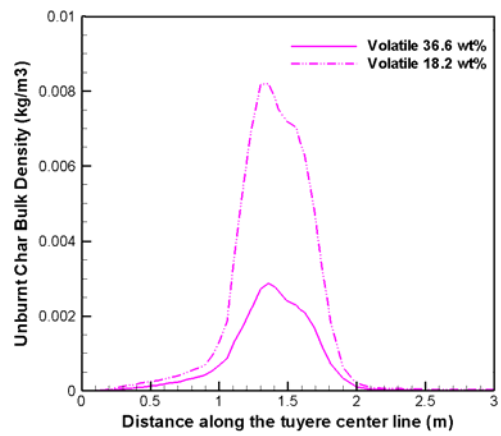

(f) Unburned Char Bulk Density

Figure 3.40 Effect of coal type on raceway combustion

The increase of volatile matter causes the lower ignition temperature of the pulverized coal particle (see temperature fields in Figure 3.41(a), (b)). Also, a more pronounced devolatization of the coal solid matrix tends to generate a more porous and reactive char (see oxygen contour profile in 3.41(c), (d)). Consequently, the combustion focus shrinks and moves close to the tuyere side (see the carbon dioxide profiles in Figures 3.41(e) and (f)).

To efficiently replace coke as a fuel in the blast furnace, the coal injected at the tuyeres should be completely gasified in the process. If the coal combustion does not go to completion inside the furnace, unburned particles will accumulate inside the solid bed, thereby deteriorating permeability conditions for the ascending gas flow and generating operational problems that will affect the productivity and fuel consumption [67,68] .

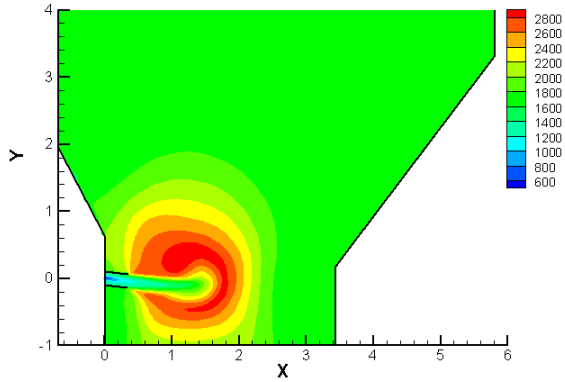

(a) Gas temperature (K), VM: 36.6 %

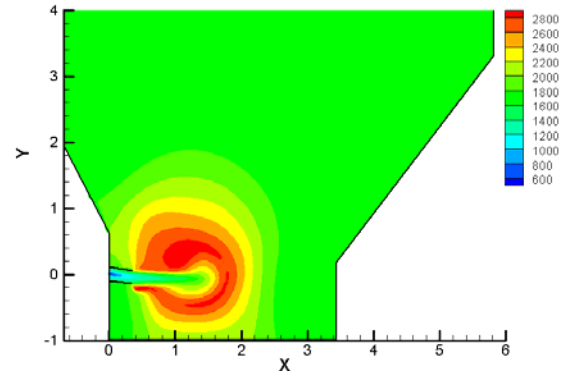

(b) Gas temperature (K), VM: 18.2 %

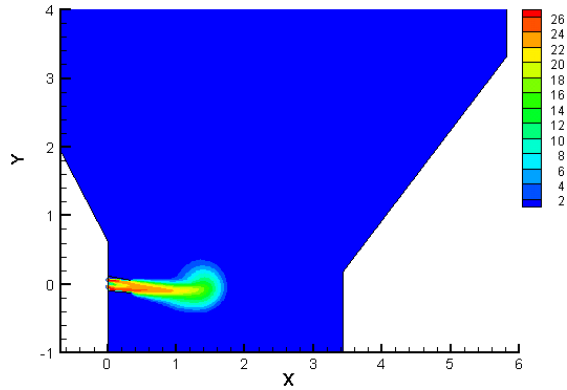

(c) O_2 concentration, VM: 36.6 %

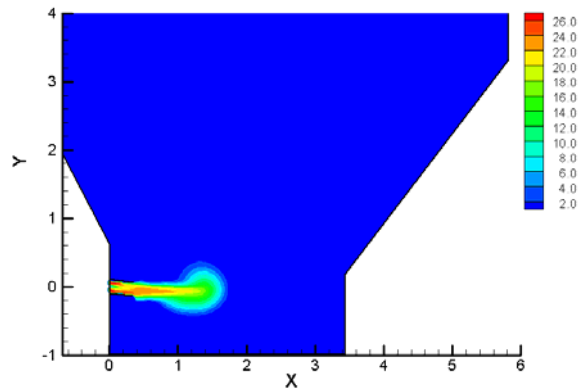

(d) O_2 concentration, VM: 18.2 %

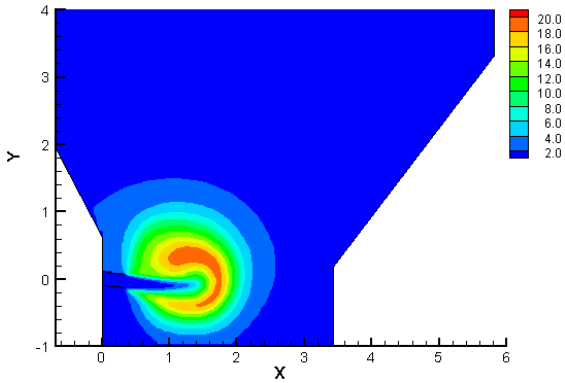

(e) CO_2 concentration, VM: 36.6 %,

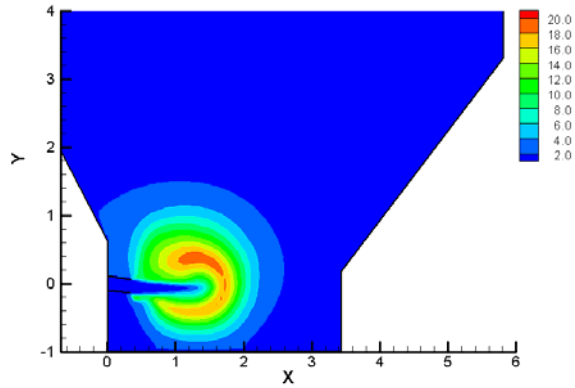

(f) CO_2 concentration, VM: 18.2 %

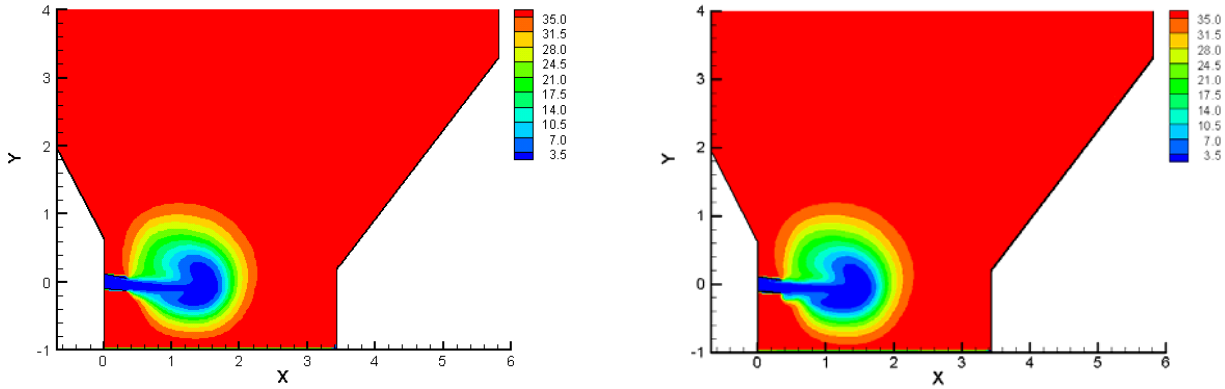

(g) CO concentration, VM: 36.6 % (h) CO concentration, VM: 18.2 %

Figure 3.41 Effect of coal type on species concentration distributions

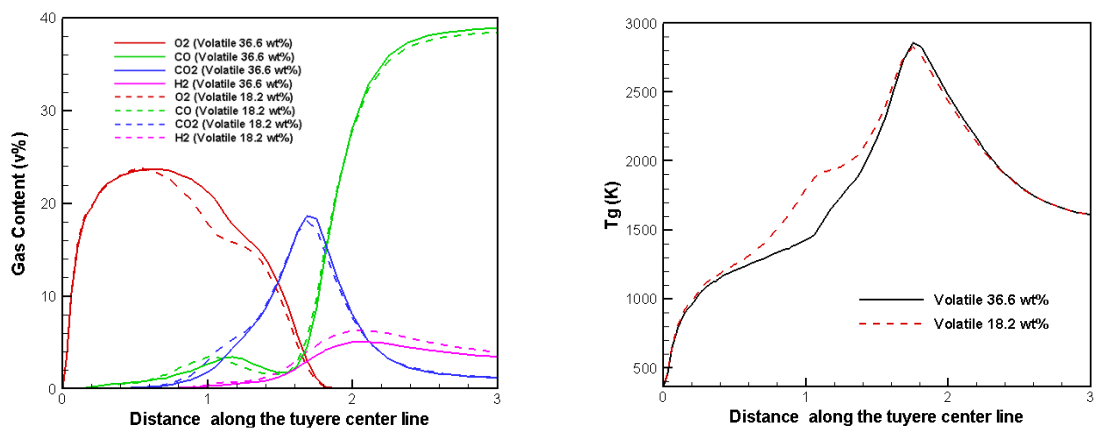

(a) Gas species (v %) (b) Temperature (K)

Figure 3.42 Effect of coal type on species and temperature distribution

The adoption of coal mixtures (high and low volatile coals combined) or medium volatile coal tends to be a reasonable alternative, since the gas volume generated at the tuyeres will decrease (in relation to a high volatile coal injection), without increasing the coke residence time significantly in the raceway (typical case of the low volatile coal injection). Both factors contribute to smaller coke degradation, preventing the formation of the bird's nest.

Effect of PCI Rate

For a long time, efforts have been made to increase the pulverized coal injection rate (PCR) to make better use of the advantages of PCI. Effects of the pulverized coal injection rate can be clearly observed in Figures 3.43 - 46. With the same oxygen concentration inside in blast supply, the O_2 is more rapidly consumed in a higher PC flow rate and more coke is replaced. Furthermore, the combustion flame comes closer to the tuyere nose in the case of higher PC concentration. However, due to the lower heat value of the coal, the flame temperature decreases

as the pulverized coal injection rate increases. More unburned char arises in the condition of higher coal flow rate due to lower combustion efficiency.

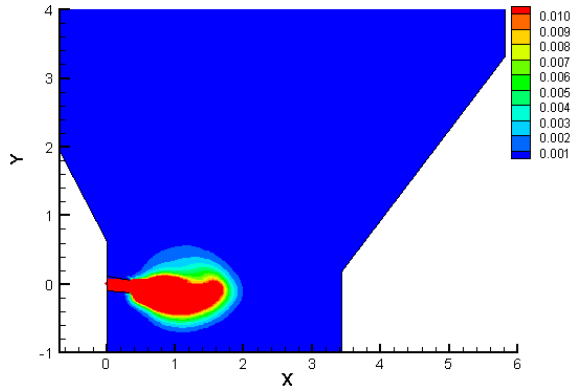

(a) Coal bulk density for 250/thm (kg/m^3)

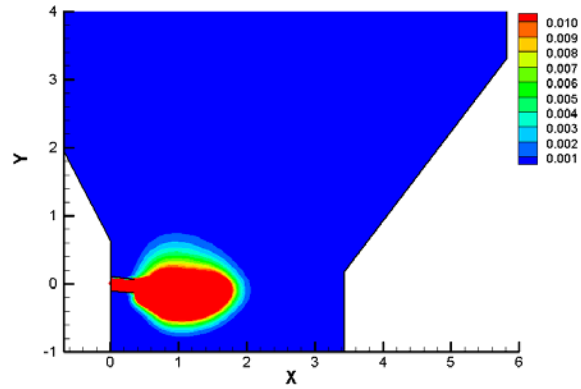

(b) Coal bulk density for 450/thm (kg/m^3)

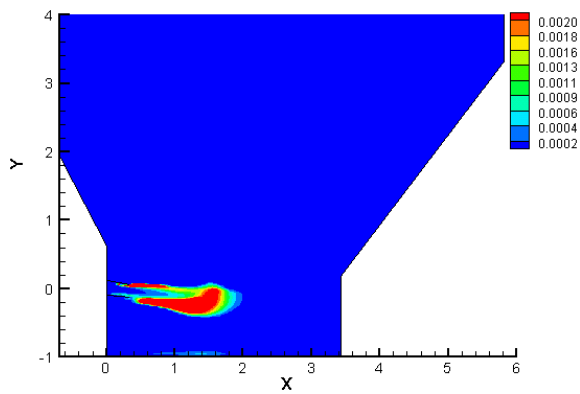

(c) Unburned char bulk density for 250 lb/thm (kg/m^3)

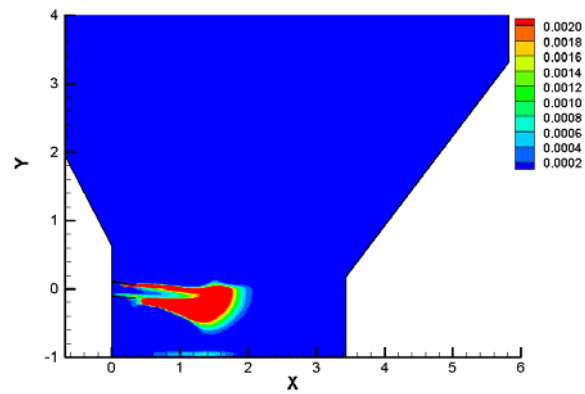

(d) Unburned char bulk density for 450 lb/thm (kg/m^3)

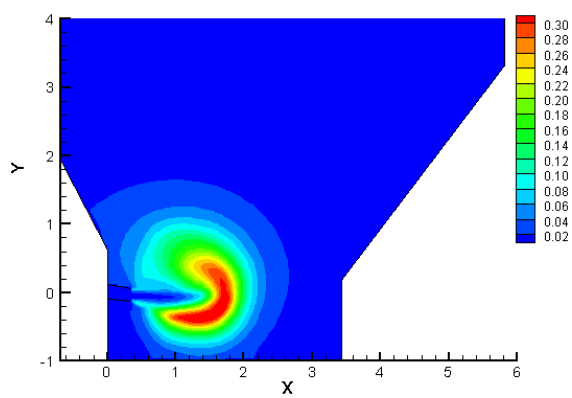

(e) Coke consumption rate for 250 lb/thm (kg/m^{3}s)

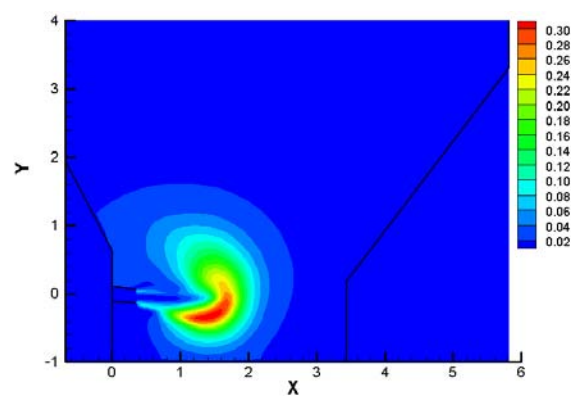

(f) Coke consumption rate for 450 lb/thm (kg/m^{3}s)

Figure 3.43 Effect of PCR on combustion process

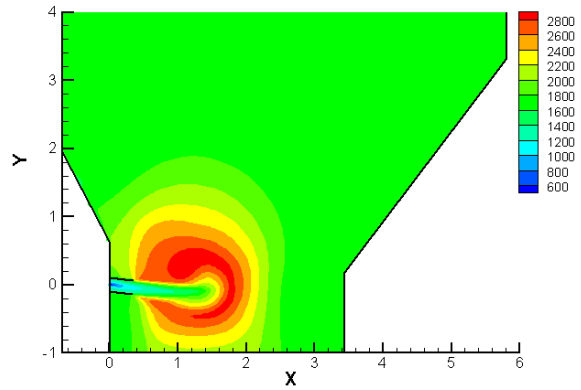

(a) Gas temperature (K) for PCR 250 lb/thm

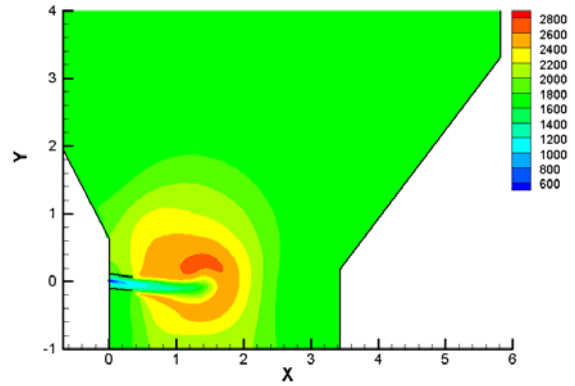

(b) Gas temperature (K) for PCR 450 lb/thm

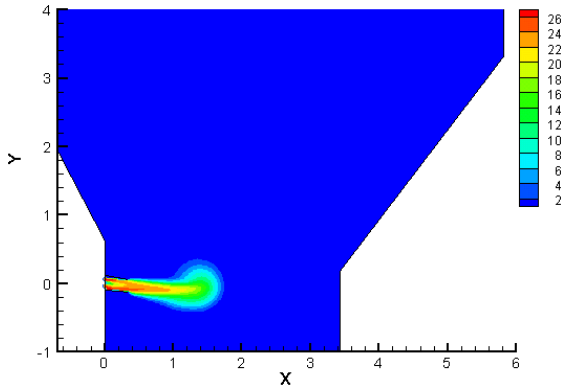

(c) O_2 for PCR 250lb/thm

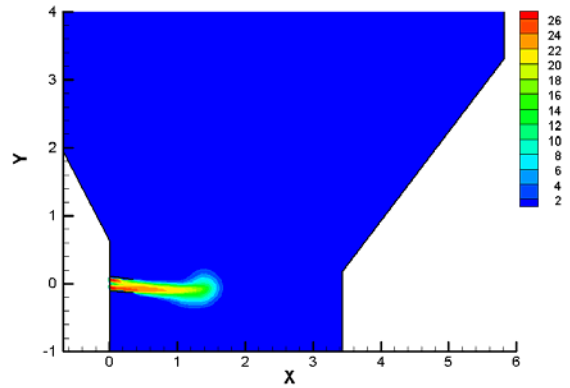

(d) O_2 for PCR 450lb/thm

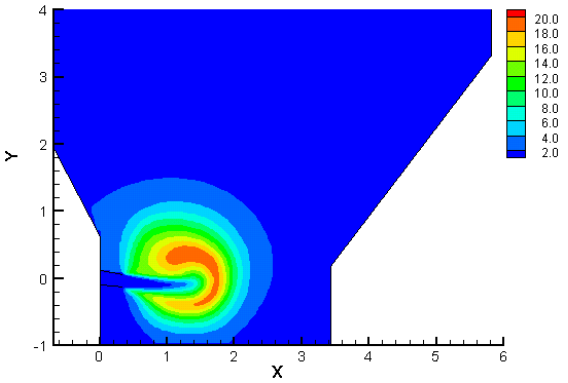

(e) CO_2 for PCR of 250lb/thm

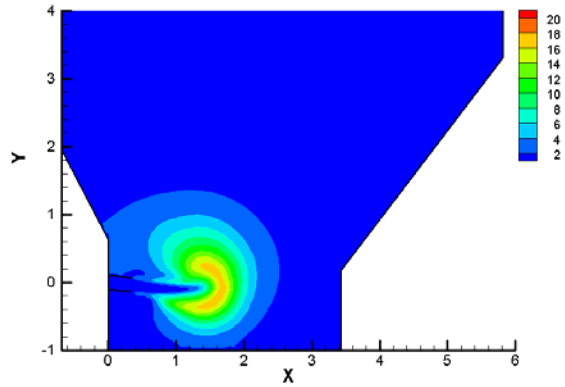

(f) CO_2 for PCR of 450lb/thm

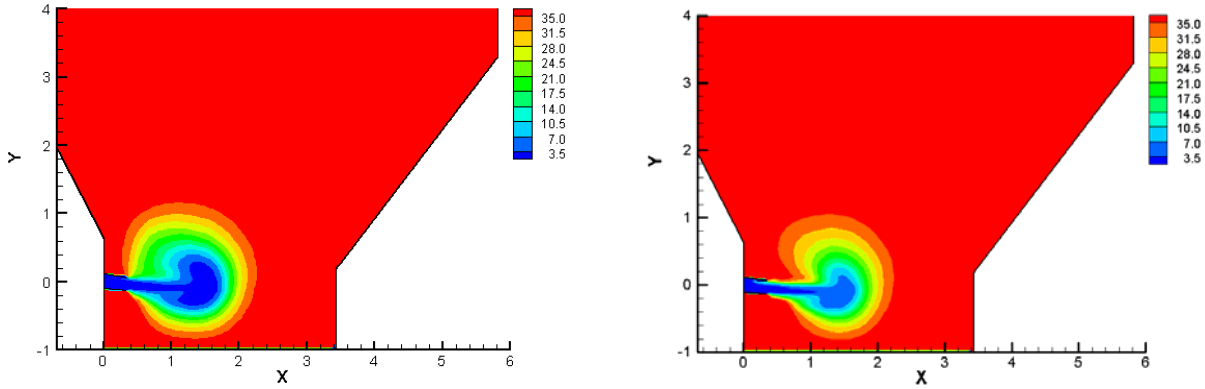

(g) CO for PCR of 250 lb/thm (h) CO for PCR of 450 lb/thm

Figure 3.44 Effect of PCR on gas species distributions

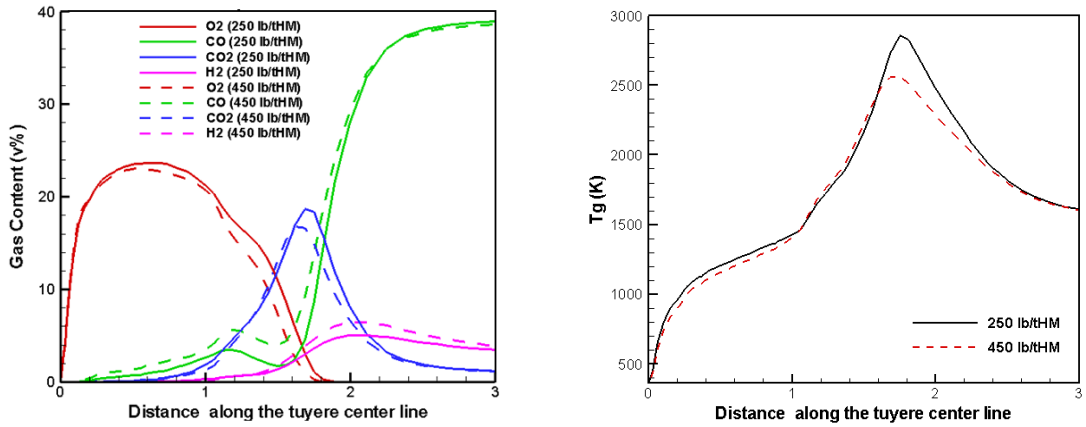

(a) Gas species (v %) (b) Temperature

Figure 3.45 Effect of PCR on species and temperature distributions

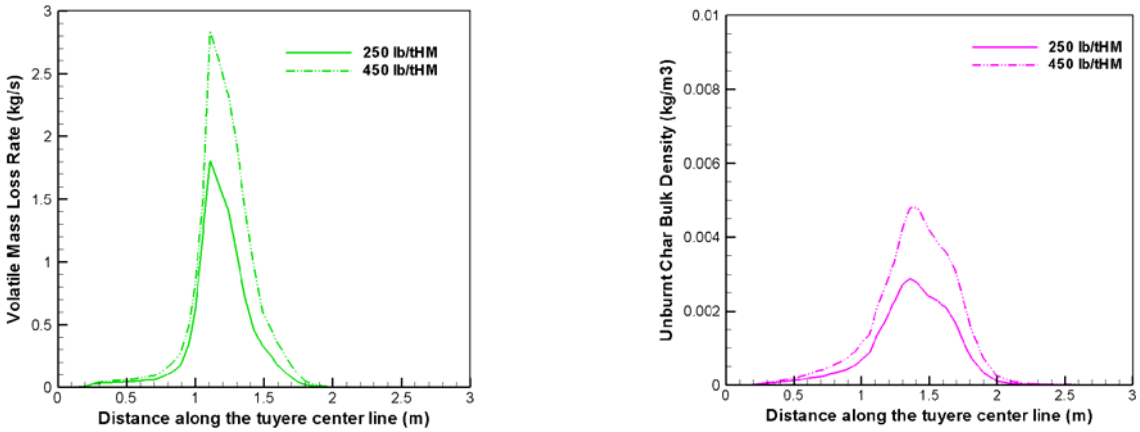

(a) Volatile releasing rate (b) Unburned char bulk density

Figure 3.46 Effect of PCR on raceway combustion

Effect of Oxygen Enrichment

An area of extreme importance for many integrated steel plants is to maximize the output of hot metal from the blast furnace. As it is usually very costly to install new facilities or to upgrade existing units for hot metal production, the most feasible way of increasing production is to increase the productivity in existing blast furnaces. One way to increase the productivity is to increase the injection rate of reductants and at the same time increase the oxygen added to blast furnace. Meanwhile, oxygen enrichment is often used to control the flame temperature in front of the tuyere under various blast conditions.

The effects of oxygen enrichment are shown in Figures 3.47-49. More specifically, these figures show the temperature and carbon consumption distribution with oxygen enrichment of the blast. Comparison indicates that the maximum temperature increases as the carbon consumption rate increases. The regions of maximum temperature and carbon consumption also move nearer to the tuyere nose with higher oxygen contents of the blast.

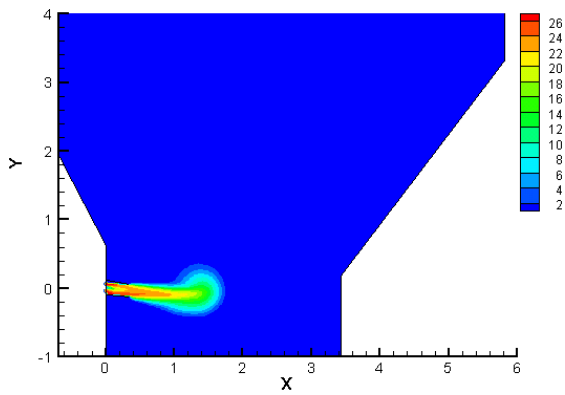

(a) O_2 for 27.26 % of O_2

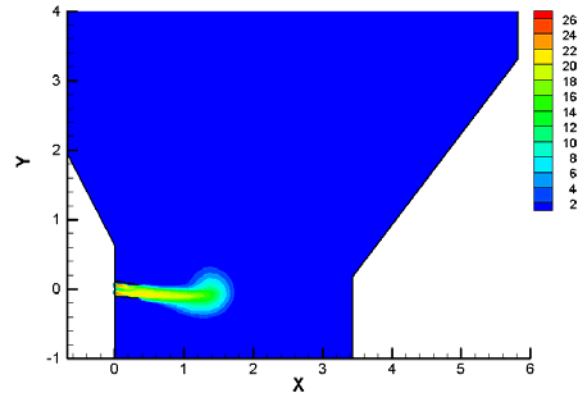

(b) O_2 for 23.55 % of O_2

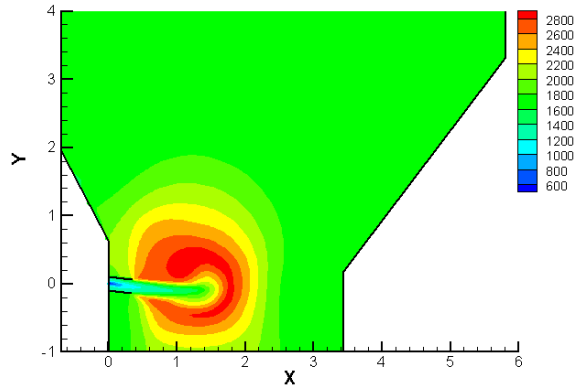

(c) Gas Temperature (K) for 27.26 % of O_2

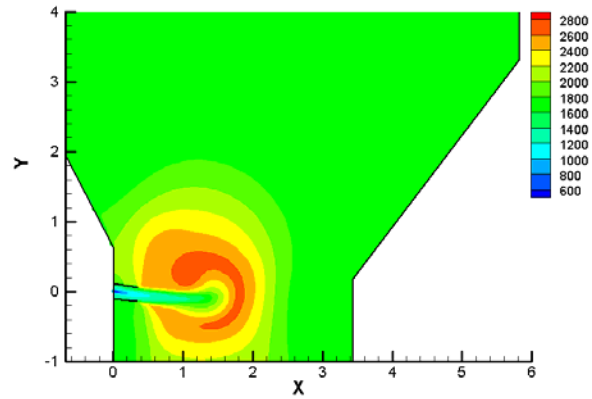

(d) Gas Temperature (K) for 23.55 % of O_2

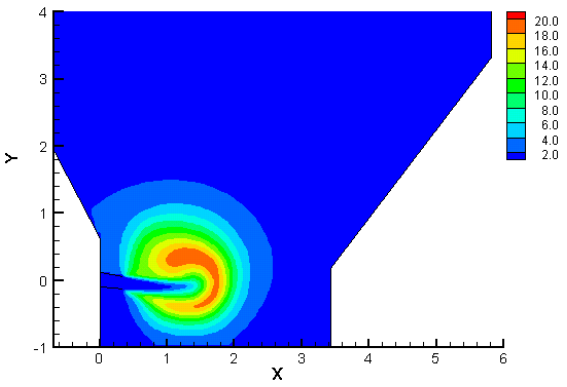

(e) CO_2 for 27.26 % of O_2

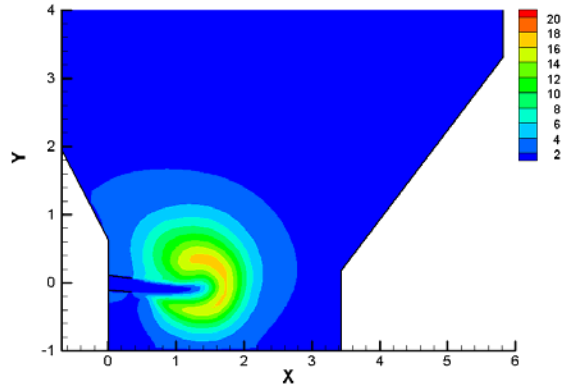

(f) CO_2 for 23.55 % of O_2

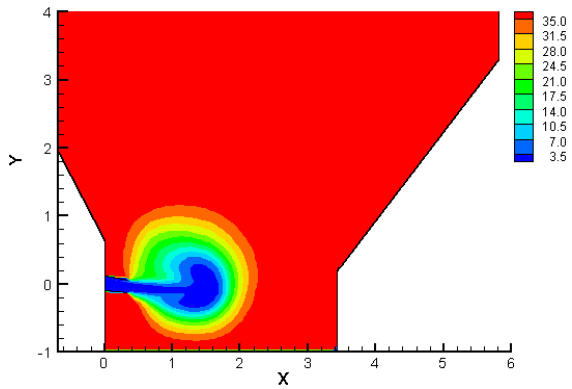

(g) CO for 27.26 % of O_2

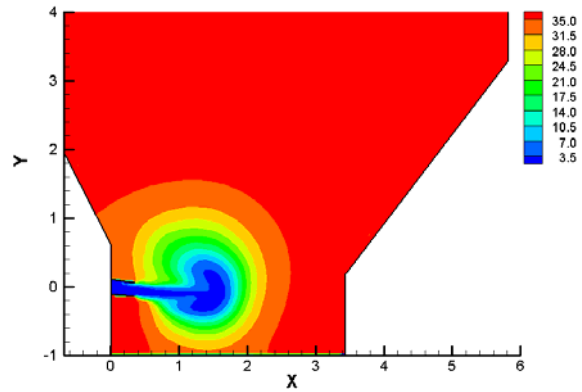

(h) CO for 23.55 % of O_2

Figure 3.47 Effect of Oxygen enrichment on gas species distributions

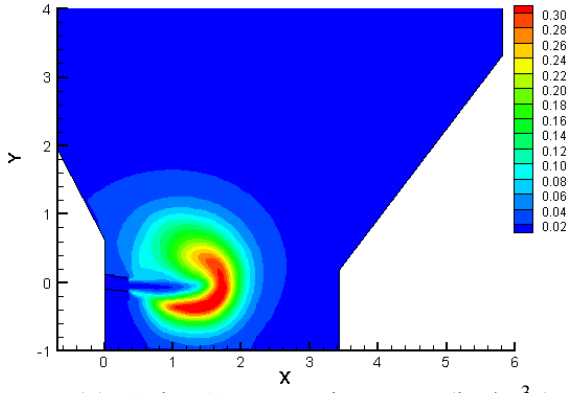

(a) Coke Consumption Rate (kg/m^{3}s)
(b) for 27.26 % of O_2

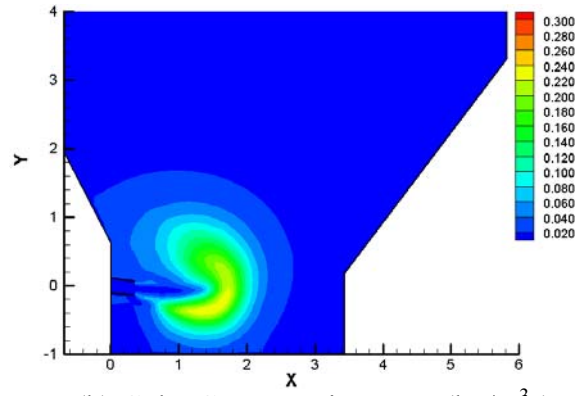

(b) Coke Consumption Rate (kg/m^{3}s)
for 23.55 % of O_2

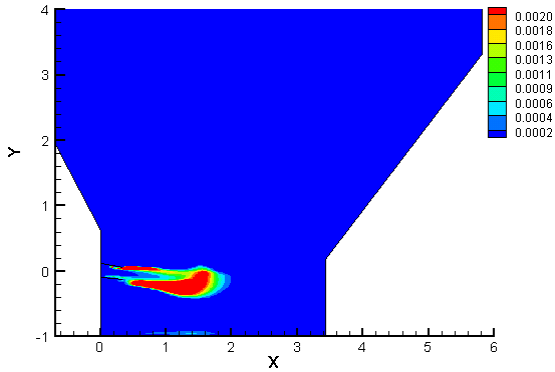

(c) Unburned Char Bulk density (kg/m^3) for 27.26 % of O_2

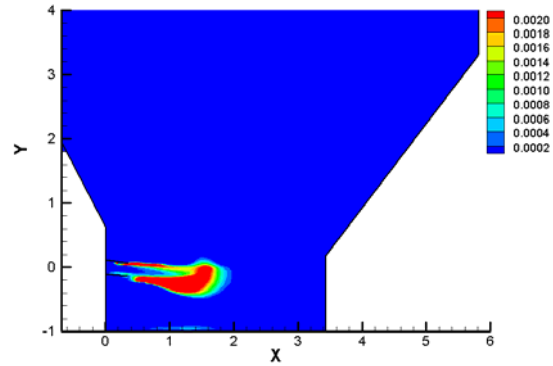

(d) Unburned Char Bulk density (kg/m^3) for 23.55 % of O_2

Figure 3.48 Effect of oxygen enrichment on raceway combustion

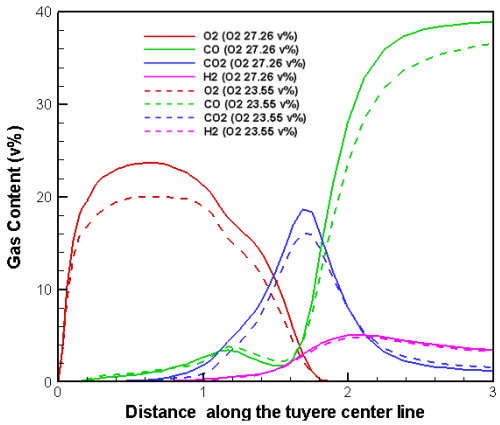

(a) Gas species

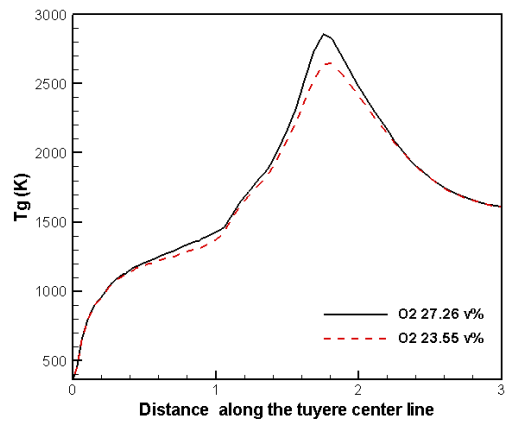

(b) Temperature

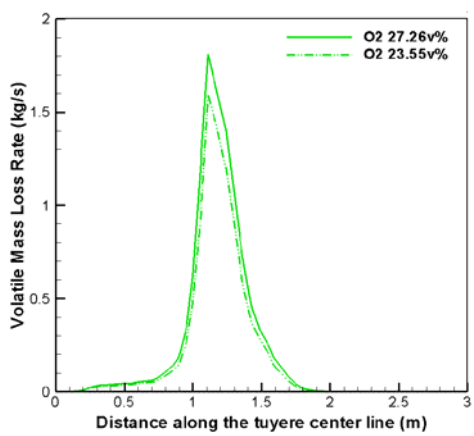

(c) Volatile releasing rate

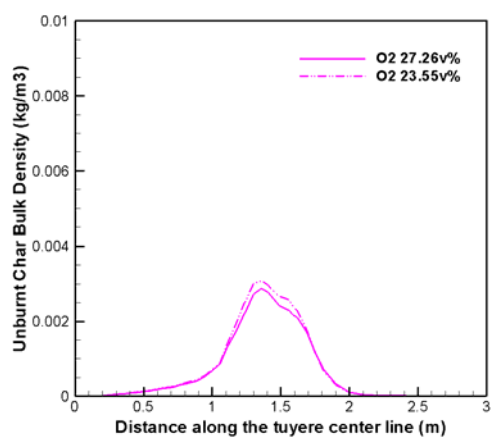

(d) Unburned char bulk density

Figure 3.49 Effect of oxygen enrichment on gas species and temperature distributions

Summary

The newly developed 3D multiphase reacting flow model is used to investigate the pulverized coal combustion behavior in the blast furnace. The results have provided detailed information of gas and coal particle flow properties such as velocity, temperature, gas species, coke and coal consumption rate. The parametric studies have shown that PCI can partially replace the coke to provide heat in a blast furnace. The coke consumption rate decreases when the coal volatile, O_2 enrichment, and PCR increase. The percentage of coal burnout increases with the increase of the volatile and O_2 enrichment.

Table 3.17 Summary of coke and coal burnout

Case	Coke consumption (kg/s)	% Coal burnout
Base Case (36.6% of Volatile, PCR of 250 lb/thm, 27.88% of O_2)	0.465	92.5
Coal B (18.2% of Volatile)	0.477	90.5
PCR of 450lb/thm	0.380	71.8
23.55% of O_2	0.475	87.3
All Coke	0.845	-

.

3.2.4 Investigation of Natural Gas Co-Injection

Conventional techniques, such as trial and error, have shown that high rate PCI reaches an upper injection rate limit because of incomplete coal burning. There are several ways to increase char burnout rate, such as oxygen enrichment, modified lance geometries, and natural gas co-injection. Natural gas co-injection is an attractive option because many blast furnaces already have natural gas injection lances installed. Natural gas also increases hydrogen levels, which has more advantages in reducing iron oxide to iron. It is for these reasons that a CFD model is needed to maximize the benefits of this proven technology. The understanding and insight provided through CFD parametric studies will push PCI rates beyond the current upper limits, and maximize energy efficiency. Modeling and understanding of the raceway formed by the hot blast stream and injectants will lead to the optimization of the complex PCI process.

Operating Conditions

Industrial participants provided information based on actual furnace conditions. A baseline case was established followed by five other cases for parametric studies. Operating conditions for the baseline case and other cases are summarized in Table 3.18. The cases were chosen so that the calculated Raceway Adiabatic Flame Temperature (RAFT) was kept approximately constant. Parameters were varied to investigate the effects of wind rate, PCI carrier air flow rate, natural gas injection rate, blast temperature, and lance oxygen content. Case 1 reduced the carrier air by 20%. Case 2 reduced the methane flow by 33%. Case 3 reduced the methane flow by an additional 33%, while blast oxygen enrichment was reduced by 7% and steam was doubled to maintain furnace chemistry. Case 4 reduced the blast air temperature

8.5%, reduced the methane flow rate by 20%, and increased the steam by 17%. Case 5 reduced the lance oxygen by 50%.

Table 3.18 Parametric Study Operating Conditions

Case	Wind rate per tuyere (kg/s)	Blast temperature (˚C)	Oxygen mass fraction in blast	Mass fraction steam in blast	PCI rate per tuyere (kg/s)	PCI carrier rate per tuyere (kg/s)	Lance oxygen rate per tuyere (kg/s)	Methane rate per tuyere (kg/s)
Base	3.12	1,099	0.308	0.0117	0.308	0.0575	0.107	0.180
1	3.12	1,099	0.308	0.0117	0.308	0.0460	0.107	0.180
2	3.12	1,099	0.297	0.0176	0.308	0.0575	0.107	0.146
3	3.12	1,099	0.286	0.0231	0.308	0.0575	0.107	0.114
4	3.12	982	0.308	0.0137	0.308	0.0575	0.107	0.144
5	3.12	1,099	0.318	0.0117	0.308	0.0575	0.0711	0.180

Coal proximate and ultimate analyses are given in Table 3.19. An average particle size of 50 μm is used in the simulations.

Table 3.19 Coal properties for natural gas co-injection

(a) Proximate analysis (wt. %)

Fixed carbon	Volatile matter	Ash
58.6	35.6	5.8

(b) Ultimate analysis (wt. %)

C	H	O	N	S	Ash
81.7	5.0	4.9	1.5	0.87	5.8

Coal and Natural Gas Injection System

In order to avoid lance burnout and have a better PCI performance, detailed analysis have been made by simulations of the PCI and natural gas injection system in Step 1 in the methodology descried earlier. Figure 3.50 shows a generic representation of the geometry from the industry, which includes a blowpipe, a tuyere, and three lances. Certain dimensions have been excluded to avoid proprietary concerns. Oxygen enriched air is supplied at the inlet of the blowpipe. A co-annular injection with pulverized coal carried by air in the inner lance and oxygen in the outer lance enters at an angle to the blowpipe. A natural gas lance also enters at an angle to the main blast air flow. The centerline of the blowpipe is perpendicular to the centerline of the blast furnace.

The lances are constructed of stainless steel with a thermal conductivity of 9.42 Btu/ft-hr-F. The wall thickness of the methane lance is 0.113 in. The wall thickness of the PCI lance is 0.179 in. The oxygen lance is 0.218 in. thick. Heat transfer by conduction was modeled for the lances. The tuyere exit is tilted downward with an angle between the centerlines of the blowpipe and the tuyere. One of the objectives of this work is to examine the heat transfer behavior in the lances. Adiabatic boundary conditions are imposed at the tuyere walls, the blowpipe and the outer surface of the lance in the region outside the blowpipe.

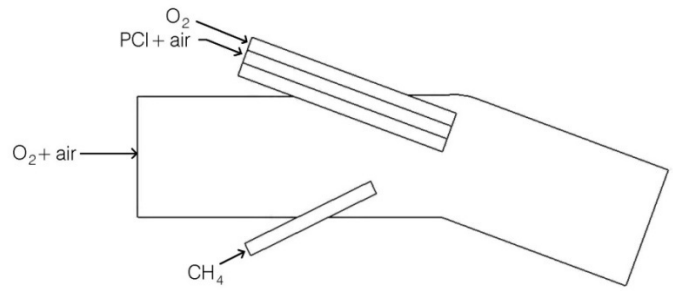

Figure 3.50 Schematic of the injection system

Flow Characteristics of Baseline Case

Detailed information on flow characteristics and kinetics reactions has been analyzed for the baseline case. The information includes velocity, temperature, pressure, combustion reaction, particle trajectories, the evolution of volatile matter from those particles, and their subsequent burnout. Figure 3.51 (a) shows the velocity in a 2D plan. The higher velocities near the exit of the tuyere are generated by the gas density change caused by combustion. Figure 3.51(b) shows 3D view of the velocities that are normal to the flow out of the tuyere. This illustrates the swirl effect induced by the lance arrangement.

The temperature distributions are shown in Figure 3.51(c). It can be seen that the natural gas is burning almost as soon as it is released from the lance because the high temperature blast contains more energy than is needed to activate the initial combustion reaction. It can also be seen that the combustion reaction continues throughout the entire length of the blowpipe and tuyere. This is beneficial to the coal combustion, but it is harmful to equipment because of the high temperatures it generates. Figure 3.51(d) shows the devolatilization happening within the tuyere. This devolatilization is increased by the hydrogen and high temperatures that are generated by the natural gas combustion.

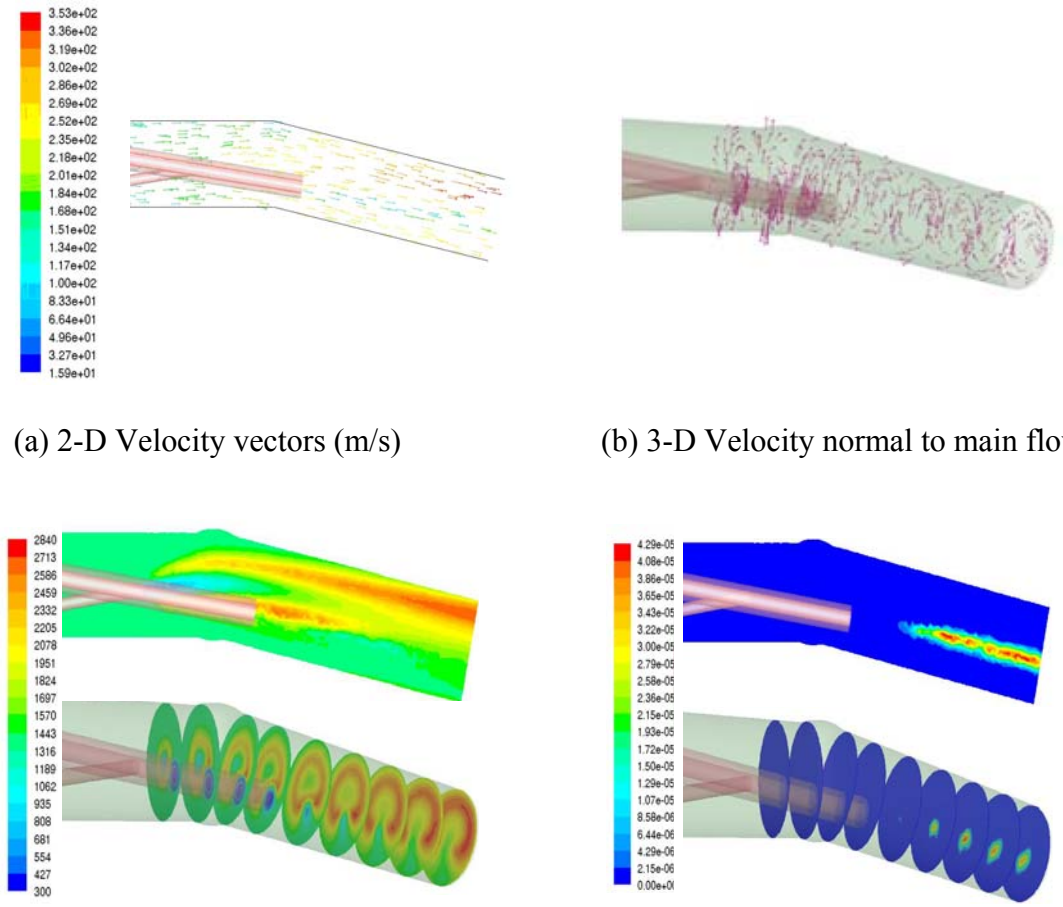

(a) 2-D Velocity vectors (m/s)

(b) 3-D Velocity normal to main flow (m/s)

(c) Contours of temperature (K)

(d) Contours of devolatilization (kg/s)

Figure 3.51 Baseline velocity, temperature and devolatilization

Figures 3.52 (a) and (b) show the contours of mass fraction of hydrogen and CO. It is important to model these radical species concentrations since these are the primary reducing agents within the blast furnace. Figure 3.52(c) shows contours of mass fraction of CO_2. It can be seen that the mass fraction is the highest in the stream of oxygen from the oxy/coal lance. By comparing Figures 3.52(d) and 3.52(e), it is obvious that the methane displaces much of the oxygen initially, and after combustion occurs, the less dense products exiting the tuyere further displace oxygen. Also, the 3-D view shows the oxygen leaving the oxy/coal lance and dissipating or being consumed by volatile and methane combustion. Figure 3.52(f) shows contours of mass fraction of water vapor. The higher mass fractions of water vapor near the oxygen stream leaving the oxy/coal lance is further evidence of the more complete combustion in this region.

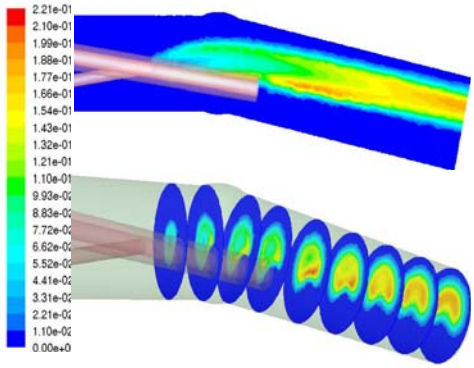

(a) Contours of mass fraction H2

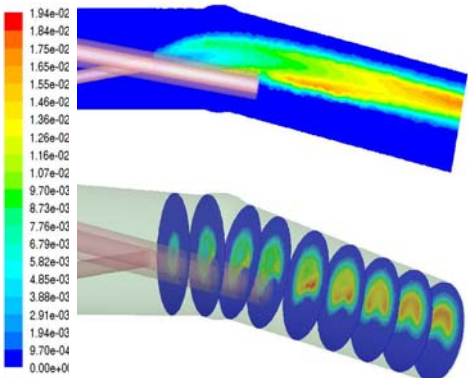

(b) Contours of mass fraction CO

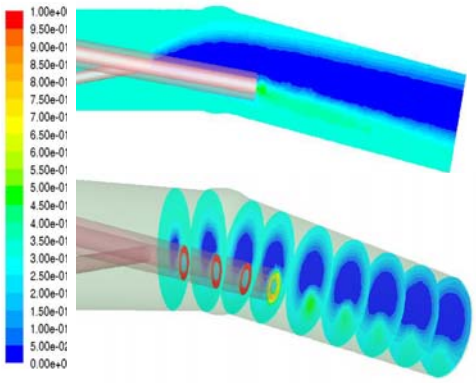

(c) Contours of mass fraction CO_2

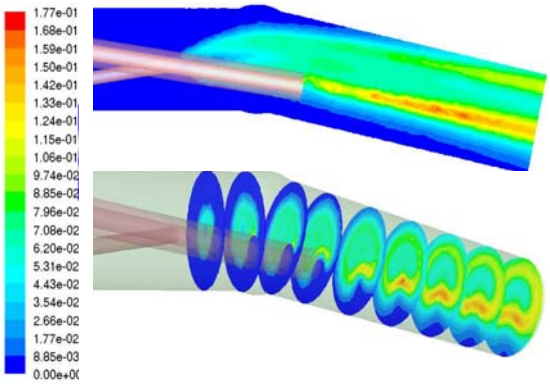

(d) Contours of mass fraction O_2

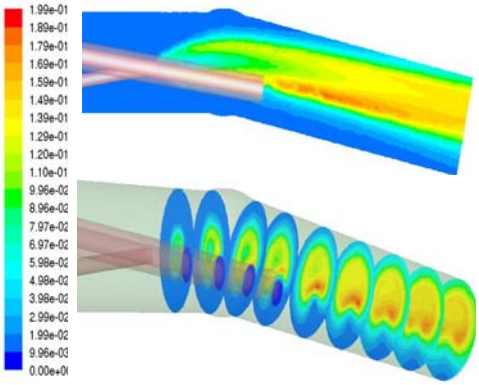

(e) Contours of mass fraction CH_4

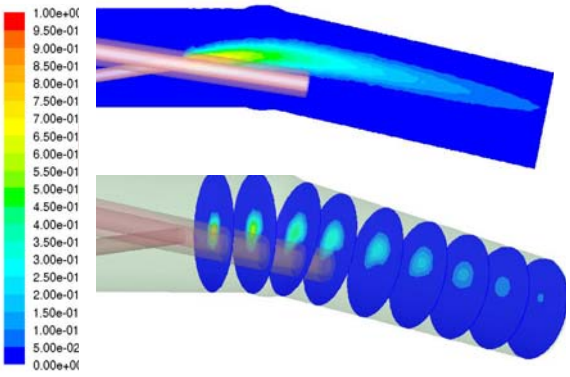

(f) Contours of mass fraction H_2O

Figure 3.52 Species concentrations of the baseline case

Effect of Carrier Air

Figure 3.53 shows the effect of carrier air flow on the devolatilization. As indicated in Figure 3.53(a), the devolatilization rate is 3.5% higher for the case with 20% less carrier air flow. This effect is illustrated in Figure 3.53(b). The reason for this is that as the carrier air flow rate is reduced, the residence time of the coal particle inside the tuyere region increases, thus increasing the devolatilization rate for the lower carrier air flow rates. The volatiles are generally evolved in about 100ms at 400K and play an important role in flame stabilization inside the raceway. It was found that the carrier air rate has no significant effect on lance temperature since the PCI lance temperature depends mainly on the co-annular oxygen flow rate. It should be also noted that even though lowering of the carrier air flow rate might increase PCI devolatilization, as shown by this CFD simulation, the limitation on this parameter is the choking of the PCI lance with accumulated coal particles. Therefore, care should be taken while reducing the carrier air flow rates.

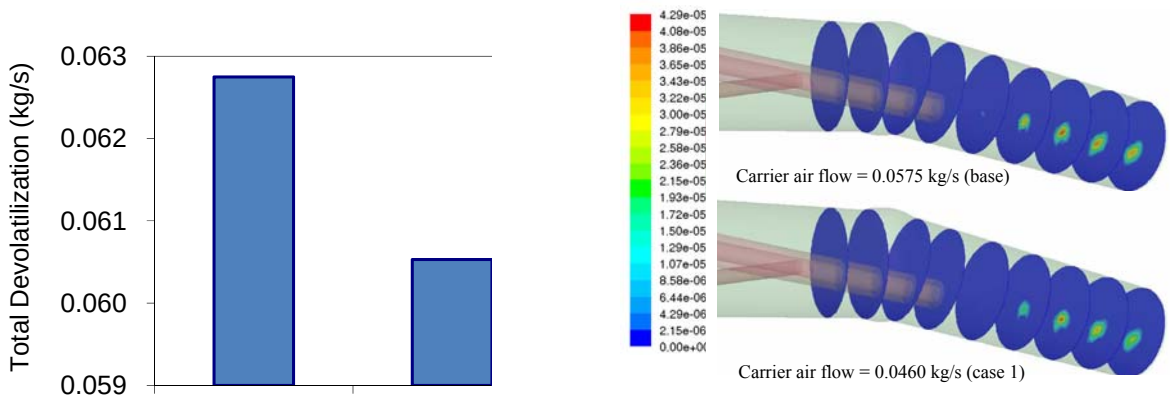

(a) Devolatilization vs. carrier air mass flow rate (b) Contours of devolatilization (kg/s)

Figure 3.53 Effect of carrier air flow on the devolatization

Effect of Natural Gas Flow rate

Figure 3.54 shows the effect of natural gas flow rate. As indicated in Figure 3.54(a), the total devolatilization within the blowpipe and tuyere increases with the mass flow rate of methane. The higher temperatures caused by methane combustion contribute to the increase in devolatilization. Figure 3.54(b) shows 3-D view of devolatilization on different cross sections. It can be clearly seen that the devolatilization is greater when the methane flow rate is higher. The variation of devolatilization of PCI with methane flow rate is not linear because the air-fuel ratio limits the maximum flame temperature near the PCI stream.

Once the air-fuel ratio is below the stoichiometric value, the flame temperature will reduce, lowering the devolatilization rate of the coal particle. H_2 flow rate is highest for the baseline case and case 1. These cases have the highest flow rates of methane. Since methane contains a lot of hydrogen, there is more hydrogen available to the system. This high amount of

hydrogen replaces carbon monoxide as reducing gas in the shaft of the blast furnace. The hydrogen gas is a better reducing gas compared with carbon monoxide and allows savings of energy by decreasing the amount of direct reduction, which demands considerable amount of energy for the reaction. This observation proves that methane injection improves hydrogen production, increasing the reducing reactions due to hydrogen.

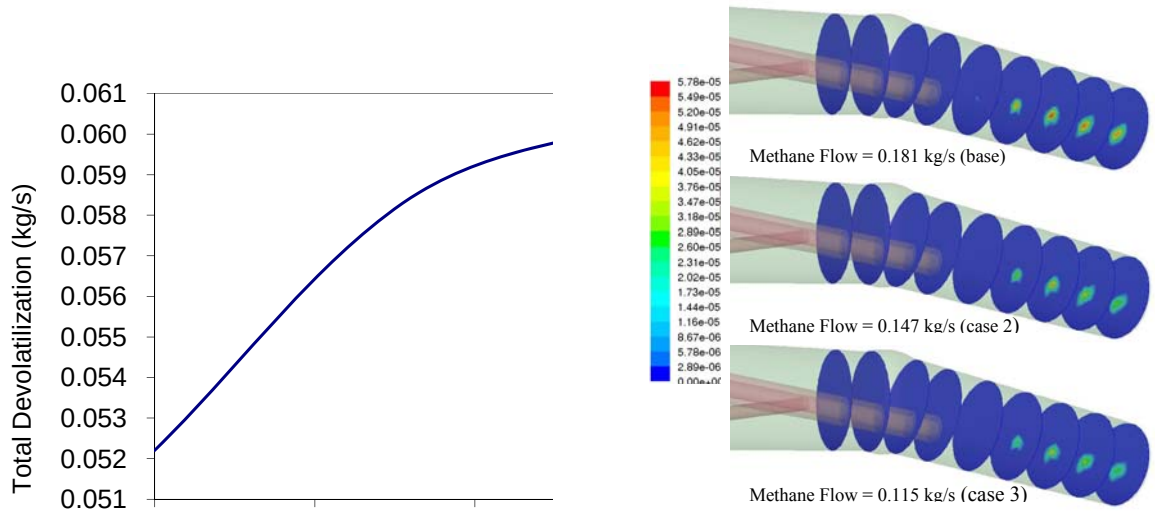

(a) Total devolatilization vs. methane flow rate (b) Contours of devolatilization (kg/s)

Figure 3.54 Effect of natural gas flow rate on the devolatization

Figure 3.58 shows the wall temperatures for different methane flow rates. It can be seen that the lance outer wall temperature profiles are similar for each of the three cases, which are consistent with industrial observations. The highest wall temperatures vary by about 10 degrees for these three cases because the walls of the PCI lance are affected mainly by the oxygen flow rate in the oxygen lance, which acts as a thermal shield between the hot methane flame and the PCI. The temperature increases towards the flame front where the combustion is at the stochiometric ratio. This is followed by the reduction in the temperature due to the rich flammability limit inside the flame.

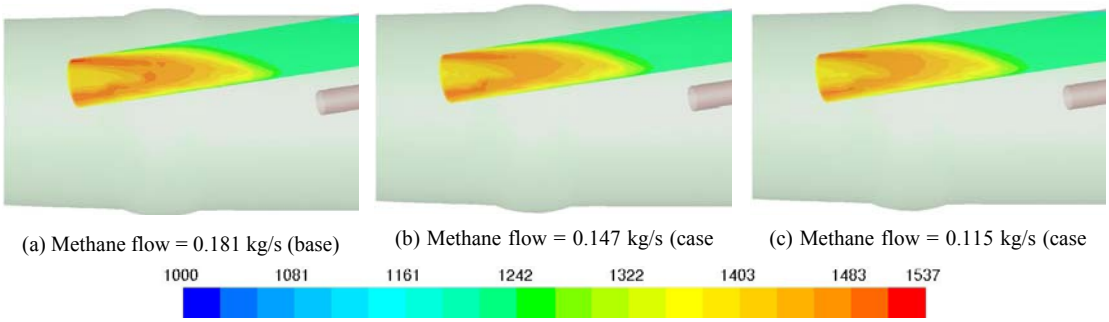

(a) Methane flow = 0.181 kg/s (base) (b) Methane flow = 0.147 kg/s (case (c) Methane flow = 0.115 kg/s (case

Figure 3.55 Contours of oxy-lance outer wall temperature (K)

Effect of Oxygen Enrichment in Oxygen Lance

The effect of oxygen enrichment in the lance is shown in Figures 3.56 and 3.57. The effect on devolatilization can be seen in Figure 3.59. Two effects are observed from these figures. The first is that the lower oxygen flow rate through the lance causes a lesser relative PCI velocity, and increases the residence time of the coal particles and the devolatilization inside the tuyere. The second effect is that the lower oxygen flow rate provides lesser thermal isolation of the PCI lance and increases the temperature and the devolatilization of the coal particles. The net result of these two effects is that the total devolatilization is about 10% higher for the case with 33% less oxygen through the oxygen lance. Figure 3.60 shows that lance oxygen flow rate has some effect on the maximum temperatures reached on the outer wall of the oxygen lance. However, further parametric studies of natural gas flow rate and lance oxygen flow rate will be required to have better understanding of these flow rates on lance wall temperature.

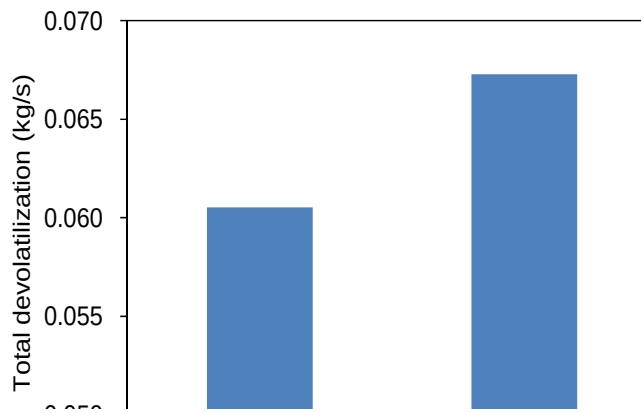

Figure 3.56 Effect of oxygen lance flow rate on devolatization

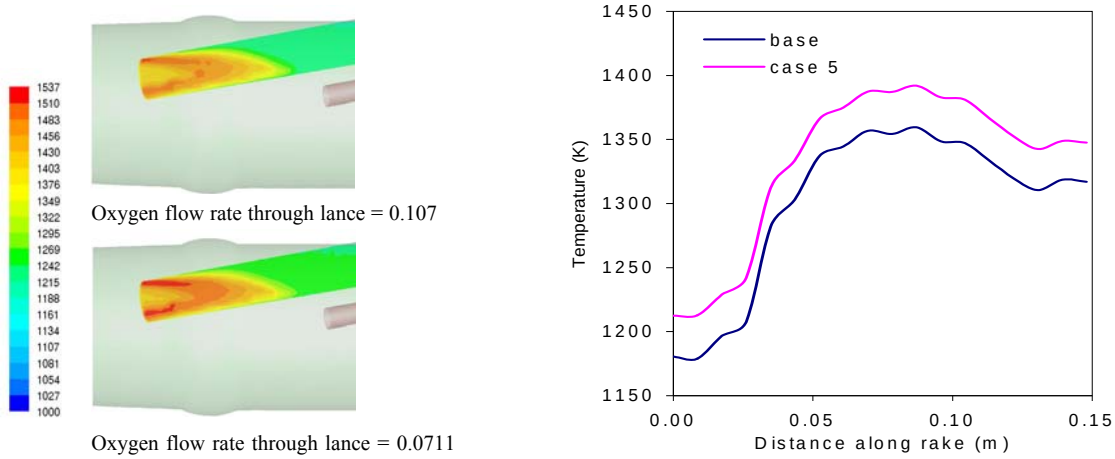

(a) Contours of temperature (K)

(b) Oxy-lance wall temperatures along rake

Figure 3.57 Effect of oxygen enrichment on oxygen lance wall temperatures

Effect of Blast Air Temperature

The effect of an 8.5% reduction in blast air temperature and a 20% reduction in natural gas flow rate are also modeled. The Figure 3.58 shows the contours of the blast air temperature effect. It can clearly be seen that the overall temperatures are reduced. Since the methane flow is also reduced in this case, the total devolatilization reported in Figure 3.58(b) is increased by the amount predicted by case 2 for the sake of comparison. It can be seen in the Figure 3.58 that devolatilization is decreased by 10%. This decrease in devolatilization is accompanied by a reduction in maximum lance temperature of only 9 K, Figure 3.58(d). This effect is mainly due to the reduction in the flame temperature which accompanies the reduction of the blast air temperature. A similar trend is observed for the lance wall temperature. A cooler blast air causes a lower lance temperature as one might expect.

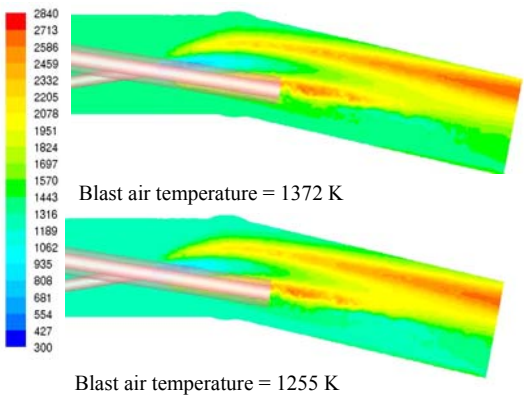

(a) 2-D contours of temperature (K)

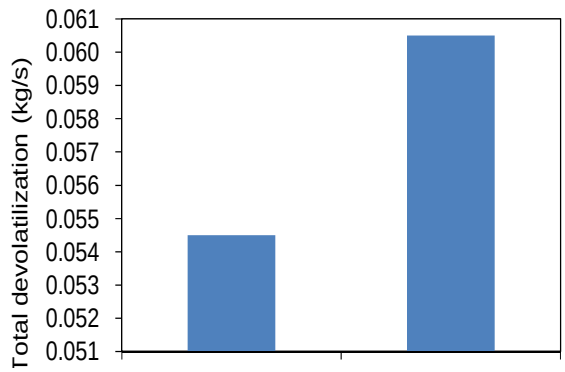

(b) Total devolatilization vs. blast air temperature

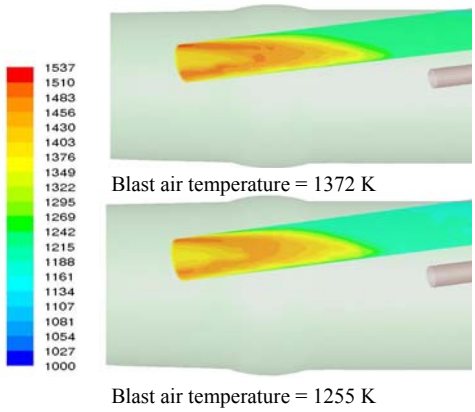

(c) 2-D and 3-D contours of temperature (K)

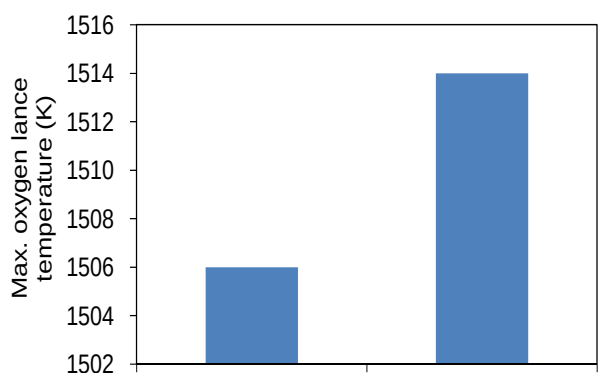

(d) Maximum oxygen lance temperatures (K)

Figure 3.58 Effect of blast air temperature on lance wall temperature

Natural Gas, Coal and Coke Combustion inside Raceway

Detailed analysis of combustion inside the raceway has also been made for the cases listed in Table 3.18. According to the multi-step methodology, the information obtained from the simulation of injection system in Step 1 is used as the input of simulations of other steps. Figure 3.59 shows the contours of data that were obtained from Step 1. The data is recorded at the tip of the oxygen/PCI lance where the oxygen and PCI enters the tuyere. The location of this data plane is illustrated in Figure 3.50. The "halo" shape of high temperature can be seen where some methane combusts upwind from the PCI/oxygen lance tip. A similar distribution can also be seen for the resulting product species.

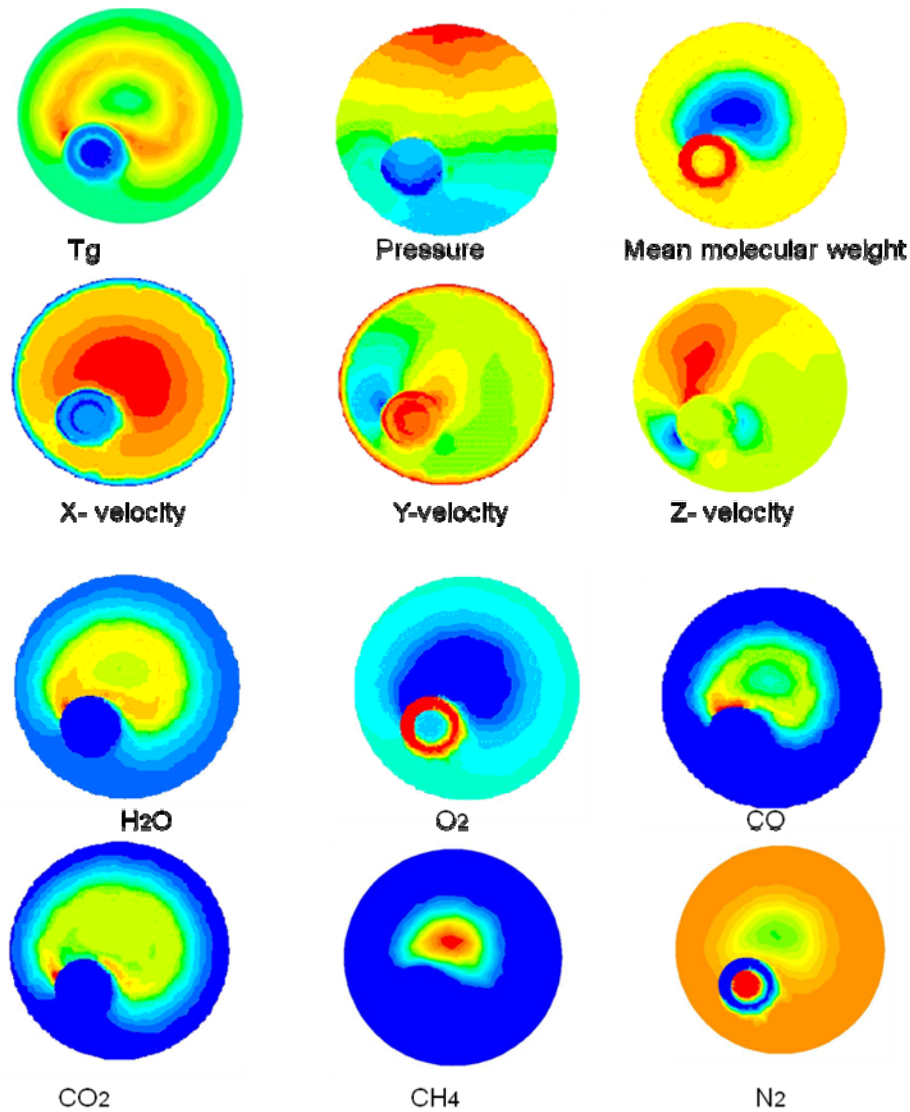

Figure 3.59 Data used as input to in-house code for the baseline case

Figure 3.60 shows the raceway formation simulated based on the multi-step methodology. The term porosity, i.e., bulk porosity in this paper, is defined as the volume fraction of the gas phase with respect to the total volume of gas and solid phases, which is 1 minus the solid particle volume fraction ($\varepsilon = 1 - \alpha_p$). The porosity inside the particles is not taken into account for the bulk porosity. This raceway shape and coke distribution is used to simulate the coke, coal and natural gas combustion inside the blast furnace. .

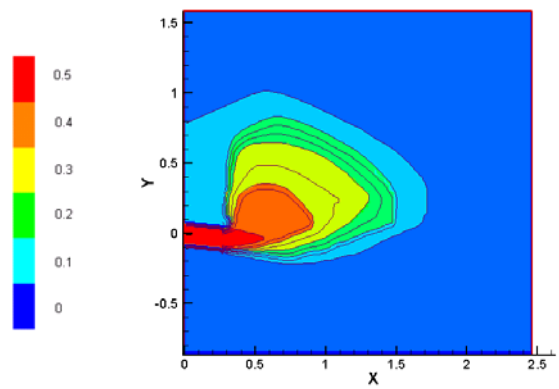

Figure 3.60 Coke particle distributions for baseline case (volume fraction of coke)

Baseline Case

Results of baseline case are displayed in Figures 3.64 and 3.65. Figure 3.64(a) shows that most of the combustion happens toward the center of the raceway. The curved line in the figures represents the outermost porosity iso-surface of the raceway. Almost all of the CO_2 is consumed before leaving the raceway as shown in Figure 3.64(b). The methane is consumed almost immediately upon entering the raceway as displayed in Figures 3.64(c). The oxygen is also consumed almost immediately upon entering the raceway as indicated in Figures 3.64(d).

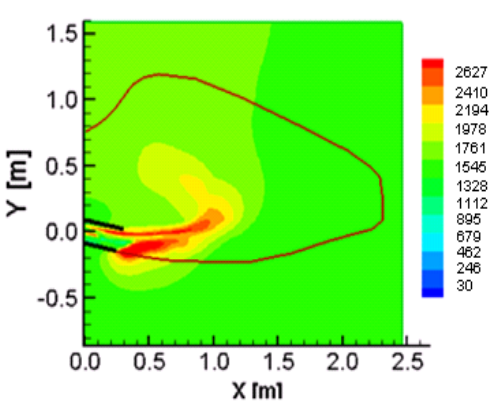

(a) T_g (C)

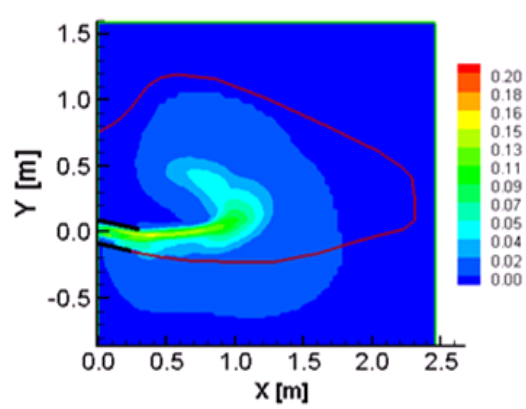

(b) CO_2

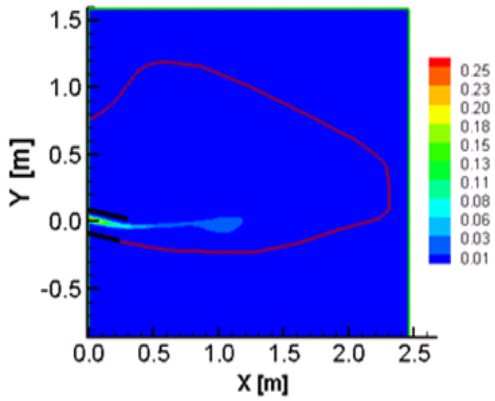

(c) CH_4

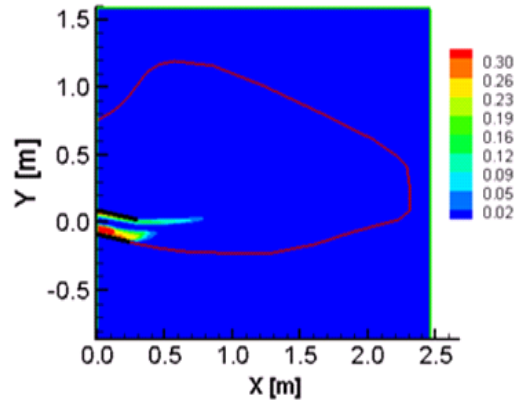

(d) O_2

Figure 3.61 Gas temperature and compositions for baseline case

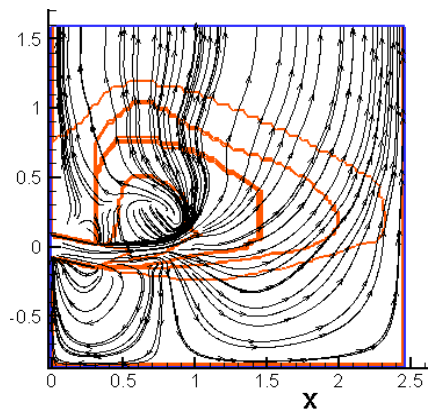

(a) Gas stream lines

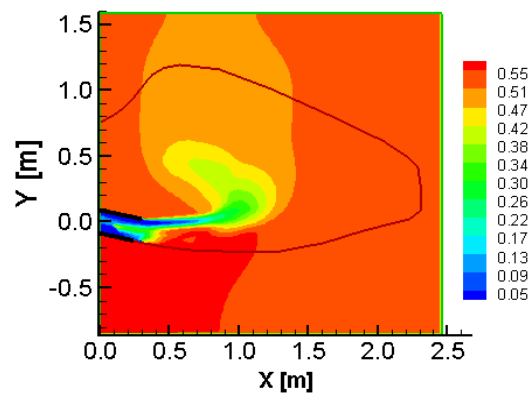

(b) CO (mass fraction)

Figure 3.62 Gas flow filed and CO distribution for baseline case

Figure 3.65 (a) shows the streamlines of the gas phase. Two major recirculation zones can be seen above and below the tuyere. Figure 3.65 (b) shows the contours of mass fraction of CO. A build up of CO can be seen below the tuyere. This is because of the low gas velocity in this region.

Effect of Carrier Air Rate

Figure 3.66 shows the effect of carrier air rate on gas temperature. It indicates that carrier air rate has little effect on combustion. This is because even though the carrier air rate is changed, the PCI rate is held constant, and the PCI has about the same velocity once it reached the raceway due to the high velocity of the blast air. The curved lines in the figures represent iso-surfaces of porosity within the raceway. Analysis also shows that carrier air rate also has little effect on coke consumption and species concentrations for the same reason as discussed above.

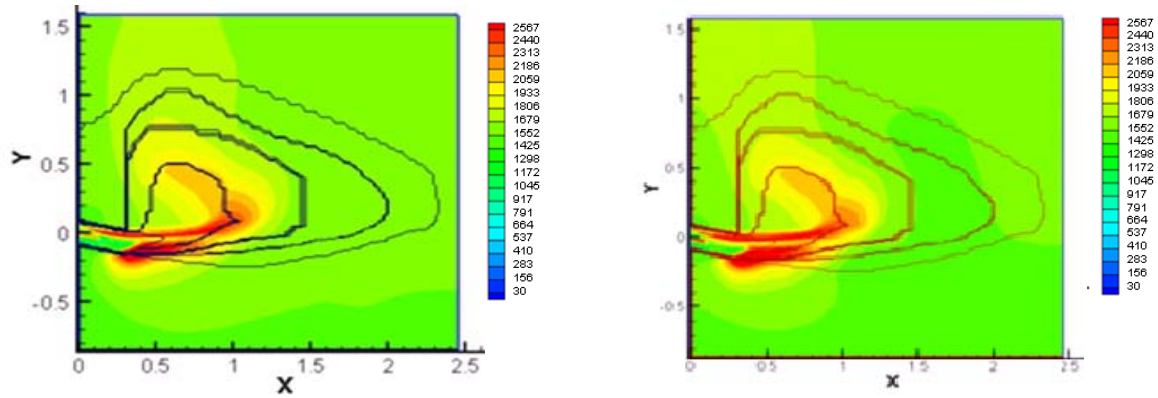

(a) Baseline case (Carrier air = 0.0575kg/s) (b) Case 1 (Carrier air = 0.046kg/s)

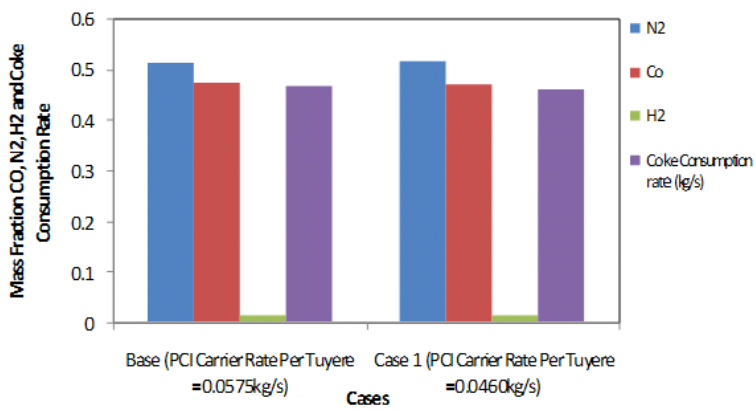

(c) Gas species concentrations and coke consumption

Figure 3.63 Effect of carrier gas flow rate on raceway combustion

Effect of Natural Gas Flow Rate

Three cases have been studied with different natural gas flow rates, which are 0.180 kg/s, 0.146 kg/s, 0.114 kg/s per tuyere for Baseline case, Case 2, and Case 3 respectively. Figures 3.64(a), 3.64(b), and 3.64(c) compare the effect of natural gas flow rate on the gas temperature in the raceway. The natural gas flow rate was increased from Figure 3.64(a) to 3.64(b), and increased more from 3.64(b) to 3.64(c). From this, it can be seen that although the maximum temperature remains about the same, the temperature distribution is changed. With higher natural gas rates, the high temperature does not penetrate as far into the furnace since the oxygen is consumed much faster by the natural gas. Figures 3.64(d), 3.64(e), and 3.64(f) show the effect of natural gas flow rate on methane mass fractions in the raceway. It can be seen that reducing the natural gas flow rate causes a reduction in methane penetration into the raceway.

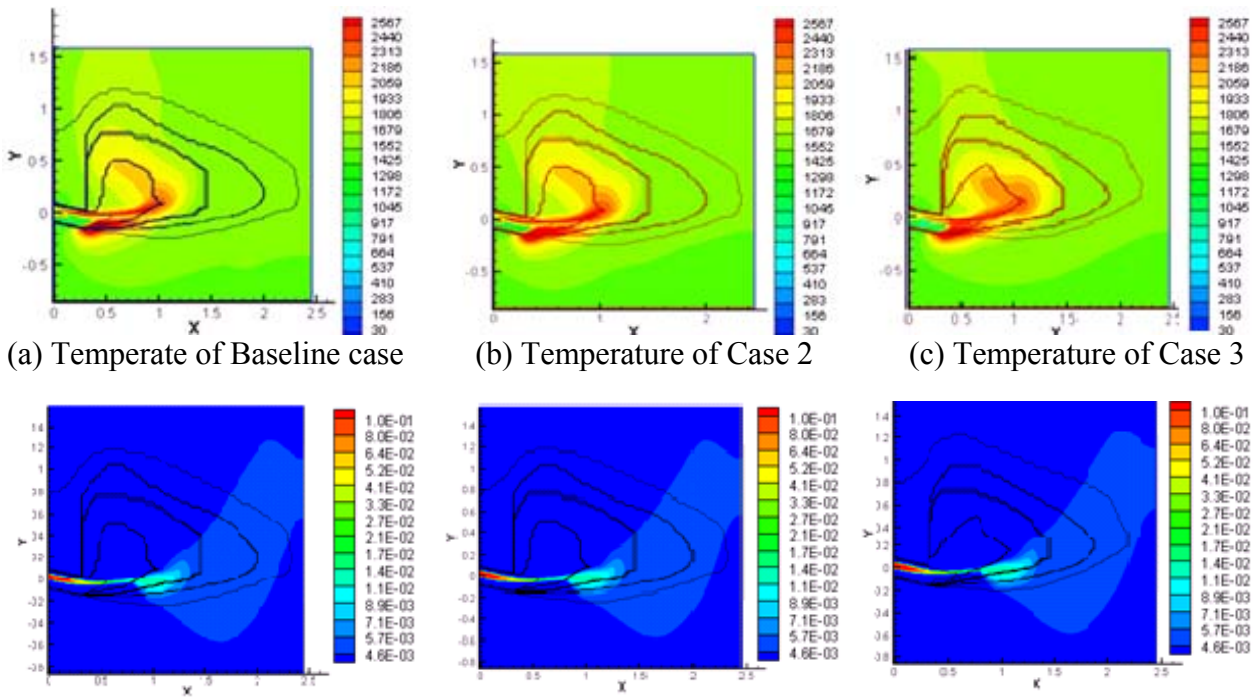

(a) Temperate of Baseline case (b) Temperature of Case 2 (c) Temperature of Case 3

(d) CH_4 of Baseline case (e) CH_4 of Case 2 (f) CH_4 of Case 3

Figure 3.64 Effect of natural gas flow rate on raceway combustion

Figure 3.68(a) shows the effect of reducing natural gas rate on major species and Figure 3.68(b) shows the coke consumption at the outlet of the model. Reducing the natural gas rate increases coke consumption as expected. Mass fraction of CO increases, since the combustion shifts from CH4 to coke due to the higher availability of oxygen to the coke. The increase in hydrogen mass fraction from the Baseline case to Case 3 is a result of keeping the RAFT (raceway adiabatic flame temperature) constant as the methane rate decreased, by increasing steam injection and decreasing the oxygen content of the blast. However, the hydrogen is produced at the expense of increased coke consumption.

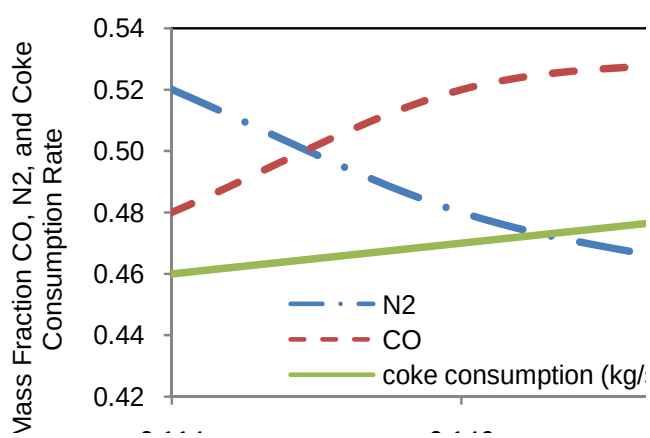

(a) The effect of reducing natural gas rate on major species

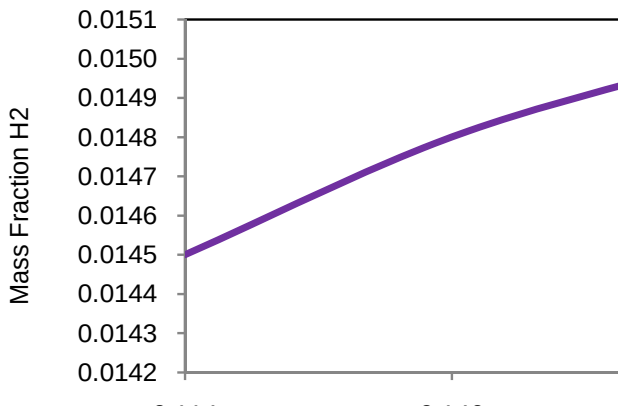

(b) Coke consumption at the outlet of the model

Figure 3.65 Coke consumption and major species distributions

Effect of Oxygen Lance Flow Rate

The effects of oxygen lance flow rate on raceway temperature, size, and O_2 distribution have been investigated. Figures 3.69 (a) and (b) show the results of the Baseline case with the oxygen flow rate at 0.107 kg/s. The Figures 3.69 (c) and (d) show the results of Case 5 with the oxygen flow rate at 0.0711 kg/s. It can be seen in Figures 3.69 (a) and 3.69(c) that oxygen lance flow rate changes the combustion rate inside the tuyere, and changes the raceway shape and size. It can be seen that the region of high temperature in 3.69 (c) is larger and more pronounced that in 3.69 (a). One may ask why lowering the oxygen lance injection rate would cause more combustion? It has been shown in a previous paper that inside the tuyere, the co-annular oxygen injection around the PCI produces an insulating effect, and less coal combustion happens inside the tuyere as a result. These results show that this effect carries over into the raceway, and less combustion is the outcome.

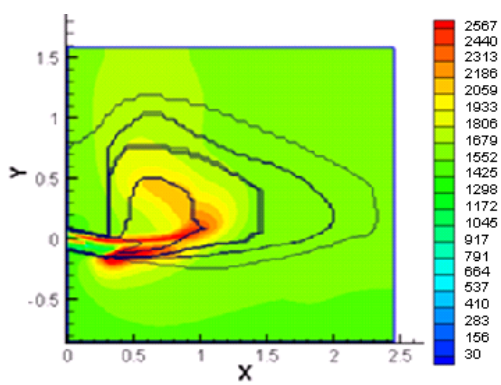

(a) Temperature (˚C) for Baseline case

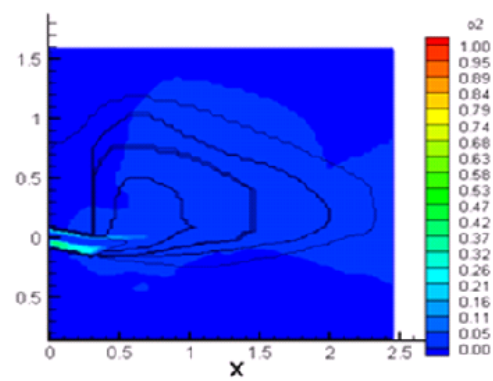

(b) Oxygen mass fraction for Baseline case

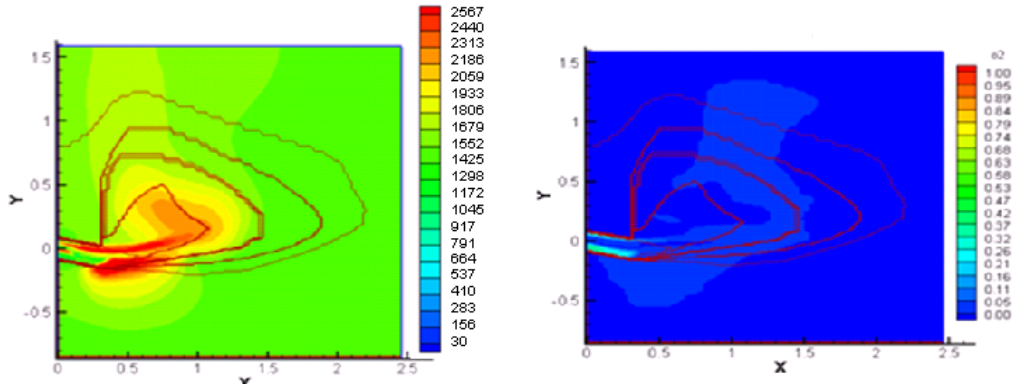

(c) Temperature (˚C) for Case 5 (d) Oxygen mass fraction for Case 5

Figure 3.66 Effect of oxygen lance flow rate on raceway combustion

Effect of Blast Temperature

Two blast temperatures (1099 ˚C for Baseline case and 982 ˚C for Case 4) have been considered. Figures 3.67 (a) and 3.67 (b) show that gas temperature in the raceway decreases when the blast temperature is lower. Although the gas temperature is higher in the Baseline case, the RAFT was kept constant for Case 4 by decreasing the methane rate, and increasing the steam's mass fraction.

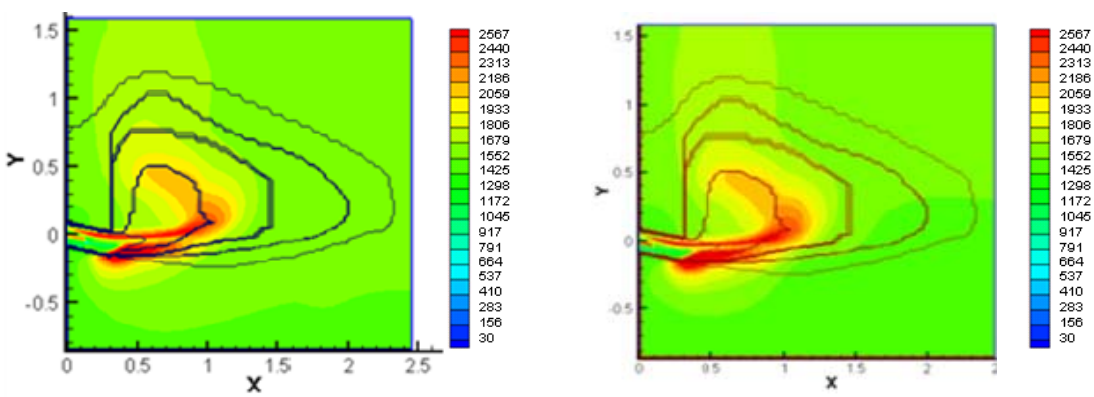

(a) Baseline case (˚C) b) Case 4 (˚C)

Figure 3.67 Effect of blast temperature on temperature distribution

Figure 3.68 shows that Case 4 demonstrated slightly higher coke consumption in the raceway, and a higher mass fraction CO at the outlet. This effect is due to gasification of coal and coke by the higher level of steam in the blast gas.

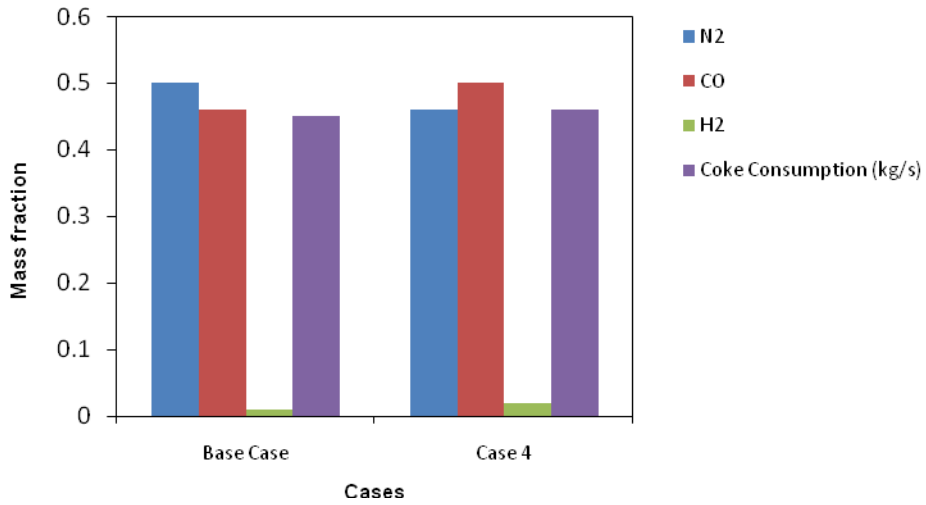

Figure 3.68 Species concentrations and coke consumption in the raceway

Figure 3.69 shows the average gas temperature on the outlet of the model for all six cases. Due to the careful formulation of the operating parameters with the intent of maintaining a constant raceway adiabatic flame temperature (RAFT), the average gas temperature has remained very close for all of the cases. The reason for choosing the cases in this way was to make the simulation as close as possible to realistic operating conditions.

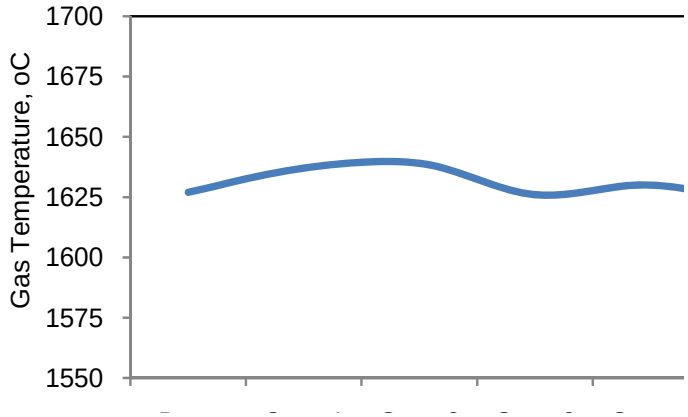

Figure 3.69 Average gas temperature for all cases

As a means of showing the ability of the co-injectants (methane and PCI) to combust instead of coke, the concept of coke consumption ratio is introduced. It should be made clear that this should not be confused with so-called "coke replacement ratio", as this has been defined in many different ways, and now has very specific meaning. Here, coke consumption ratio is defined as:

$$\frac{\left(\begin{array}{c}\text{Total mass of coke required to}\\ \text{react with all oxygen in the system}\end{array}\right) - \left(\begin{array}{c}\text{Total mass of coke}\\ \text{consumed in the simulation}\end{array}\right)}{(\text{PCI mass flow rate}) + (\text{CH4 mass flow rate})}$$

Figure 3.70 shows the coke consumption ratio for the different cases. It can be seen that the highest coke consumption ratio occurred in case 3, and the lowest in case 1.

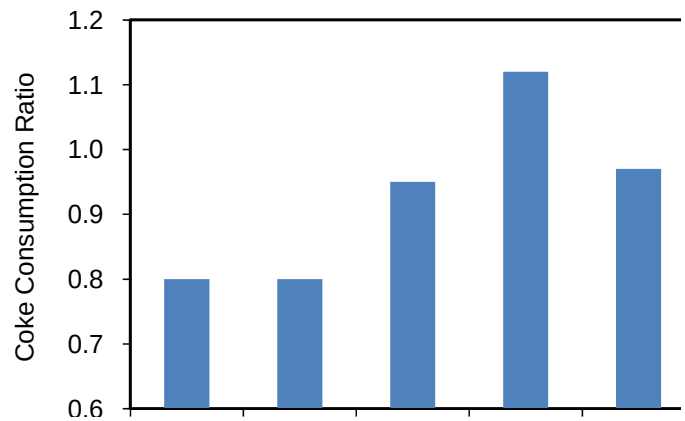

Figure 3.70 Coke consumption ratio for all cases

Summary

CFD simulations have been performed to evaluate the benefits of natural gas co-injection with pulverized coal injection. Detailed analyses have been conducted to investigate the heat transfer between hot blast, lance wall and flows inside the lance, temperature distribution in the lance wall, natural gas combustion and coal devolatilization and combustion. The flow characteristics and combustion of coke, coal and natural gas in the raceway have also been analyzed in detail. It has been found that the addition of natural gas greatly increases devolatilization rates and the availability of hydrogen to the furnace. With the current lance arrangement, varying the natural gas flow rate has little effect on the maximum oxygen lance temperature. Carrier air flow rate and oxygen flow rate through the oxygen lance have similar effects on devolatilization. Reducing either of these parameters causes an increase in devolatilization. PCI carrier rate has no significant effect on lance wall temperature. Reducing blast air temperature not only reduces devolatilization, but also decreases the amount of reducing gases going into the furnace. It has also been shown that blast air temperature has little effect on lance temperatures as well. It was found that while the carrier air rate has little effect on combustion in the raceway, other parameters such as natural gas flow rate can have high impact on raceway combustion. It has also been shown that the oxygen flow rate through the annular oxygen lance blankets the PCI, and hinders the coal combustion process. The CFD simulations have also confirmed that the RAFT calculation used to determine the various parameters (i.e. blast temperature, steam injection rate, natural gas injection rate, etc.) would in fact result in constant overall raceway temperatures.

These simulation results have provided good references for PCI lance design, lance arrangement, lance protection, and selection of tuyere practices to achieve the optimized natural gas and PCI rate. Some of these results have been implemented in the operation of a blast furnace by one of the industrial participants.

.

3.2.5 Design of PCI Conditions

One of industrial participants is in the process of introducing PCI technology into their blast furnace operations. In order to help the design of the PCI system and determine operating conditions, a number of simulations have been performed based on conditions provided by the industrial participant. The injection system is shown in Figure 3.71. The tuyere diameter is 0.165m at a downward angle of 7°. The simulation parameters and conditions are listed in Tables 3.20 and 3.21. Effects of the blast temperature, extent of oxygen enrichment, tuyere size, and the pulverized coal mass flow rate have been investigated.

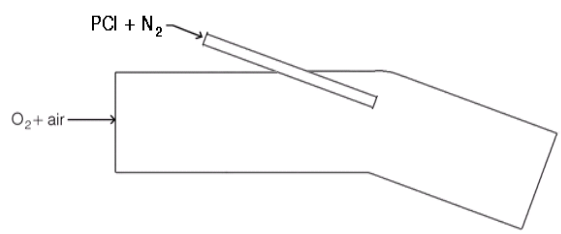

Figure 3.71 Geometry for injection system simulations

Table 3.20 Baseline operating conditions for PCI design

Hot Blast Conditions	
Temperature	1338 K
Pressure	3.313 atm
Mass flow rate	3.412 kg/s
Oxygen content	25 wt %
Proximate analysis of coal	
Fixed carbon	52.64 %
Volatile matter	33.81 %
Ash	7.02 %
Moisture	6.53 %
Other conditions	
Tuyrene	165.1 mm
Lance diameter	25.0 mm
Carrier mass flow rate	0.037 Kg/s
PCI Rate	0.357 Kg/s

Table 3.21 Parameters Studied for PCI design

Case Number	Study Detail	Blast Temperature (K)	Volume Nm3/min	Pressure atm(abs)	Oxygen %	Moisture gr/Nm3	Coal Rate kg/min	Tuyere Diameter, m
1	Base Case	1338.6	160.6	3.313	25.02	14.483	21.394	0.1651
2	Vary Blast Temperature	1283.0	160.6	3.313	25.02	14.483	21.394	0.1651
3	Vary Blast Temperature	1394.1	160.6	3.313	25.02	14.483	21.394	0.1651
4	Vary Blast Temperature	1449.6	160.6	3.313	25.02	14.483	21.394	0.1651
5	Vary Tuyere Diameter	1338.6	160.6	3.313	25.02	14.483	21.394	0.1397
6	Vary Blast Oxygen	1338.6	160.6	3.313	26.02	14.483	21.394	0.1651
7	Vary Blast Oxygen	1338.6	160.6	3.313	27.02	14.483	21.394	0.1651
8	Vary Blast Oxygen	1338.6	160.6	3.313	29.02	14.483	21.394	0.1651
9	Vary Coal Rate	1338.6	160.6	3.313	25.02	14.483	24.451	0.1651
10	Vary Coal Rate	1338.6	160.6	3.313	25.02	14.483	27.507	0.1651

PCI Injection System

Baseline case

Figure 3.72 shows the gas velocity and coal particle trajectories in the injection system. The slower nitrogen flow from the lance gradually gets momentum from the surrounding blast air, with its velocity close to the later at the exit of the tuyere as shown in Figure 3.72(a). From Figure 3.72(b), it can be shown that after escaping from the narrower lance tip, pulverized coal particles disperse gradually as they move forward. The legend of Figure 3.72(b) indicates that residence time of coal particles before the tuyere is no more than 0.04s.

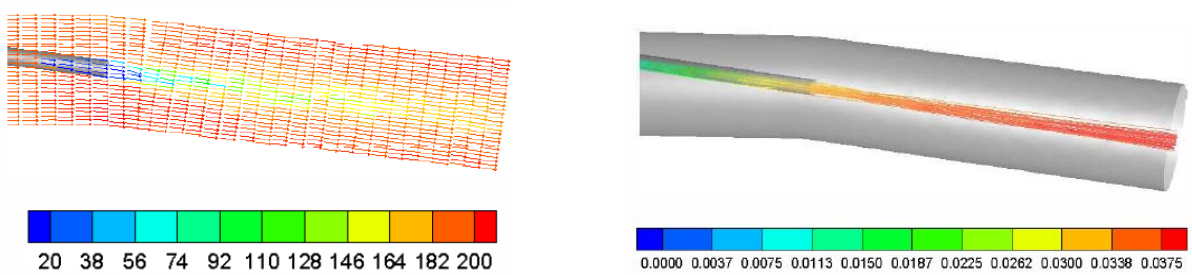

(a) Gas velocity colored by magnitude (m/s) (b) Coal trajectories colored by residence time(s)

Figure 3.72 Gas and solid flow characteristics in the injection system

In a blast furnace, hot blast constitutes the main source for coal particle heating. The mixing of the primary stream of pulverized coal and hot blast is identified by the gas phase temperature distribution. Figure 3.73 shows the temperature distributions of the gas phase in the reacting flow. Obviously, the temperature is relatively low in the vicinity of the lance. This helps to keep the lance cool, thus prolonging the lifespan of the lance. The cooler carrier flow from the lance gets heat from the hot blast air. With the temperature high enough, the heated coal particles

begin to evaporate and release volatile matter, see Figure 3.74. The volatiles are generally evolved in about 100ms at 400K and, play an important role in flame stabilization inside the raceway. After that, gas combustion concentration of carbon dioxide (see Figure 3.75) in the center of the tuyere exit.

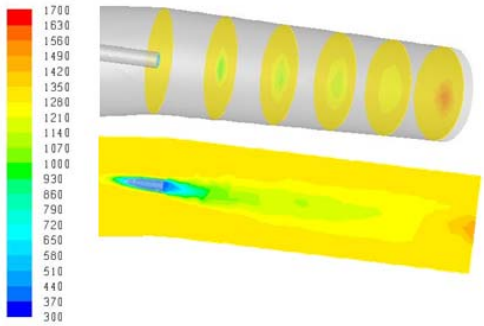

Figure 3.73 Gas temperature (K)

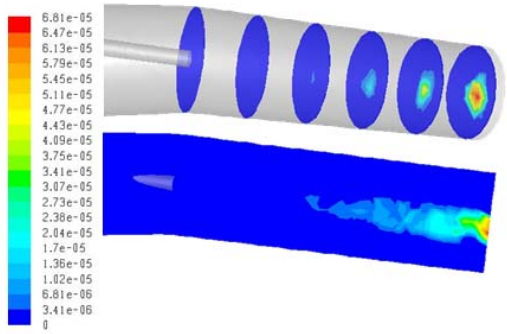

Figure 3.74 Devolatilization rate (kg/s)

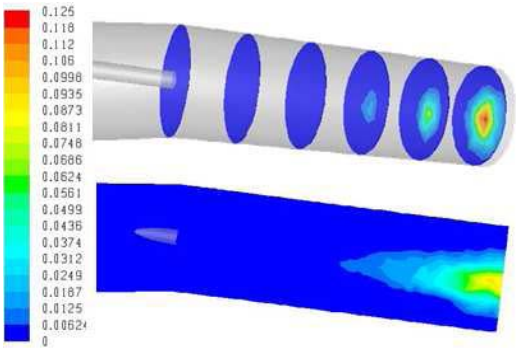

Figure 3.75 Mass fraction of CO_2

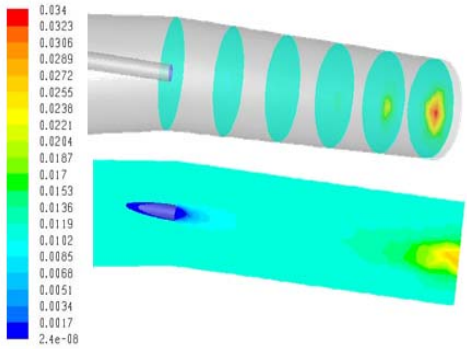

Figure 3.76 Mass fraction of H_2O

Effect of Blast Temperature

Three cases of different hot blast temperature were also conducted. Figure 3.77 describes the rising behavior of the coal temperature. As shown in the figure, generally, once the coal particles enter into the major flow, they will be heated up quickly by the background hot blast, and experience rapid vaporizing process and the successive devolatization. However, from Figure 3.78, it can be seen clearly that the blast temperature has notable impact on the volatile releasing pattern. With the increasing blast temperature, devolatilization rate becomes higher. When the temperature increases from 1283K to 1449K, corresponding devolatilization rate remarkably shifts 0.004kg/s to 0.045 kg/s.

As indicated in Figure 3.79, in the circumstance of elevated blast flow and enriched oxygen, combustion happens to the released volatile matter. Similarly, increasing blast temperature induces wider and denser CO_2 distribution, earlier combustion flame and higher

burnout fraction than one might expect. All these in turn result in higher coal temperature in the later phase for hotter blast air, as shown in Figure 3.79. This arises from the fact that the devolatilization phenomena are principally determined by particle temperature, which is closely related to the hot blast temperature. Therefore, the higher the hot blast temperature is, the more effective are the coal reactions, as predicted.

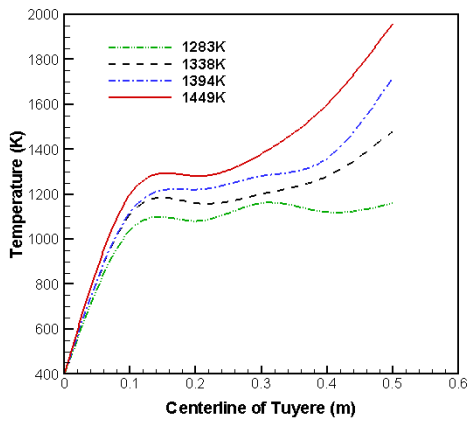

Figure 3.77 Effect of blast temperature on the coal temperature along the tuyere centerline

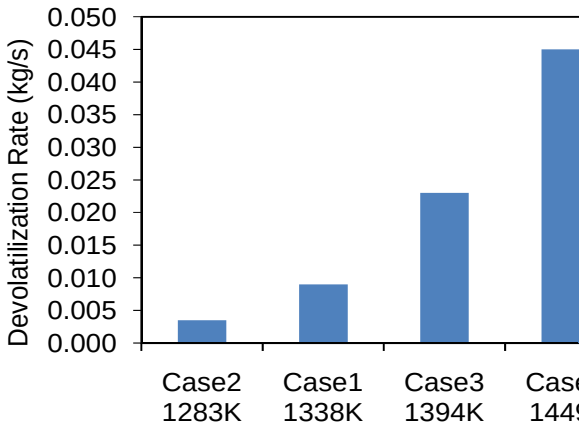

Figure 3.78 Effect of blast temperature on the devolatilization rate (kg/s)

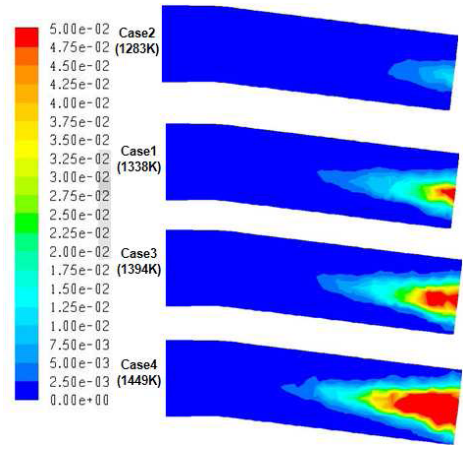

Figure 3.79 Effect of blast temperature on the mass fraction of CO_2

Effect of Tuyere Diameter

From different aspects, Figures 3.80 - 3.82 manifest the effect of the tuyere diameter on the pulverized coal combustion behavior. With all other operating conditions identical with each other, only the tuyere diameter is different between Case 1 and Case 2, 165.1mm and 139.4 mm, respectively. Having the same mass flow rate, for the case of smaller tuyere diameter, pulverized coal particles pass through the tuyere more quickly than that of larger one. Consequently, higher

velocity results in a shorter residence time in a smaller tuyere and a lower volatile release rate when compared with the condition of the Case 1, see Figure 3.80. Correspondingly, Figure 3.81 shows that more combustion takes place near the exit of tuyere in Case 1 than that in Case 2 with the smaller tuyere diameter. Also, there are corresponding trend in the distributions of temperature in Figure 3.82. Based on the above discussion, it can be shown that, to some extent, the tuyere of larger size may be an option to lengthen the residence time and improve the coal combustion efficiency.

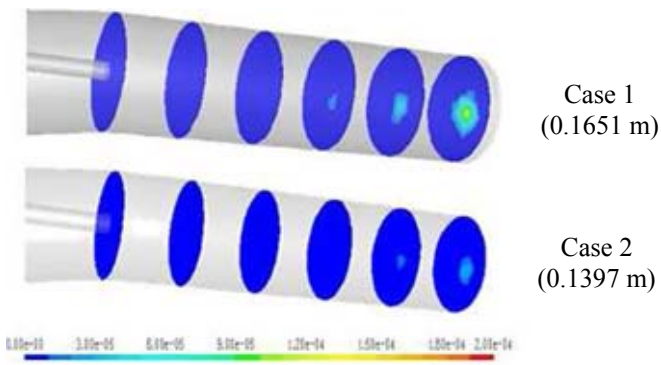

Figure 3.80 Effect of tuyere diameter on the devolatilization rate (kg/s)

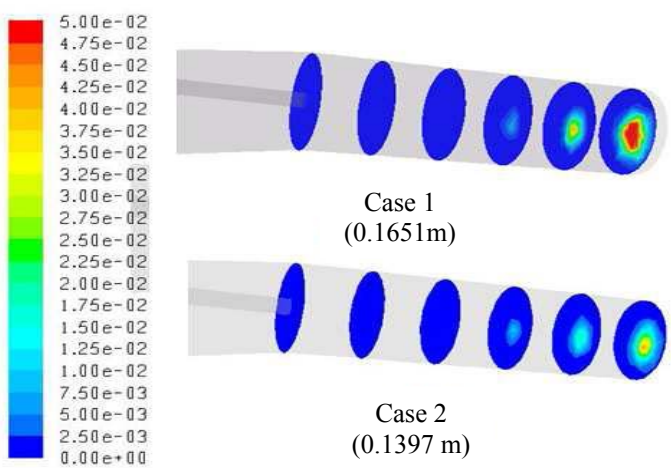

Figure 3.81 Effect of tuyere diameter on the mass fraction of CO_2

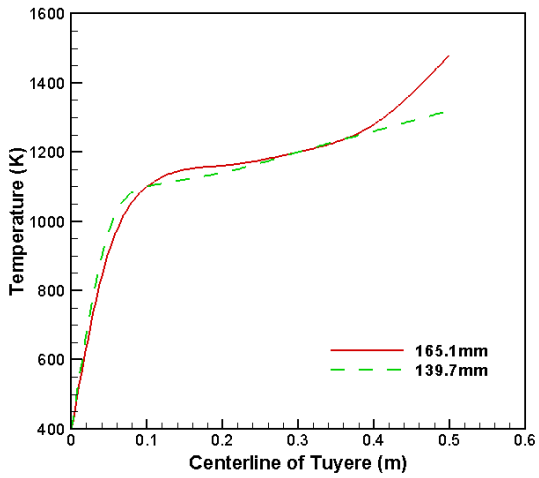

Figure 3.82 Effect of tuyere diameter on the coal temperature along the tuyere centerline

Effect of Oxygen Enrichment

Oxygen enrichment plays an important role in optimizing the furnace operation and enhancing the productivity. To understand the role played by oxygen concentration upon PC combustion, the temperature fields of PC at four different oxygen concentrations, consisting of 25% (Case 1), 26% (Case 6), 27% (Case 7), and 29% (Case 8), are simulated and demonstrated in Figure 3.83. The figure depicts that pulverized coal combustion in the blowpipes and tuyeres will be intensified if the oxygen concentration in the hot blast is increased. Figure 3.84 indicates that the volatile release rate increases a bit as the oxygen concentration is enriched from 25% to 27%, and a little higher for the case of 29% O_2. However such increments are as notable as that caused by the change in blast temperature. The reason causing this feature is that the characteristic times for particles traveling in the tuyere are very short, whereas the time required for unburned char to react with oxygen is much longer. Consequently, coal devolatilization becomes the dominant reaction in the tuyere, and the reaction is as sensitive to the oxygen concentration as expected.

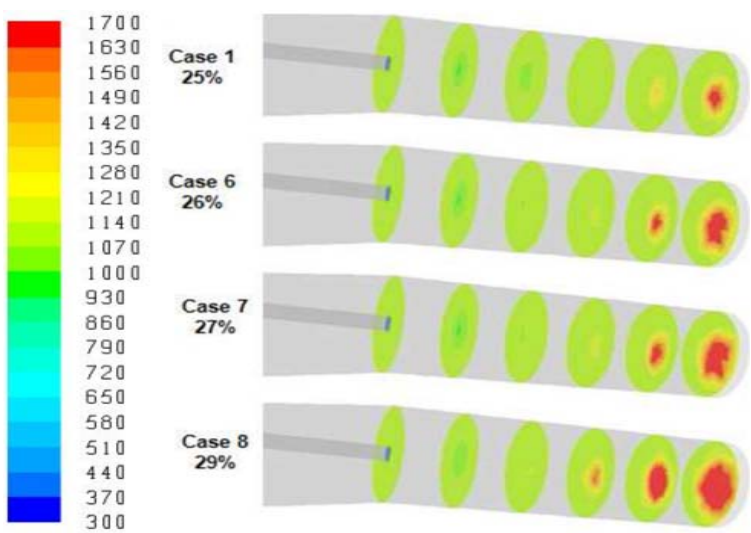

Figure 3.83 Effect of oxygen enrichment on the gas temperature distributions (K)

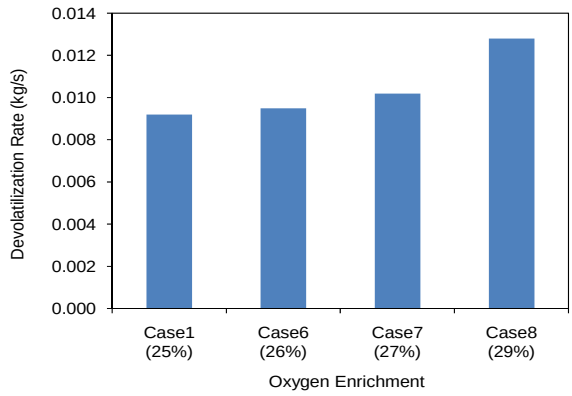

Figure 3.84 Effect of oxygen enrichment on the devolatilization rate (kg/s)

Coal and Coke Combustion inside Raceway

Detailed analysis of combustion inside the raceway has also been made. According to the multi-step methodology, the information obtained from the simulation of injection system in Step 1 is used as the input of simulations of other steps.

Baseline Case

Figure 3.85 shows the gas temperature in a plane across the tuyere centerline. The inlet has a lower temperature region due to low injection temperature of the pulverized coal and carrier compared with the high blast air temperature. The central zone gas and injected coal particle temperature increase rapidly due to the heat exchange between the gas and the coal particles.

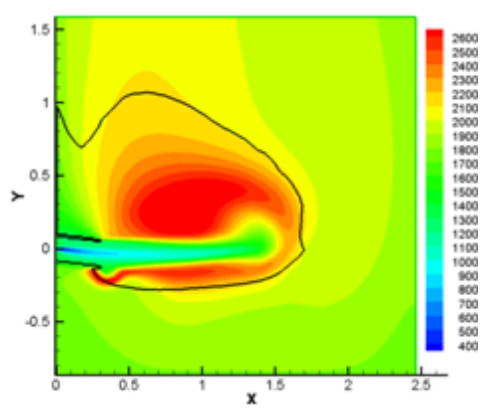

Figure 3.85 Gas temperature distributions

Species distributions along the tuyere central line are shown in Figure 3.86. The oxygen distribution is shown in Figure 3.86 (a), the oxygen concentration in the coal plume region is

lower as the carrier gas used is N_2 and the volatile matter is released from the coal particle in this region. The combustion procedure can also be seen clearly from the temperature and species distributions along the tuyere central lines. Along the centerline of the tuyere to its nose, the O_2 concentration decreases rapidly, the gas temperature and CO_2 concentration increase, meaning that combustion is occurring.

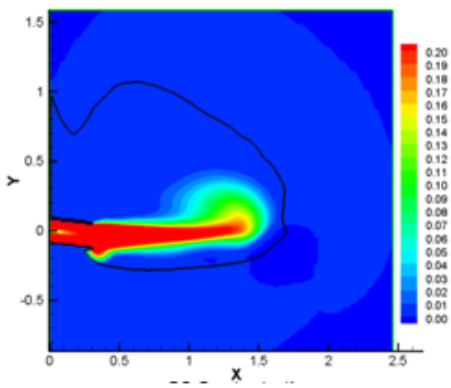

(a) O_2

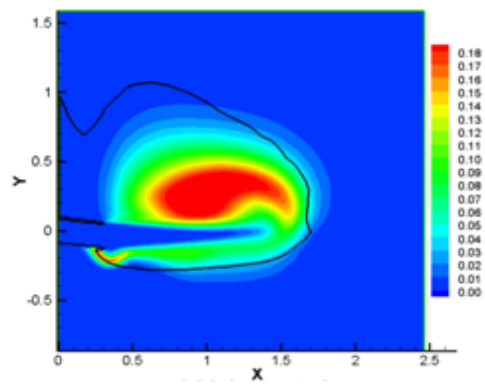

(b) CO_2

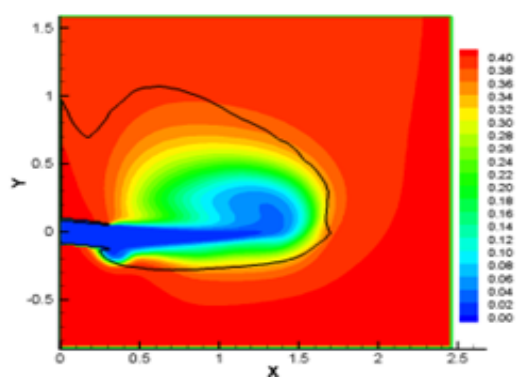

(c) CO

Figure 3.86 Species distribution along the tuyere central line

Effect of Blast Temperature

Four different blast temperatures are considered including the Baseline case temperature (Case 1 and Cases 2 to 4). The gas temperature distributions for the four cases are shown in Figure 3.87. The higher the blast temperature the higher the observed gas temperature in the raceway, as well as the higher the exit temperature, Figure 3.88.

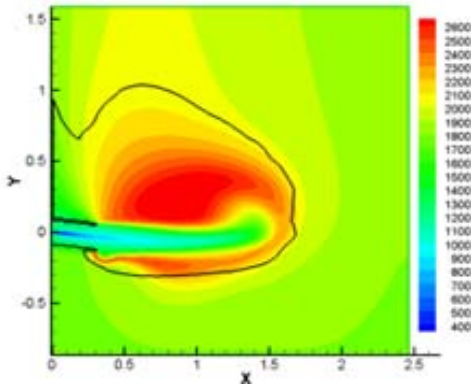

(a) T = 1283.0 K

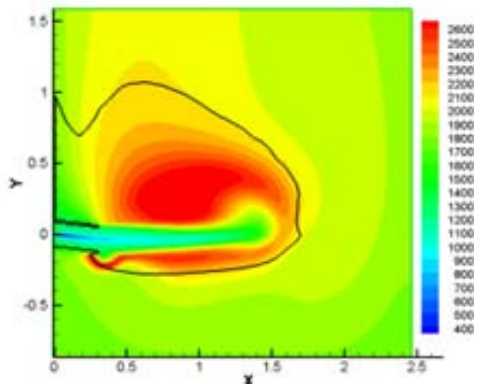

(b) T = 1338.6 K (Baseline case)

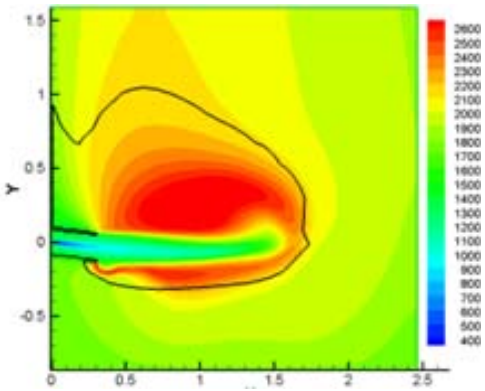

(c) T = 1394.1 K

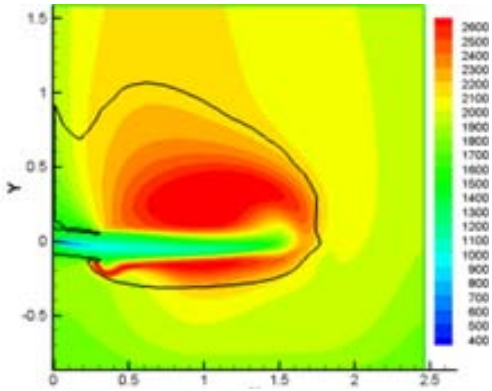

(d) T = 1449.6 K

Figure 3.87 Gas temperatures (K) for different blast temperature

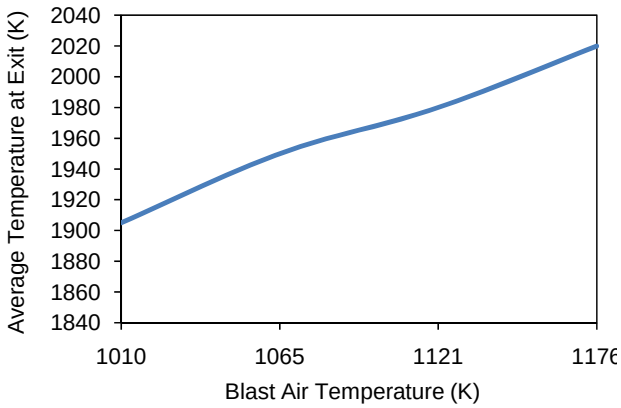

Figure 3.88 Exit temperatures at different blast temperature

The effect of blast temperature vs. the percentage of burned coal is also analyzed. The higher the blast temperature, the greater is the observed percentage of burnt coal, as shown in Figure 3.89.

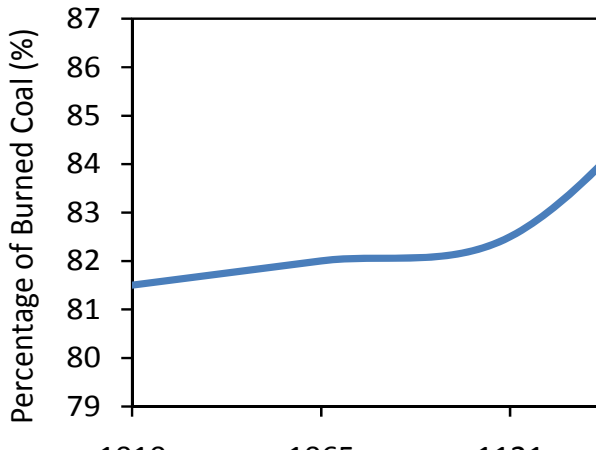

Figure 3.89 Percentage of burned coal vs. blast temperature

Effect of Oxygen

Four different oxygen percentages are considered including the Baseline case temperature (Case 1, Cases 6 to 8). The gas temperature distributions for the four cases are shown in Figures 3.90 (a) to (d). The higher the oxygen's percentages, the higher the observed gas temperature was in the raceway.

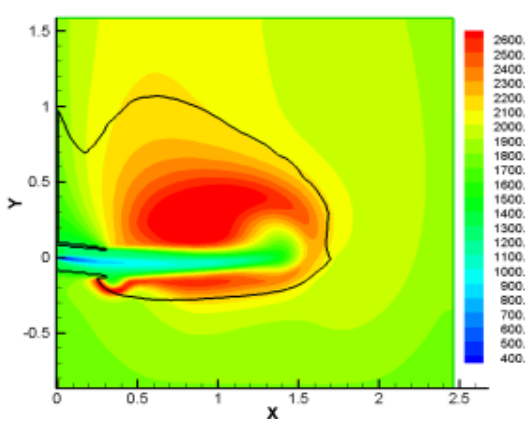

(a) O_2 = 25.02% (Baseline case)

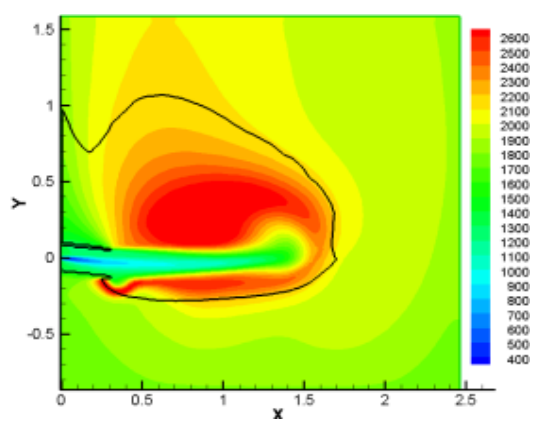

(b) O_2 = 26.02%

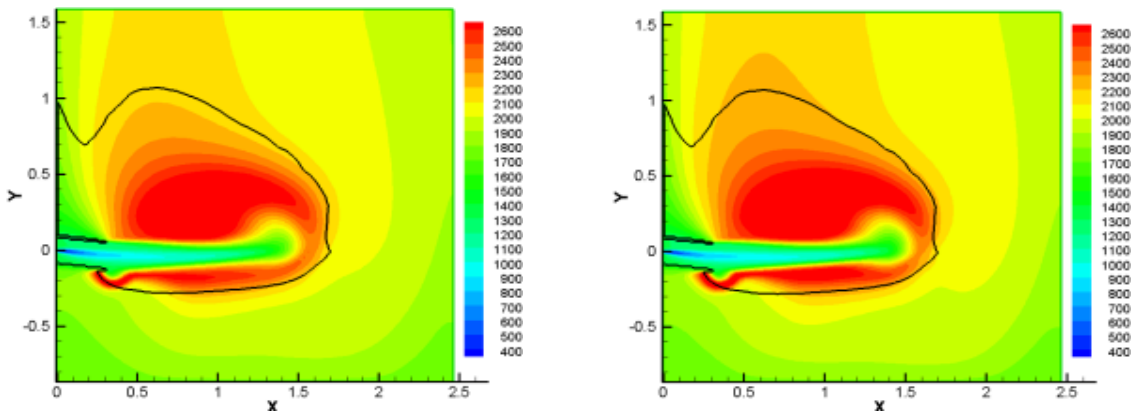

(c) O_2 = 27.02% (d) O_2 = 29.02%

Figure 3.90 Gas temperatures as the effects of oxygen (K)

Effect of PCI Rate

Three different PCI injection rate are considered including the Baseline case (Case 1, Cases 9 and 10). The effects for the average temperature at exit vs. the PCI injection rate are shown in Figure 3.91. The lower the PCI injection rate, the higher the average temperature at exit. As a result, the lower the PCI injection rate, the higher the observed percentage of burned coal, as shown in Figure 3.92.

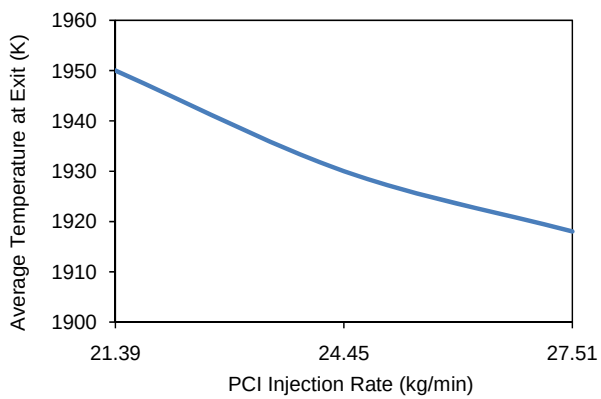

Figure 3.91 Exit temperatures at different PCI injection rate

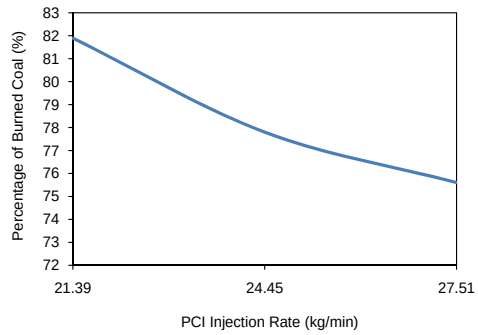

Figure 3.92 Burned coal % at different PCI injection rate

Effect of Tuyere Size

Two different tuyere diameters are considered including the Baseline case (Case 1 and Case 5).The effects of tuyere size on gas temperate are shown in Figure 3.93. The larger diameter corresponds to the lower gas temperature, which indicates that the combustion condition for bigger diameter tuyere is better than the smaller diameter tuyere. It can also be seen clearly in Figures 3.94. The larger the tuyere's diameter, the higher percentage of burned coal and the lower the averaged temperature at exit.

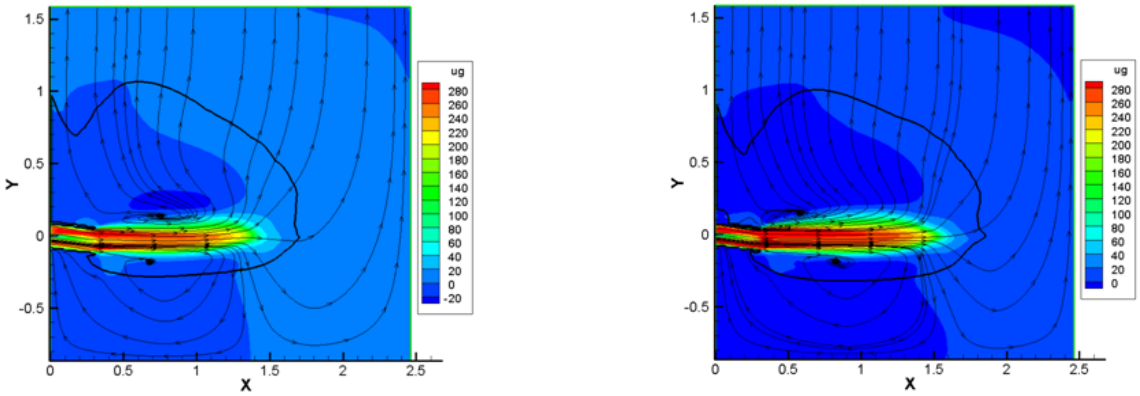

(a) Tuyere diameter = 0.1651m (b) Tuyere diameter = 0.1397m

Figure 3.93 Gas temperature vs. different tuyere diameter

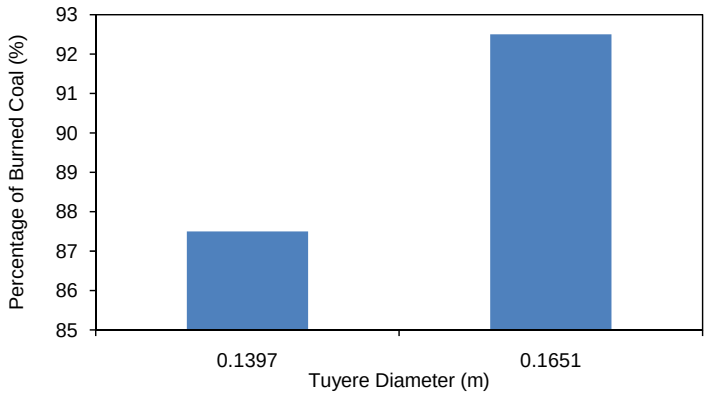

Figure 3.94 Coal burnt ratio at different tuyere diameter

Summary

A 3-D multiphase reacting computational model has been developed to simulate pulverized coal and coke combustion inside tuyere and raceway. Simulation results show that higher blast temperature has a higher coal burned out percentage, and a higher average exit gas temperature. As PCI flow rate increases, the coal burned out percentage will decrease, and the exit average gas temperature will decrease. When tuyere size is decreased, the depth of the raceway becomes larger because of the higher blast air velocity. The coal burned out percentage will increase, and the exit average gas temperature will decrease since the total burned out coke will decrease. The simulation results have provided information for the design and operation of PCI process.

4 CONCLUSIONS

Introduction of pulverized coal injection (PCI) to the blast furnace has been recognized as one of the most important developments in the iron making industry. In order to have a better understanding of the complex phenomena in the PCI process as well as to determine the impact of key parameters for the design and optimization of the system, efforts have been made to develop comprehensive 3-D multiphase CFD models for the PCI process simulations. To have more efficient and accurate simulations, a multi - step methodology has been developed. The main features of these CFD models and the methodology are summarized below:

1. CFD model for injection systems:
    - Complete geometry of blowpipe, lance and tuyere
    - Simulation of 3-D, turbulent, multiphase multispecies reacting flows
    - Lagrangian tracking of particles
    - Pulverized coal injection
    - Natural gas co-injection
    - Combustion of coke, coal, and natural gas
2. CFD model for raceway formation
    - Real geometry of blast furnace
    - Simulation of 3-D, transient, turbulent, multiphase flows
    - Eulerian approach
    - A multi-fluid granular model for describing the flow behavior of the fluid-solid mixture.
    - Non-uniform porosity distribution of coke bed
    - Consideration of combustion effects by including additional mass and volume expansion due to combustion
3. CFD model for combustion in raceway
    - Simulation of 3-D, turbulent, multiphase, multispecies flows
    - Coke combustion
    - Coal combustion
    - Natural gas co-injection
    - Non-uniform porosity distribution of coke bed
    - Predicted raceway shape
4. Multi-step methodology
    - Integration of all the CFD models
    - Complete simulation of PCI process

The CFD models have been validated by comparing simulation results with experimental data with acceptable agreements. A large number of simulations have been conducted to apply the CFD models and the methodology to actual blast furnace conditions for various industrial participants. Detailed information of flow and combustion properties has been analyzed for all the simulations. These simulations have served for the following purposes based on industrial requests:

1. Better understanding of the flow characteristics and combustion behavior

2. Identification of the cause of problems (trouble shooting)
3. Guidance for PCI lance design, lance arrangement, and lance protection
4. Determinations of impacts of key parameters on PCI combustion performance
5. Direction of optimization strategies for PCI operating conditions

During the course of this research, close interactions between academia and industry as well as collaborations between project participants have ensured the successful completion of the project. A number of undergraduate and graduate students have gained valuable research experience and are well trained for solving real world iron/steel making problems.

5 LIST OF REFERENCES

[1]. Petel, R., Hutny W., Price J.T. (2002). Energy and Energy Consumption and CO_2 Emissions in an Ironmaking Process. Advances in Environmental Research, 6, 157-170.

[2]. Peacey J. G., Davenport W. G. (1979). The Iron Blast Furnace: Theory and Practice. Oxford: Pergamon Press.

[3]. Biswas A. K. (1981). Principles of Blast Furnace Ironmaking: Theory and Practice. Australia: Cootha Publishing House

[4]. Huang, D. ., Zhang Yu, Deshpande Rohit, Chaubal Pinakin, Zhou Chenn Q. (2007). Simulation of the Hearth Draining Process and Thermal Stress of a BF Hearth. AISTech 2007 : Proceedings of the Iron and Steel Technology Conference, 1, 475-485.

[5]. Burgess J. M. (1979). The Potential of Coal as a Blast Furnace Injecting. BHP Tech. Bull., 23, 66.

[6]. Wakuri Shinijiro, Mochizuki Shiro, Baba Masaki, Misawa Junji.(1984). Operation of Pulverized Coal Injection into Large Blast Furnace with High Top Pressure. Transactions ISIJ, 24, 622-630.

[7]. Worrell Ernst, Price Lynn, Martin Nathan. (2001). Energy Efficiency and Carbon Dioxide Remissions Reduction Opportunities in the US Iron and Steel Sector. Energy, 26, 513-536.

[8]. Schofield N., Fisher R., Anderson D. R. (2004). Environmental Challenges for the Iron and Steelmaking Process. Ironmaking and Steelmaking, 31 (6), 428-431.

[9]. Ameling Dieter, Steffen Rolf. (2005). Challenges for the EU Steel Industry. Ironmaking and Steelmaking, 32 (3), 187-190.

[10]. Wu Long, Paterson N., Dugwell D. Kandiyoti R., R. (2007). Simulation of Blast-Furnace Tuyere and Raceway Conditions in a Wire Mesh Reactor: Extents of Combustion and Gasification. Energy & Fuels, 21, 2325-2334.

[11]. Nomura Shin-Ichiro. (1987). One Method for Optimizing Pulverized Coal Injection in Ironmaking Blast Furnaces. Transactions ISIJ, 27: 552-559.

[12]. Aoki HideYuki, Nogami Hiroshi, Tsuge Hideo, Miura Takatoshi and Furukawa Takeshi. (1993). Simulation of Transport Phenomena around the Raceway Zone in the Blast Furnace with and without Pulverized Coal Injection. ISIJ Int., 33(6): 646-654.

[13]. Nogami Hiroshi, Richard Peter Austin, Yagi Jun-Ichiro, Yamaguchi Kazuyoshi. (2004). Numerical Investigation on Effects of Deadman Structure and Powder Properties on Gas and Powder Flows in Lower Part of Blast Furnace. ISIJ Int., 44(3), 500-509.

[14]. Umekage Toshihiko, Yuu Shinichi, Kadowaki Masatomo. (2005). Numerical Simulation of Blast Furnace Raceway Depth and Height, and Effect of Wall Cohesive Matter on Gas and Coke Particle Flows. ISIJ Int., 45(10): 1416-1425.

[15]. Abdel Halim K.S.(2007). Effective utilization of using natural gas injection in the production of pig iron. Materials Letters, 61, 3281-3286.

[16]. Ishii K. (2000). Advanced Pulverized Coal Injection Technology and Blast Furnace Operation. Oxford: Pergamon- Elsevier Science Ltd.

[17]. Yamaguchi K., Ueno H., Tamura K. (1992). Maximum Injection Rate of Pulverized Coal into Blast Furnace through Tuyeres with Consideration of Unburned Char". ISIJ Int, 32, 716.

[18]. Suzuki T., Smoot L.D., Fletcher T.H., Smith P.J. (1986). Prediction of high-intensity Pulverized Coal Combustion, Combustion Science and Technology, 45, 167-183.

[19]. Jamaluddin A.S., Wall T.F., Truelove J.S. (1986). Mathematical Modeling of Combustion in Blast Furnace Raceways, including injection of Pulverized Coal. Ironmaking and Steelmaking, 13, 91-99.
[20]. Nogami H., Miura T., Furukawa T. (1992). Simulation of Transport Phenomena around Raceway Zone in the lower part of Blast Furnace. Tetsu-to-Hagane, 78, 1222-1229.
[21]. Takeda K., Lockwood F.C.(1997). Integrated Mathematical Model of Pulverized Coal Combustion in a Blast Furnace. ISIJ International, 37, 432-440.
[22]. Guo B., Zulli P., Rogers H., Mathieson J.G., Yu A. (2005). Three-dimensional Simulation of the Combustion Behavior of Pulverized Coal Injection. 5th International Symposium on Multiphase Flow, Heat Mass Transfer and Energy Conversion, Xi'an, China.
[23]. Picard M. (2001). Pulverized Coal Combustion in the Blast Furnace Raceway, Using a 3D Numerical Simulation. Proceedings of the 2001 Ironmaking Conference.
[24]. Guo Y.C., Chan C.K., Lau K.S.(2003). Numerical Studies of Pulverized Coal Combustion in a Tubular Coal Combustor with Slanted Oxygen Jet, Fuel, 82, 893-907.
[25]. Rajneesh S., Sarkar S., Gupta G S. (2004). Prediction of Raceway Size in Blast Furnace from Two Dimensional Experimental Correlations. ISIJ International, 44.
[26]. Gupta G.S., Rudolph V. (2006). Comparison of Blast Furnace Raceway size with Theory. ISIJ International, 46(2), 195-201.
[27]. Flint P. J and Burgess. (1992) Metal Trans, 23, 267-83
[28]. Szekely J. and Poveromo J. J. (1975) Metal Trans, 6, 119-30
[29]. Mondal S. S., Som S. K., Dash S. K. (2005). Numerical Predictions on the Influence of the Air Blast Velocity, Initial Bed Porosity and Bed Height on the Shape and Size of Raceway zone in a Blast Furnace. Journal of Physic:. Applied Physics, 38, 1301
[30] Clifford Tetrault, Yongfu Zhao, D. (Frank) Huang, Pinakin Chaubal, Chenn Zhou, "CFD modeling of pulverized coal injection in a blast furnace", presented at 2005 ASME International Mechanical Engineering Conference and Exposition, paper, November 5-11, 2005, Orland, Florida (abstract only)
[31] Roldan, David ,Tetrault, Clifford, Zhao Yongfu, Atkinson Mark, Zhou, Chenn Q. (2005). Heat Transfer Analysis in a Blast Furnace Tuyere Nose. Proceedings of the ASME Summer Heat Transfer Conference, 3, 179-187.
[32] Gu, Mingyan; Chen, Zumao; Selvarasu, Naresh K.; Huang, D.; Chaubal, Pinakin; Zhou, Chenn Q.; "Simulation of pulverized coal injection in a blast furnace", Proceedings of 2006 ASME International Mechanical Engineering Congress and Exposition, IMECE2006 - Power, 2006, 7p
[33] Selvarasu, Naresh K.; Huang, D.; Chen, Zumao; Gu, Mingyan; Zhao, Yongfu; Chaubal, Pinakin; Zhou, Chenn Q.; "Prediction of raceways in a blast furnace", Proceedings of 2006 ASME International Mechanical Engineering Congress and Exposition, IMECE2006 - Power, 2006, 7p
[34] Chenn Q. Zhou, D. (Frank) Huang, Zumao Chen, Naresh K Selvarasu, Mingyan Gu, Yongfu Zhao, and Pinakin Chaubal, "Simulations Of Raceway Conditions in a Blast Furnace", presented at the 4th International Congress on the Science and Technology of Ironmaking, Japan, November 2006 (5 pages)
[35] Walker, William; Zhou, Chenn Q., "Study of pulverized coal injection with natural gas co-injection, and pre-combusted natural gas in the blast air", poster presentation at 2006 PUC Graduate Spotlight, Oct 2006 (abstract only)

[36] Selvarasu, Naresh K; Zhou, Chenn Q; "Prediction of raceways in a blast furnace", poster presentation at 2006 PUC Graduate Spotlight, Oct 2006 (abstract only)

[37] Gu, M.; Chen, Z.; Huang, D.; Chaubal, P.; Zhou, C.Q.; "Heat transfer, devolatilization and combustion of injected coal before entering raceways", AISTech 2006 - Proceedings of the Iron and Steel Technology Conference, 2006, v 1, p 345-355

[38] Chenn Q Zhou., Huang Frank D., Zumao Chen, Selvarasu Naresh K., Mingyan Gu., Yongfu Zhao and Pinakin Chaubal. (2006). ISIJ ICSTI proceedings, 500-503

[39] Selvarasu Naresh K., Huang D., Zumao Chen., Mingyan Gu., Yongfu Zhao., Pinakin Chaubal., and Chenn Q. Zhou. (2006). Prediction of Raceways in a Blast Furnace, Proceedings of 2006 ASME International Mechanical Engineering Congress and Exposition, IMECE2006-15573, 7 pages

[40] Gu, Mingyan; N.K.C. Selvarasu; Yongfu Zhao; Dennis Lu; Chenn Q. Zhou; "Numerical Analysis of Coal Combustion in a Raceway", presentation at the 5th US Combustion Meeting, the Combustion Institute, San Diego, CA, March 25-28, 2007 (6 pages).

[41] Gu, Mingyan; Selvarasu, Naresh K.; Huang, D.; Chaubal, Pinakin; Zhou, Chenn Q.; "Numerical analysis on the coke combustion inside raceway", AISTech 2007 - Proceedings of the Iron and Steel Technology Conference, 2007, v 1, p 609-618

[42] Walker, William; Gu, M.; Selvarasu, N.K.C.; D'Alessio, John; Macfadyen, Neil; Zhou, C.Q.; "Numerical study of pulverized coal injection with natural gas Co-injection in a blast furnace", AISTech 2007 - Proceedings of the Iron and Steel Technology Conference, 2007, v 1, p 453-462

[43] Selvarasu, Naresh K., Gu Mingyan, Zhou Chenn Q., Zhao Yonufu. (2007). Computer Modeling of Blast Furnace Raceway Formation Kinetics. Proceedings of the Iron and Steel Technology Conference, 1,425-433.

[44] Mingyan Gu, N.K.C. Selvarasu, William Walker, and Yongfu Zhao, "Numerical Analysis on Pulverized Coal Combustion in the Raceway of a Blast Furnace", Processing of ASME-JSME Thermal Engineering and Summer Heat Transfer Conference, HT2007-32141, 8 pages

[45] Gu Mingyan, Naresh K Selvarasu, D. (Frank) Huang, Pinakin Chaubal, and Chenn Q. Zhou, "Numerical Analysis on the Coke Combustion inside Raceway", presentation at presentation at the 2007 Chinese Society for Metals (CSM) Annual Meeting, Chengdu, China, Nov. 2007

[46] Fengguo Tian, Lijian Sun, Bin Wu,Yongfu Zhao, and Chenn Q. Zhou, "Numerical Analysis of Combustion Behavior of Pulverized Coal in Blast Furnace Raceway", Combustion Fundamentals and Applications, Proceedings of 2008 Central States Spring Technical Meeting, (7 pages)

[47] Fengguo Tian, Lijian Sun, Mingyan Gu, Yongfu Zhao, and Chenn Q. Zhou, "Numerical Analysis on Pulverized Coal Combustion in the Blast Furnace Raceway", AISTech 2008 - Proceedings of the Iron and Steel Technology Conference, 2008, paper No. 8198, 9 pages

[48] William Walker, Mingyan Gu, Naresh Selvarasu, John D'Alessio, Neil Macfadyen, and Chenn Zhou, "Simulation of Natural Gas and Pulverized Coal Combustion in a Blast Furnace and their Effects on Coke Consumption in the Raceway", AISTech 2008 - Proceedings of the Iron and Steel Technology Conference, 2008, paper No. 8121, 12 pages

[49] William Walker, Mingyan Gu, Naresh Selvarasu, John D'Alessio, Neil Macfadyen, and Chenn Zhou, "Methodology For The Numerical Simulation Of Natural Gas, Coal, And Coke Combustion in a Blast Furnace", Proceedings of 2008 ASME Summer Heat Transfer Conference, HT2008-56363, 8 pages

[50]. Suhas Patankar. (1980). Numerical Heat Transfer and Fluid Flow. Taylor & Francis, 1st ed.

[51] M. Jazbec, D.F. Fletcher and B.S. Haynes, "Simulation of the Ignition of Lean Methane Mixtures using CFD Modeling and a Reduced Chemistry Mechanism", Applied Mathematical Modelling, Vol. 24, 2000, pp. 689-696.

[52]. Austin P.R., Nogami H. and Yagi J. (1997). A Mathematical Model of Four Phase Motion and Heat Transfer in the Blast Furnace. ISIJ Int., 37, 458-467.

[53]. Austin P.R., Nogami H. and Yagi J. (1997). A Mathematical Model for Blast Furnace Reaction Analysis based on the Four Fluid Model. ISIJ Int., 37, 748-755.

[54]. Zhou, L.X. (1993). Theory and Numerical Modeling of Turbulent Gas-Particle Flows and Combustion. New York: Science Press & CRC Press.

[55]. Ren Yan., Mahinpey Nader., Freitag Norman. (2007). Kinetic Model for the Combustion of Coke Derived at Different Coking Temperatures. *Energy & Fuels*, 21: 82-87.

[56] Hiroshi Nogami, Hideyuki Yamaoka And Kouji Takatani, Raceway Design For The Innovative Blast Furnace, ISIJ International, Vol. 44 (2004), No. 12, pp. 2150–2158

[57] Rajneesh S., Sarkar S. and Gupta G. S. (2004). Comparison of Blast Furnace Raceway Size with Theory. ISIJ International, 44, 195-201.

[58] Zhang Y., Wei X. L., Zhou L. X., Sheng H. Z. (2005). Simulation of Coal Combustion by AUSM Turbulence-Chemistry Char Combustion Model and a Full two-Fluid Model. Fuel, 84,1798-1804.

[59]. Ichida Morimasa., Orimoto Takashi, Tanaka Tsuyoshi, Koizumi Fumio. (2001). Behavior of Pulverized Coal Ash and Physical Property of Dripping Slag under High Pulverized Coal Injection Operation. ISIJ Int., 41(4): 325-332.

[60]. Hiroshi NOGAMI., Hideyuki Yamaoka., Kouji Takatani. (2004). Raceway Design for the Innovative Blast Furnace. ISIJ Int., 44(12),2150-2158.

[61]. Pipatmanomai Suneerat., Herod Alan A., Morgan Trevor J., Paterson Nigel. (2004). The Fate of Volatiles from Injectant Coals and Soot Formation in Blast Furnaces. Energy & Fuels, 18, 68-76.

[62]. Badzioch S. and Hawksley P.G.W. (1970). Kinetics of Thermal Decomposition of Pulverized Coal Particles. Ind. Eng. Chem. Process Design and Development, 9, 521-530.

[63]. Hiroshi NOGAMI., Sungging Pintowatoro., Jun-Ichiro Yagi. (2005). Numerical Analysis on Behavior of Unburned Char and Fine Coke in Blast Furnace. ISIJ Int., 45(10), 1489-1495.

[64]. Lu, Liming., Sahajwalla, Veena., Harris, David. (2001). Coal Char Reactivity and Structural Evolution during Combustion-Factors Influencing Blast Furnace Pulverized Coal Injection Operation. Metallurgical and Materials Transactions B, 32B, 811-820.

[65]. Kalkreuth, W., Borrego, A., Alvarez, D., Menendez, R. (2005). Exploring the Possibilities of using Brazilian sub-bituminous Coals for Blast Furnace Pulverized Fuel Injection. Fuel, 84, 763-772.

[67]. Yamagata, Suyama, Horisaka. (1992). Fundamental Study on Combustion of Pulverized Coal Injection into Coke Bed at High Rate. ISIJ International, 32, 725-732
[68]. Yamaguchi, Ueno, Matsunaga, Kakiuchi. (1995). Test on High-rate Pulverized Coal Injection Operation at Kimitsu No 3 Blast Furnace. ISIJ International, 35, 148-155